THE CONCENTRATION OF LIGHT IN THE HUMAN LENS

BY *John C. Merriam,* MD

ABSTRACT

Purpose: This thesis explores the idea that light energy, especially ultraviolet light, contributes to the unequal distribution of cataract around the world and to the development of cortical opacities.

Methods: In the first section, the thesis reviews historical concepts of the function of the lens and the nature of cataract, epidemiologic data on the global distribution of cataract, and clinical observations of the predominant location of cortical opacification. Second, computer ray tracings and geometric optics demonstrate the passage of light of varying angle of incidence within the lens. Third, two models of the human eye are used to study the refraction of light by the cornea and lens and illustrate the concentration of energy at the equatorial plane of the lens.

Results: Cataract prevalence increases with proximity to the earth's equator, and cortical cataract is most common in the inferior and inferonasal lens. Theoretical studies and the eye models both demonstrate that the concentration of light within the lens increases with angle of incidence, and the eye models suggest that the inferior and inferonasal lens receives significantly more energy than other sections of the lens.

Conclusion: The prevalence of cataract and exposure to ultraviolet energy both increase with decreasing latitude. The most common location of cortical cataract in the inferonasal lens is consistent with the greater dose of light energy received by this portion of the lens. These studies suggest that the global distribution of cataract and the development of cortical cataract are at least in part dependent on the dose of ultraviolet light received by the lens.

INTRODUCTION

DEVELOPMENT OF CONCEPTS OF THE LENS AND CATARACT

The practice of cataract surgery began long before the position of the lens within the eye was known.[1-11] The ancient Greeks debated whether vision was due to the release of visual spirit from the eye, as Plato wrote, or the

reception of stimuli by the eye, as Aristotle thought.[12] No mention of the lens is found until after the founding of Alexandria, Egypt, in 332 BC. The astronomy of Ptolemy and the geometry of Euclid were developed in Alexandria, and scientific anatomy also began there. Alexandrian anatomists placed the lens in the center of the eye and assumed it was the principal organ of visual perception.[5] The retina, choroid, and sclera nourished and protected the lens, and the optic nerve was thought to be hollow to permit visual spirit to pass from the brain to the lens and the visual impression to pass from the eye to the ventricles of the brain for interpretation and memory. Alexandria and at least part of its famous Library were burned by Caesar's troops in 48 BC, and the Library was finally destroyed by the Arabs after the capture of Alexandria in 641 AD. The writings of Herophilus, Eristratus, and other Alexandrian anatomists were lost, but their texts were familiar to Roman physicians, in whose work Greek medical knowledge survived.[5]

The Roman physician Aurelius Cornelius Celsus (25 BC-25 AD) accepted Alexandrian teachings. The oldest surviving description of couching is found in Celsus' *De Medecina*, and Celsus refers to an Alexandrian surgeon named Philoxenes who was skilled at couching 270 years before Christ.[13,14] Undoubtedly, couching was practiced long before Philoxenes, and in Europe this ancient procedure remained the principal surgical procedure for cataract until at least the late 18th century and was practiced in some parts of Asia into the 20th century.[13,15] Celsus located the lens or "crystalloides" in the center of the eye. Between the small central lens and the iris, Celsus described an empty space, the locus vacuus, in which coagulated humors obstructing vision were thought to settle. Couching was not an operation on the lens but a means of clearing the visual axis. This idea would influence concepts of ocular anatomy and function for at least 1,500 years.

Another Roman physician, Claudius Galenus (131-201 AD), born in Pergamon in Hellenic Asia Minor, would have more influence than Celsus.[16] He may have participated in human dissection, but many of his original anatomical observations were based on the dissection of animals, especially dogs and apes.[5,17,18] He described seven extraocular muscles, six plus the retractor muscle found in some animals. He denied the decussation of the optic nerves but recognized their union at the chiasm, which served to distribute "visual spirit" evenly to the two eyes to create a single sensation from two.[5] Galen's conception of the globe is more accurate than that of Celsus. Galen moved the lens anteriorly, noted the difference in the curvature of its anterior and posterior surfaces, but retained a space between the lens and the iris where cataract or hypochyma, a morbid

humor from the brain, settled. His vast corpus was not all preserved; but when rediscovered in Europe in the late Middle Ages, his anatomic and physiologic concepts initially had the authority of doctrine.

After the decline of Rome and the division of the Empire into eastern and western sectors, Greek and Roman medical concepts were preserved by Arab scholars.[2,5,8,9,18] The Arabs referred to cataract as "mä", or water, suggesting that the opacity flowed into the eye.[2] The lens retained some properties of perception, and glaucoma was attributed to a drying up of the lens.[5] Couching remained the principal treatment for cataract, although the Egyptian Ammar is said to have aspirated soft cataracts with a hollow needle.

The Eastern Caliphate was overrun by the Turks in 1058, Baghdad was destroyed by the Mongols in 1258, and after the 11th century the Western Caliphate increased in importance. At its peak, Arab Spain had 70 libraries and 17 institutes of higher learning.[5] In the late Middle Ages, classical and Arabic medical knowledge was discovered, copied, and translated by European monks. Universities were not founded until the late Middle Ages, initially at Bologna (1158) and later at Padua (1222), Siena (1246), Montpellier (1220), and Oxford (1249).[5,9] The widespread distribution of books did not become possible until after Gutenberg's invention of the printing press and moveable type in 1450 in Mainz, Germany. By 1467 universities could obtain printed texts from Strasbourg. The first Latin *Opera* of Galen was printed in Venice in 1490, and the first printed Greek edition of Galen's collected works was published by the Aldine Press in Venice in 1525.[19]

The first incunabulum printed in Ferrara in 1474 was Benevenutus Grassus' *De Oculis*.[20] Benevenutus probably was born in the 11th century, was educated at Salerno, and taught at Montpellier. Although he apparently had dissected the globe, his little book repeats classical misconceptions of ocular anatomy and function. He placed the "crystalline body" centrally within the eye, described the path of visual spirit from the brain down the optic nerve to the vitreous, and accepted the conventional belief that cataract was an opacity in front of the crystalline that prevented the escape of the visual spirit. Another physiologic observation that is curiously charming to the 20th century is his explanation of the source of tears. The major and minor lacrimal glands were unknown. Benevenutus stated that tears "that escape through the puncta in the lower lid come from the heart, when one is in great pain. Those tears that flow from the upper lid originate in the brain, as the result of some corrupting or excess of humors."[21]

Credit for the establishment of anatomy as an objective science is

given to Andreas Vesalius (1514-1564).[16, 22] Raised in Brussels, Vesalius began his medical studies in Paris (1533-1536), where in 1531 Johannes Guinter, professor of medicine, published a translation of the first nine books of Galen's *Anatomical Procedures*, assuring the ascendancy of Galenism.[17,22] Vesalius' studies in Paris were interrupted by war, and he completed his studies in Padua. Upon graduation, he was appointed to the chair of surgery and anatomy, a position not held in especially high esteem. In 1537 in reference to the first anatomy witnessed in Paris, he wrote: "I gave careful consideration to the possibility that anatomical dissection might be used to check speculation."[23] With access to cadavers, Vesalius became convinced that much of Galen's anatomy was in error because it was based on animals. His conviction that human anatomy could be learned only by human dissection led to the first great anatomical and medical text of the Renaissance, *Humani Corpora Fabrica*, published in 1543, when Vesalius was 28.[22,24-27] In the same year the heliocentric planetary system of Nicholas Copernicus (1473-1543) was published.

Vesalius made some original observations relevant to ophthalmology. He described atrophy of the optic nerve after loss of an eye in childhood, derided the common belief that nerves were hollow, and expressed skepticism that the lens was the principal organ of vision.[8,22] However, he could not divorce himself completely from Galen. He attributed raising the lids to the orbicularis and described six extraocular muscles plus a seventh, the retractor bulbi. His representation of the eye is no more sophisticated than the classical authorities he criticized (Fig 1). The lens is a small structure in the center of a spherical globe, similar to Celsus' conception.

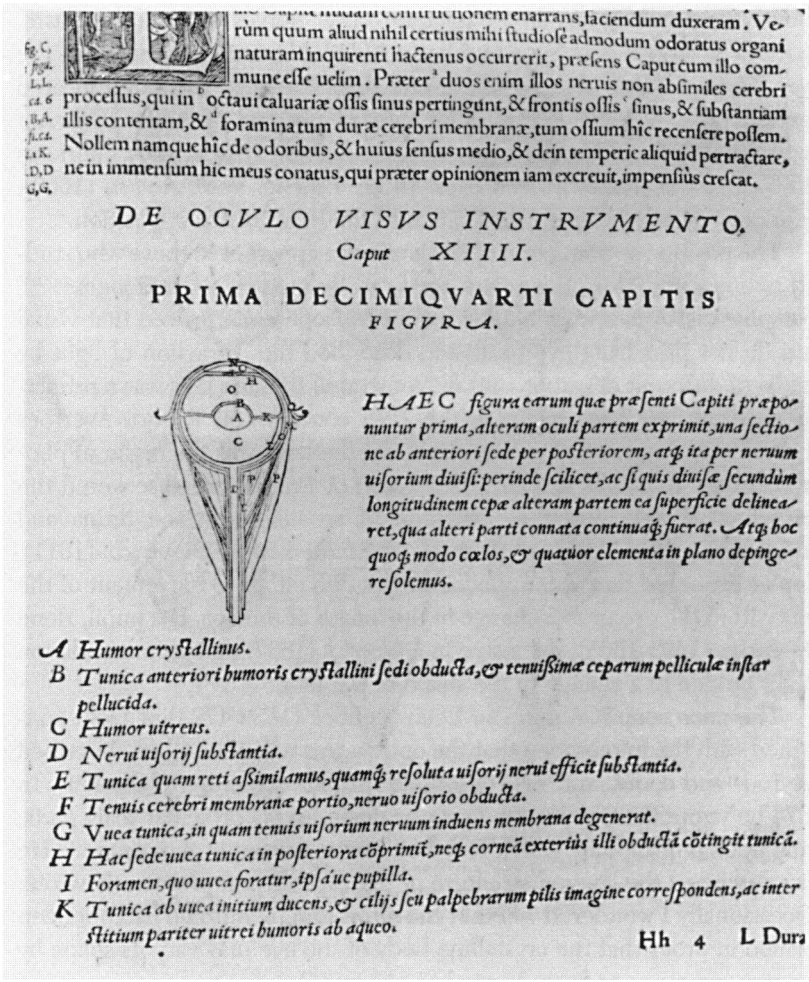

rùm quum aliud nihil certius mihi ſtudioſè admodum odoratus organi naturam inquirenti hactenus occurrerit, præſens Caput cum illo commune eſſe uelim. Præter duos enim illos neruis non abſimiles cerebri proceſſus, qui in octaui caluariæ oſſis ſinus pertingunt, & frontis oſſis ſinus, & ſubſtantiam illis contentam, & foramina tum duræ cerebri membranæ, tum oſſium hîc recenſere poſſem. Nollem namque hîc de odoribus, & huius ſenſus medio, & dein temperie aliquid pertractare, ne in immenſum hic meus conatus, qui præter opinionem iam excreuit, impenſiùs creſcat.

DE OCVLO VISVS INSTRVMENTO.
Caput XIIII.

PRIMA DECIMIQVARTI CAPITIS
FIGVRA.

HAEC figura earum quæ præſenti Capiti præponuntur prima, alteram oculi partem exprimit, una ſectione ab anteriori ſede per poſteriorem, atq; ita per neruum uiſorium diuiſi: perinde ſcilicet, ac ſi quis diuiſæ ſecundùm longitudinem cepæ alteram partem ea ſuperficie delinearet, qua alteri parti connata continuaq; fuerat. Atq; hoc quoq; modo cœlos, & quatuor elementa in plano depingere ſolemus.

A Humor cryſtallinus.
B Tunica anteriori humoris cryſtallini ſedi obducta, & tenuiſsimæ ceparum pelliculæ inſtar pellucida.
C Humor uitreus.
D Nerui uiſorij ſubſtantia.
E Tunica quam reti aſsimilamus, quamq; reſoluta uiſorij nerui efficit ſubſtantia.
F Tenuis cerebri membranæ portio, neruo uiſorio obducta.
G Vuea tunica, in quam tenuis uiſorium neruum induens membrana degenerat.
H Hac ſede uuea tunica in poſteriora cõprimit, neq; corneã exteriùs illi obductã cõtingit tunicã.
I Foramen, quo uuea foratur, ipſa uue pupilla.
K Tunica ab uuea initium ducens, & ciliis ſeu palpebrarum pilis imagine correſpondens, ac interſtitium pariter uitrei humoris ab aqueo.

FIGURE 1
Vesalius' illustration of the eye. Lens is located centrally within a spherical globe (from Versalius[24]).

Vesalius' book undoubtedly became known to the practicing medical community. The first textbook in the vernacular devoted exclusively to the eye was published in 1583 by the barber-surgeon George Bartisch at his expense. The style of *Das Ist Augendienst* is reminiscent of the *Fabrica*, but its more than 80 illustrations are cruder than those of the *Fabrica*.[28,29] The first is a multilayered depiction of the skull and brain seen from

above; the final figure shows separate optic nerves without a chiasm. Bartisch practiced couching, and he included a layered illustration of the eye. When the last "flap" is lifted, one finds the lens, small and located centrally as in Vesalius (Fig 2). The anterior position of the lens was not proved until one of Vesalius' successors in Padua, Hieronymus Fabricius (1537-1619), sectioned frozen eyes. In *De Visione, Voce, Auditu* (1600), Fabricius included a crude illustration of the lens in correct position.[30]

The position and function of the lens were apparent to those who studied optics long before they were accepted by medical practitioners.[2,4,5,8-10] The physicist Alhazen (965-1038 AD) of Mesopotamia proved that visual rays do not pass from eye to object, described the refraction of light by media of different densities, and demonstrated that the lens was a refracting medium. In Arab Spain in the 12th century Ibn Rushdi Averroes (1109-1162) suggested that the retina, not the lens, was the organ of photoreception. Johannes Kepler (1571-1631) of Frankfurt rediscovered the refraction of light and the formation of an image on the retina and explained various types of glasses. In *Mathematica Dioptrice* (1611), Kepler proposed that accommodation was due either to movement of the lens within the eye or to a change in the length of the eye. His pupil, René Déscartes (1595-1665), suggested in *Dioptrics* (1637) that accommodation might be due to a change in the shape of the lens.[4]

The microscopist Anton van Leeuwenhoek (1638-1723) of Delft confirmed with the microscope that the optic nerve was not hollow, described the rods and cones, and first described the fine structure of the lens. In 1674 he wrote that the bovine lens was made up of "orbicular scaly parts, lying upon one another, which had their beginning out of the center."[31] He also described the layered structure of the capsule and presciently wrote: "Occasionally I wondered whether the afore-said membrane had not been formed in order that the crystalline body of the eye may vary its shape by a certain pressure or force exerted on the eye."[32]

The medical community was slow to accept these new ideas and their implications for the nature and location of cataract. Some physicians had argued that cataract was a disease of the lens in the latter half of the 17th century, but two Frenchmen proved it.[5,11,33] On April 6, 1705, Pierre Brisseau (1631-1717) of Tournay depressed the cataract of a soldier who succumbed to tuberculosis. After clearing the visual axis, he opened the eye and found that he had depressed an opaque lens into the vitreous.[11] Brisseau's observation that cataract was a disease of the lens was reported to the Academy of Medicine at Paris in November 1705, but was initially disputed and not accepted by the Academy until 1708. In 1709 Brisseau documented his observations in *Traité de la Cataracte et du Glaucome.*

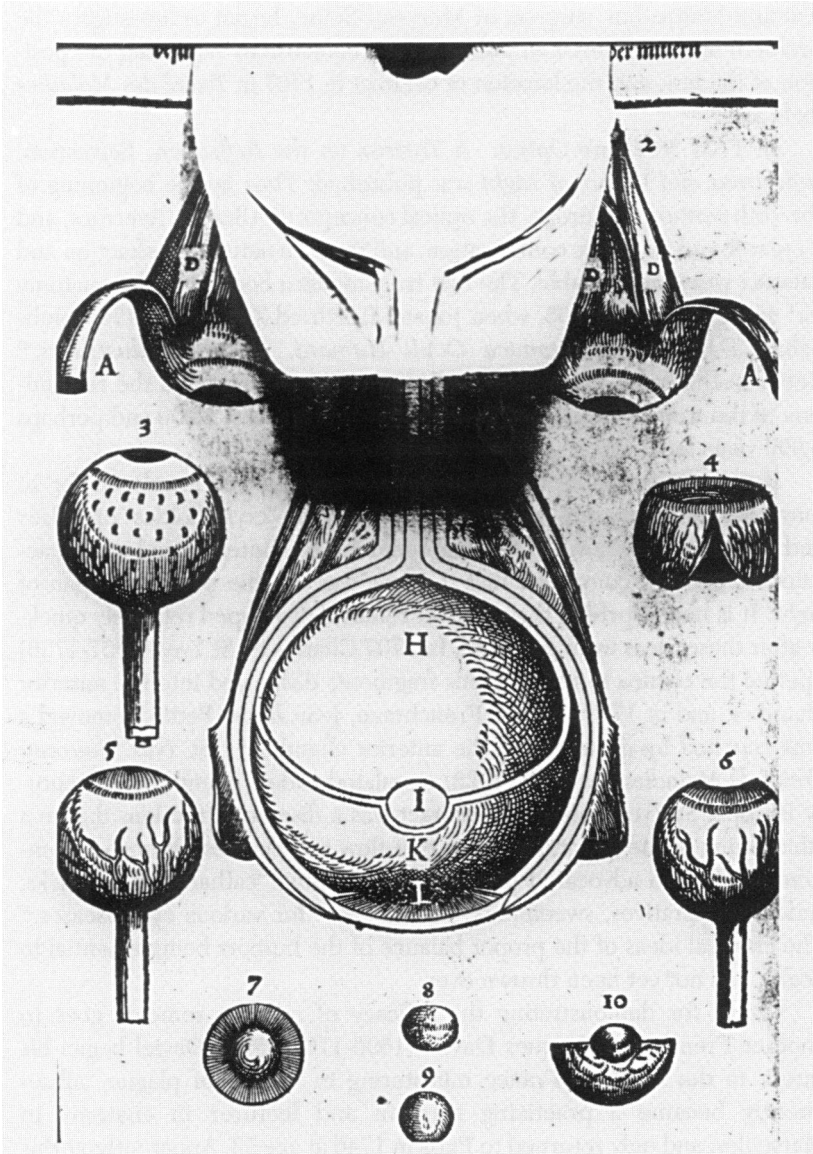

FIGURE 2
Bartisch's illustration of the eye is nearly identical to that of Vesalius. Flaps have been lifted to reveal small crystalline within eye (from Bartisch[28]).

Antoine Maître-Jan, surgeon of Mery-sur-Seine, began to investigate the problem in about 1682 and published his conclusions regarding the position of the lens and the location of cataract in 1707 in *Traité des Maladies de l'Oeil*.[34]

In 1704 Newton's *Optics: A Treatise on the Reflection, Refraction, Inflections and Colors of Light* was published. Thus by the beginning of the 18th century in Europe, the optical concepts of Alhazen, Averroes, and Kepler found anatomic confirmation, and the true nature of refraction and cataract were indisputable. The first truly modern book of ocular anatomy did not appear until 1755, when Johann Gottfried Zinn (1727-1759) published *Descriptio Anatomica Oculi Humani, Iconibus Illustratus*.[35] Between the beginning of cataract surgery by couching and the recognition of the true location of cataract and the lens at least 2,000 and perhaps 3,000 years had passed.

It seems reasonable to conclude that the lens was misplaced for so long because theory required a space between the "crystalloides" of Celsus and the iris; and removal of the lens could not be contemplated until practitioners became convinced that the lens was not the principal organ of sight. It is not surprising that cataract removal developed relatively quickly after these ideas were accepted. In 1707 Charles de St Yves (1667-1736) opened the cornea to remove lens fragments dislocated into the anterior chamber, and in 1708 another Frenchman, Jean Louis Petite, removed a lens couched by mistake into the anterior chamber.[5,11] St Yves' *Nouveau Traité de Maladies des Yeux* (1722) circulated widely in eighteenth century Europe. St Yves stated that cataract was a disease of the lens due to a "thickening of the nutritious juices that flow into the vessels of the membrane". He also advocated purging, bloodletting, "catharticks, emeticks, sudorifs, alteratives, sweeteners, coolers, etc" for various eye diseases.[36] The classical ideas of the proper balance of the humors being essential to health had not yet been thrown over.

Credit for demonstrating the efficacy of cataract removal goes to another Frenchman, Jacques Daviel (1696-1762).[1,2,5,10,33] Daviel began his career in the south of France ministering to victims of plague, subsequently became a practicing surgeon and lecturer in anatomy in Marseilles, and only returned to Paris in 1746 at age 53. Apparently, at this time he become dissatisfied with the results of couching and devised blunt instruments to make the procedure safer. In 1747 he attempted depression on a Monsieur Garion, a master wigmaker of Paris.[33] Failing to depress the lens, he opened the lower part of the cornea and pushed the lens out, along with a "small" amount of vitreous. The eye healed uneventfully, and by 1750 extraction had become his method of choice. In late

1751 his success with extraction was reported to the Royal Academy of Surgery of Paris. Daviel formally presented his results to the Academy in April and November 1752; and they were published in 1753. Daviel's original curved incision was made inferiorly with a scissor. He later tried an inferior triangular incision and a temporal triangular corneal incision.[33]

Many surgical refinements followed the acceptance of Daviel's demonstration of the safety and efficacy of lens removal.[2,5-7,10,11,37,38] For at least another hundred years the lens could be examined clinically only with the unaided eye or a loupe. It is not surprising that some of the most lavishly illustrated and detailed textbooks of the first half of the 19th century are devoted almost exclusively to external disease or the so-called "ophthalmias," "scirrhous" disease or malignancies, and congenital anomalies.[39-44] The broad term "amaurosis" encompassed essentially all causes of blindness not visible to the naked eye. This terminology was criticized by James Wardrop,[45] but not until the introduction of Helmholtz's ophthalmoscope in 1851 was a more precise etiologic definition of blindness possible. Amaurosis as a blanket term disappeared. In 1855 Jaeger published the first atlas of newly discovered disorders of the retina and optic nerve.[46] The ophthalmoscope also provided a more objective means of assessing the lens and the refractive state of the eye. Ruete was among the first to recognize the utility of the new instrument for studying the lens, and his *Lehrbuch* (1854) devotes 100 of its 751 pages to cataract.[47]

In the latter half of the 19th century clinicians used a handheld loupe and direct or indirect ophthalmoscopy to examine the anterior segment.[48,49] A binocular loupe of sufficient magnification had the disadvantage of unsteadiness until the corneal microscope was introduced by Czapski and developed by Zeiss in the late 19th century. In 1911 Alvar Gullstrand (1862-1930) won the Nobel Prize for his work on the diffraction of light by lenses as applied to the human eye, and in that same year he demonstrated the slit lamp in Heidelberg.[50] Zeiss combined the slit lamp with Czapski's corneal microscope to create the instrument that permits detailed study of the lens.[51]

LOCATION OF CATARACT

It is interesting that careful observations of the lens were made before the introduction of the modern slit lamp. In lectures to students at the Royal London Ophthalmic Hospital, Moorfields, in June 1847, William Bowman described cortical cataract:

> In the commencing cataract of middle or declining age, we not uncommonly find the posterior surface of the lens first affected...This opacity sometimes, and indeed generally, encroaches from the margin in distinct streaks of irregular thick-

> ness, length, number and distance apart; and we usually find that when the pupil is widely dilated by belladonna, some at least of these streaks are traceable round the margin for some way over the anterior surface.[52]

In 1889 Magnus noted that one type of opacity, presumably cortical, initially developed in the inferior half of over 90% of the 166 patients studied.[53] In 1891 Brailey suggested that while nuclear cataract appeared to be a true degenerative change, the course of cortical opacification might be affected by "hygienic measures and...other remedial measures."[54] In a textbook published in 1900, Edward Jackson observed that cortical cataract initially was most prominent in the lower nasal quadrant of the lens.[55] Writing in the *Journal of the American Medical Association* in 1908, Greene reported that cortical cataract could be "..detected in the lower inner one-third or one-half of the periphery in more than 95% of all cortical cases."[56] In 1909 Handmann confirmed these observations in a larger study of 845 eyes. He tabulated the incidence of ten locations of cataract, including the quadrants and the upper, lower, nasal, and temporal halves of the lens. Opacities of the inferior and nasal lens were the most common, and Handmann speculated that sunlight or perhaps toxic metabolites that settled in the inferior aqueous might be responsible. He also suggested that a large nose might help to protect the eye from sunlight.[57]

Handmann urged that the observation that cortical cataract began inferiorly be incorporated into textbooks to broaden appreciation of this phenomenon and interest in its etiology. With the slit lamp, more refined studies of the lens became possible; yet one finds few references to the predominant location of cortical opacification in texts. In 1922 Schild[58] reported that in 218 eyes lamellar opacities were most common inferonasally. In 1934 Clapp[59] referred to Handmann's 1909 study and confirmed that the "position of the first area of clouding of the lens in senile cataract is usually in the sector down and in." He also discussed the available evidence linking ultraviolet light to cataract. In his textbook of slit lamp biomicroscopy, Berliner noted that "cuneiform opacities, like the lines of lamellar separation with which they are usually associated, are localized mostly in the lower nasal periphery."[60] In 1950 Kirby[61] also noted that cuneiform cataract develops in the inferior periphery of the cortex.

Documentation that cortical cataract is not distributed evenly around the equator of the lens preceded appreciation that the prevalence of cataract is not distributed evenly around the world. In 1937 Wright[62] noted the difference in the incidence of cataract in the Deccam and Malabar regions of southern India, and he speculated that differences in exposure to sunlight might account for the difference. In 1967 the prevalence of cataract was found to be greater among Punjabis over age 40 residing in

Kurali, Punjab, than among Punjabi immigrants in western Canada and northern California; and among the immigrants, the prevalence of cataract increased with years spent in India prior to emigration.[63] In 1972 van Heyningen[64, 65] observed that as many cataract operations were performed per week in Shikarpur, Pakistan, as per year in Oxford and that cataracts were more advanced at the time of operation in Pakistan than England. In 1979 Zigman[66] reported that the frequency of brunescent cataract was correlated with latitude and was higher in Manila than Tampa and higher in Tampa than Rochester. In a survey of five climatic zones of the Punjab, Chatterjee[67, 68] noted that cataract prevalence was not equally distributed over the Indian subcontinent. In 1977 the authors of the Framingham Eye Study[69] noted that cataract prevalence rates were similar in Framingham (Mass), New York City, and Edinburgh, and that the rates in these areas were considerably lower than in the Punjab. In 1982 Chatterjee calculated that the age-adjusted prevalence of cataract in the Punjab was almost three times higher than in Framingham.[70]

Studies from the Indian subcontinent linking cataract prevalence to latitude have been confirmed in other parts of the world. In 1962 Halevi[71] found that male and female immigrants to Israel from the Orient developed cataracts requiring surgery at a younger age than immigrants from Europe; and he reviewed available data to suggest that cataract incidence decreased with increasing latitude. In 1970 Jamieson[72] observed that cataract began at an earlier age among black Africans in the Mrewa Trust lands of Zimbabwe than Europeans. The relatively early development of lens opacities among Nigerians was confirmed in 1973.[73] In a 1978 study of the incidence of macular degeneration among 1,000 black patients over age 50 in Nigeria and 380 white patients over age 50 in London, Gregor and Joffe[74] excluded nearly 30% of Nigerians because of dense unilateral or bilateral lens opacities preventing visualization of the fundus but only 2.5% of the Londoners. In 1989 Marré and Marré[75] reported that cataract developed a decade earlier in Burma than in Leipzig, Germany. In 1980 Taylor reported that cataract in a group of 350 Australian aborigines increased with sunlight and ultraviolet B (UV-B) exposure.[76] In a large study of aboriginal and nonaboriginal residents of rural Australia, Hollows and Moran[77] correlated cataract with ultraviolet exposure and found that aborigines, who spent a greater part of their lives outdoors, were more likely to develop cataract than nonaborigines and that cataract occurred at a younger age among aborigines. In contrast, two small surveys in northern Canada failed to show a difference in the prevalence of cataract among native Indians and Eskimos and white Canadians.[78, 79]

A survey in northwest India that found cataract prevalence was greater

among residents of the plains than among those living at higher elevations in the surrounding Himalaya appeared to contradict the hypothesis that sunlight and ultraviolet exposure correlated with cataract prevalence.[68] A careful, large epidemiologic study conducted in Nepal in 1980 and 1981 confirmed that cataract prevalence was greater among residents of the lowlands than residents living above 1,000 m and increased in all groups with age. It also showed that in some areas, the mountains blocked direct sunlight. When the study population was divided into groups based on average hours of daily sunlight exposure, the correlation of cataract prevalence with sunlight was confirmed.[80]

In a blindness survey of seven rural areas of China, the incidence of senile cataract was found to increase with decreasing latitude and increasing altitude.[81] The incidence in Zedang in Tibet at the highest altitude and lowest latitude was nearly ten times greater than in the lowland areas.[82] The age- and sex-adjusted prevalence of cataract of residents near Lhasa, Tibet, at an altitude of 4,000 m was 60% higher than among residents of Shunyi County near Beijing, at an altitude of 50 m.[83]

Careful epidemiologic studies from America and Europe also have demonstrated an association of light exposure with cataract. Analysis of Medicare data indicates that the probability of undergoing cataract surgery in the United States increases by 3% for each degree of south latitude.[84] Using state blindness registries and the National Health and Nutrition Examination Survey, Hiller found an association of cataract incidence with sunlight and UV-B.[85,86] Cortical cataract appeared to be related to UV-B exposure, but no association of nuclear or posterior subcapsular opacities was detected.[87] A small survey of white patients 40 to 69 years of age in North Carolina suggested that cortical and posterior subcapsular cataracts were associated with sunlight but that nuclear cataract was not.[88]

The most carefully documented study of the relationship between ultraviolet exposure and cataract is Taylor's study of 838 Chesapeake Bay watermen,[89-91] among whom a doubling of the cumulative exposure to UV-B resulted in a 1.6-fold increase in the risk of cortical cataract. No association of UV-B exposure and nuclear cataract was detected. A separate case-control study of patients having cataract surgery on the eastern shore of Maryland, however, did report an association of posterior subcapsular cataract (PSC) with UV-B exposure. Corticosteroid use, diabetes, blue eyes, and less than high school education also were risk factors for PSC, while smoking and hypertension were not.[92] Reviewing the data from the watermen, Taylor[93-96] also noted an association of pterygium and climatic droplet keratopathy with ultraviolet exposure, and others have confirmed this association.

The Beaver Dam Eye Study documented an increased risk of cortical cataract with higher levels of UV-B exposure among men but not women; no association of ultraviolet exposure and nuclear or PSC cataract was found for men or women.[97-99] A study of 1,008 patients with cataracts in Parma, Italy,[100,101] found a significant association of pure cortical or mixed cortical and posterior subcapsular opacities with sunlight exposure. No significant relationship between sunlight exposure and other mixed types of cataract was detected.

Most interesting is the consistent observation among contemporary observers that cortical cataract begins in the inferior and inferonasal lens. Adamsons and coworkers[102] reported in 1991 that among the watermen 60% of the cortical opacities were found in the inferonasal quadrant of the lens. A more detailed study of retroillumination photographs from 1985 and 1990 revealed that approximately 63.8% of cortical opacities were inferonasal, 17% inferotemporal, 6.4% superonasal, and 12.8% superotemporal. The distribution of new cortical opacities detected between 1985 and 1990 was similar.[103] In the Beaver Dam Eye Study the lens was divided into nine segments, and cortical opacities were found more frequently in the inferonasal sectors than elsewhere.[98,99] Other smaller surveys also have shown that cortical opacities occur most frequently in the inferior lens.[104,105] The standard photographs for the Lens Opacities Classification System also suggest that cortical opacity begins in the inferior lens.[106]

The definition of cataract, the sophistication of the means of identifying cataract, the care with which sunlight exposure is assessed, and the numbers of patients studied are among the potential variables affecting the validity of epidemiologic studies. However, data from many societies and racial groups support the observation that prevalence of cataract increases with age and decreasing latitude and that the development of cortical cataract and possibly posterior subcapsular cataract is associated with exposure to ultraviolet light.[107-110] These risks are independent of country and ethnicity.

If cataract prevalence in general and cortical cataract in particular are related to the amount of sunlight exposure, the inferior portion of the lens must receive a greater dose of light energy than the upper portion of the lens. In 1909 Handmann[57] assumed that the iris helped to protect the peripheral lens from intense light, and in 1920 van der Hoeve[111] stated that light could not be implicated in cataract because lens opacities begin peripherally while only the "pupillary part of the lens" is exposed to ultraviolet rays. The refraction of oblique light by the cornea was described by Helmholtz[112] and was proposed as a diagnostic test for keratoconus in 1970.[113] Recently with elegant computer ray tracing analysis, Coroneo and

colleagues[114-116] have shown that light obliquely incident on the cornea may be concentrated on the opposite limbus and refracted into the peripheral lens.

The next sections present an overview of factors affecting terrestrial ultraviolet exposure followed by theoretical and experimental data demonstrating that the inferior half of the lens receives a greater dose of light energy than the superior half.

ULTRAVIOLET RADIATION

The ultraviolet (UV) region includes wavelengths from 10 to 400 nm and accounts for less than 9% of total solar output. UV radiation (UVR) may be divided into extreme UV (10 to 120 nm), far UV (120 to 200 nm), UV-C (200 to 280 nm), UV-B (280 to 315 nm), and UV-A (315 to 400 nm).

Because the atmosphere absorbs wavelengths below about 290 nm nearly completely, the biologically active wavelengths at the earth's surface are UV-B and UV-A.[117] The number of air molecules per unit volume is related to temperature and pressure, and with increasing altitude both pressure and density decrease. Half of the air column is contained within the lowest 5 km of the atmosphere and 90% within the lower 10 km. The stratosphere contains most of the remaining atmosphere, extending up to about 50 km, including 90% of the atmospheric ozone.

Stratospheric ozone is the result of the action of short wavelength solar UV (below 242 nm) on oxygen molecules.[118] Insufficient oxygen remains above the stratosphere to generate ozone, and short wavelength UV is filtered out before reaching lower altitudes. Spectral transmission is wavelength-dependent largely because of atmospheric ozone, and the variability in transmission is greatest in the UV-B region, where ozone absorption is most marked. Other gases, including SO_2 and NO_2, also may attenuate UV but normally are present only in trace amounts. In industrial areas, such gases and the release of industrial ozone may offset losses in the ozone column.[117]

Attenuation of UV is due to absorption and scatter.[118] Rayleigh scattering refers to scattering by gases and varies by about one order of magnitude over the visible spectrum, accounting for the blue color of clear skies. Aerosols made of dust, sea salt, soot, ammonium sulfate, and sulfuric acid droplets also may affect UV exposure and may fluctuate significantly over time and location. Clouds in the lower atmosphere are composed of liquid water droplets, while at higher elevations in the upper troposphere and stratosphere they are formed of ice crystals. The size distribution of water particles, the vertical stacking of clouds, and the geometry of sun-cloud reflection all have the potential to affect the levels of UV radiation

received at the earth's surface. These variables and atmospheric pollutants are difficult to quantify and may fluctuate quickly. Year-to-year variability in cloud cover accounts for most of the fluctuation in annual UV irradiance. [117]

Total terrestrial UV-B irradiance is a function of direct irradiance from the sun and diffuse irradiance from scatter. Scattering is most efficient in the lower atmosphere, resulting in an increase in the ratio of diffuse to direct irradiance with decreasing solar elevation. Changes in the distribution of ozone within the atmospheric column thus may affect direct and scattered solar irradiance differently. For instance, an increase in ozone in the lower atmosphere combined with a decrease in the upper atmosphere might lead to a decrease in total atmospheric ozone, yet surface UV-B irradiance might decline if the decrease in scattered irradiation more than offset the increase in direct irradiation.[117]

In general, terrestrial UV exposure increases with decreasing path length through the atmosphere, and the principal variables determining UV dose at the ground are time of day, season, and solar zenith angle and its complement, the angle between the horizon and the sun or the solar elevation angle.[117,118] Declination refers to the angle between the sun's direction and the earth's equatorial plane and varies from +23.45° on June 21 to -23.45° on December 21. The sun crosses 0° at the spring and fall equinoxes. For comparison, the position of the sun on the solstices and equinoxes at New York City and a more southern city, Caracas, is shown in Tables I and II. The position of the sun at New York on the days of some experiments is shown in Table III. The distance between the sun and the earth varies by about 3.4% from perihelion (minimum) on January 3 to aphelion (maximum) on July 5, resulting in a variation in extraterrestrial radiation of about 6.9%, which is significant when comparing UV exposure of the southern and northern hemispheres.

TABLE I: SOLAR POSITIONS, EQUINOXES AND SOLSTICES, NEW YORK CITY (40° 47′ N, 73° 59′ W)

	Vernal Equinox March 20		Summer Solstice June 21		Autumnal Equinox September 23		Winter Solstice December 22	
Time	Altitude	Azimuth	Altitude	Azimuth	Altitude	Azimuth	Altitude	Azimuth
0700	10°27′	99°28′	26°29′	80°56′	13°26′	101°51′		
0900	31°40′	122°26′	49°06′	101°05′	34°10′	125°48′	14°07′	139°15′
1100	46°37′	156°28′	68°53′	140°34′	47°45′	161°47′	24°36′	166°14′
1200	49°07′	178°37′	72°42′	181°44′	49°07′	184°24′	25°50′	181°23′
1300	47°11′	200°59′	68°20′	221°48′	46°04′	206°15′	24°04′	196°26′
1500	32°53′	235°58′	48°16′	259°49′	30°27′	239°22′	12°44′	222°53′
1800	0°37′	269°22′	14°38′	288°30′				
	sunrise 0600, sunset 1803 EST		sunrise 0425, sunset 1929 EST		sunrise 0544 sunset 1747 EST		sunrise 0717, sunset 1627 EST	

TABLE II: SOLAR POSITIONS, EQUINOXES AND SOLSTICES, CARACAS, VENEZUELA, (10°35′ N, 66°56′ W)

	Vernal Equinox March 20		Summer Solstice June 21		Autumnal Equinox September 23		Winter Solstice December 22	
Time	Altitude	Azimuth	Altitude	Azimuth	Altitude	Azimuth	Altitude	Azimuth
0700	13°22′	92°48′	17°59′	68°36′	17°08′	93°17′	10°05′	116°22′
0900	42°41′	100°13′	45°26′	67°14′	46°23′	101°20′	35°07′	128°45′
1100	70°31′	122°32′	70°52′	45°52′	73°36′	129°40′	53°18′	158°07′
1200	79°10′	172°56′	77°08′	359°22′	79°04′	193°04′	55°58′	181°33′
1300	72°40′	232°34′	70°39′	313°36′	69°37′	239°31′	52°34′	204°30′
1500	45°16′	258°57′	45°10′	292°42′	41°37′	260°16′	33°39′	232°22′
1700	16°00′	266°50′	17°43′	291°24′	12°16′	267°30′	08°24′	244°06′
1800	01°16′	269°41′	04°03′	293°06′				
	sunrise 0602, sunset 1804 EST		sunrise 0546, sunset 1749 EST		sunrise 0546, sunset 1749 EST		sunrise 0611, sunset 1737 EST	

TABLE III: SOLAR POSITIONS, NEW YORK CITY, (40°47′ N, 73°59′ W)

	August 19, 1995		August 31, 1995		September 30, 1995	
Time	Altitude	Azimuth	Altitude	Azimuth	Altitude	Azimuth
0700	19°41′	89°48′	17°40′	93°42′	12°02′	104°20′
0900	41°53′	112°17′	39°31′	116°51′	32°21′	128°21′
1100	59°09′	150°39′	55°34′	154°46′	45°14′	163°31′
1200	62°03′	180°09′	57°56′	181°40′	46°22′	185°01′
1300	59°04′	209°34′	54°56′	208°06′	43°18′	205°46′
1500	41°44′	247°46′	38°14′	244°42′	27°59′	237°52′
1800	08°10′	279°44′	4°52′	277°05′		
	sunrise 0510, sunset 1843 EST		sunrise 0522, sunset 1825 EST		sunrise 0551 sunset 1735 EST	

Another variable to be considered is albedo. Spectral albedo is the ratio of ground reflection to spectral radiation, a ratio of 1 indicating complete reflection. Spectral albedo generally decreases as wavelength decreases and varies with surface. Albedo for UV-B is about 10% for dry road concrete, 13 to 15% for bright sand, and up to 80% for snow; and albedo levels for UV-A are somewhat higher.[119,120]

The earth's surface is exposed to direct solar radiation, diffuse sky radiation from scattering, reflection from the surface or albedo, and back reflection of albedo by the atmosphere. Radiation transfer is a complex product of extraterrestrial spectral irradiance and wavelength-dependent transmission through the atmosphere. Dose to the eye thus may be affected by latitude, solar elevation, cloud cover, time of day, season, albedo and physical factors such as gaze position and squinting. These variables have been discussed in detail by Sliney.[121,124] Pupil size decreases with age, independent of gender, refraction, iris color, and illuminance level.[125] Some have speculated that by permitting the pupil to dilate, sunglasses might increase the exposure of the eye to harmful light, although ordinary sunglasses appear to offer adequate protection.[126,127]

The potential effect of ultraviolet light on human health has received more attention recently because ground-based and satellite measurements

have established that the ozone layer in the lower stratosphere has decreased, largely due to the emission of chlorine-containing compounds into the environment.[128-130] The three most important determinants of terrestrial ultraviolet exposure are solar elevation, total vertically integrated ozone, and cloud cover.[131] Ozone absorbs essentially all ultraviolet of wavelengths shorter than 295 nm and much in the range of 295 to 310 nm.[132] UV-B is the region of greatest sensitivity of many biological processes, probably because the peak response for DNA damage is between 300 and 310 nm. Damage falls off at shorter wavelengths due to fewer incident photons and decreases at longer wavelengths due to decreasing DNA absorption. It has been estimated that a 1% decrease in total ozone would increase UV-B by 1.7% to 2%.[133] The spectral dose rate, defined as the product of the biological action spectrum and suface spectral irradiance, varies with time of day, season, and latitude and is maximum at solar noon.[118] The daily dose for DNA damage is greatest for the tropics when the sun is directly overhead and at the summer solstice in the northern hemisphere, and total daily dose increases with decreasing latitude (Fig 3).

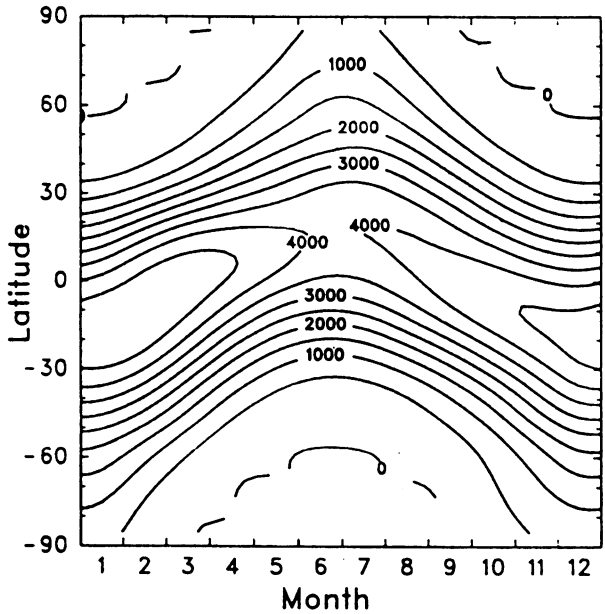

FIGURE 3

Relation of season and latitude to daily dose (J/m² per day) for DNA damage, assuming clear skies and ozone column averages from 1979 to 1989 (reproduced, with permission, from Madronich,[118] p25).

If increases of terrestrial ultraviolet exposure due to ozone loss do not exceed the normal fluctuation due to other factors such as cloud cover, the increase due to ozone loss may not be biologically significant.[130] A recent study combining satellite-based measurements of ozone and cloudiness to estimate ultraviolet radiation at the earth's surface suggests that in some parts of Europe, Central Asia, North America, and the southern hemisphere below 30°, summer levels of UVR already may exceed background cloud variability.[131]

Clinical effects probably would not be evident until after many years of elevated UVR levels. The incidence of cutaneous melanoma and basal and squamous cell carcinomas increases with decreasing latitude in Scandinavia, but no effect of decreasing ozone levels on the rate of cutaneous malignancy in Norway has been detected yet.[134] The greatest loss of ozone has occurred in the region of Antarctica where the return of sunlight in springtime results in depletion of ozone; UV-B levels there are substantially higher than a decade ago.[117] The biological implications of increasing UV-B radiation levels in Antarctica are not well understood, but one study recorded an inhibition of photosynthesis in Antarctic phytoplankton during periods of ozone depletion in 1990.[135] A recent study of animal and human populations of southern Chile and Argentina failed to reveal any acute adverse dermatologic or ocular effects of increased ambient ultraviolet-B exposure resulting from ozone depletion.[136]

PHYSICAL VARIABLES OF THE EYE

Transmission and Absorption

Interest in the effect of ultraviolet light on the eye is not new. In 1879 Soret[137] demonstrated that the aqueous and vitreous of bovine and sheep eyes transmitted ultraviolet wavelengths to at least 294 nm and that the lens absorbed wavelengths below about 383 nm. In 1912 Martin[138] showed that the rabbit cornea transmitted wavelengths longer than 295 nm but absorbed wavelengths shorter than 295 nm. The rabbit lens began to absorb at 400 nm and completely absorbed wavelengths below 350 nm. In 1915 Burge[139] reported that the pig cornea transmitted wavelengths as short as 297 nm and speculated that the higher incidence of cataract in the tropics might be due to greater ultraviolet exposure. Duke-Elder[140-141] studied the effect of UVR on the cornea and lens. In 1956 Bachem[142] determined that the wavelengths most damaging to the cornea and lens of guinea pigs and rabbits were 288 nm and 297 nm, respectively. In 1962 Boettner and Wolter[143] studied the transmission of the eye and confirmed that the aqueous transmitted all wavelengths between 220 and 2,400 nm; the cornea transmitted from 300 to 2500 nm, with 80% transmittance at

380 nm; and the lens absorbed below 390 nm with 90% transmittance at 450 nm. More recently, the spectral transmission of the human eye has been studied in 1-nm steps over the wavelengths 250 to 800 nm. The absorption of the aqueous was negligible. Various corneas showed 1% transmittance between 291 and 298 nm, and the lens showed 1% transmittance between 389 and 414 nm, except for a 7-month-old donor whose lenses had peaks of 10% and 3% at 317 nm.[144] With the reemergence of extracapsular cataract extraction, the protective role of the posterior capsule has been questioned. Keates and Murata[145,146] have shown that the lens capsule transmits more than 90% of incident ultraviolet light, and thus an intact posterior capsule does not shield the retina from ultraviolet.

Estimation of the potential absorption of ultraviolet by the lens is complicated by the change in transmission with age and by the dependency of absorption on wavelength.[107] In general, the absorption of both visible and ultraviolet light by the lens increases with age and decreasing wavelength.[147-150] Weale[148-150] studied absorption by lens homogenates over the range 327 to 700 nm and found a window of transmittance at 330 nm in young lenses but not in older lenses. As the absorption of potentially harmful radiation by the lens increases with age, the potential protection of the retina also increases.

Change in Refraction With Age

The growth and development of the lens have been reviewed in detail recently, and estimation of UVR dose to the lens is complicated by age-dependent changes in the eye.[151-154] In 1883 Smith[155] used a micrometer to document that the equatorial diameter of the lens increased from an average of 8.67 mm in the third decade of life to 9.62 mm in the ninth decade, and the average weight increased from 174 to 266 mg. In 1891 he reported significant individual variability in the dimensions of the cornea, but unlike the lens, it attained its full diameter within the first year of life.[156] Tscherning[157] also documented the variability of ocular dimensions, and initial measurements made on cadaveric eyes were incorporated into the textbooks of the early 20th century.[158-160] In 1946 Huggert[161] measured the lens optically and found that lens thickness increased from an average of 3.5 mm at age 10 to 4.3 mm at age 80; the cortex increased on average by 0.007 mm per year. With ultrasonography, Weekers and colleagues[162,163] estimated in 1973 that the lens grows sagittally by 0.023 mm per year. Using immersion ultrasonography, Hoffer[164] reported that the mean axial length of the human lens was 3.78 mm in the third decade and 5.03 mm in the 10th decade of life. The anterior lens capsule also increases in thickness with age.[165] Recently, ultrasonography has been used to document the

dimensions of the eyes of term and preterm infants.[166,167] With the Scheimpflug camera the optical density of the lens may be studied even more precisely.[168]

The mean refractive index of the corneal epithelium, anterior stromal surface, and posterior stromal surface differ,[169] and the refractive index of the lens also decreases from the center of the lens to the surface.[170] While the refractive indices of the cornea are relatively stable over time, the refractive gradient of the lens changes with age. It is not possible to consider all the potential variables of ocular and lens growth, and in the next section a standard eye model and computer ray tracing are used to study the patterns of light transmission by the cornea and lens.

ESTIMATION OF IRRADIANCE OF THE LENS BY RAY TRACING ANALYSIS

MATERIALS AND METHODS

Geometric optics and a standard eye model (Fig IV) were used to estimate irradiance of various regions of the human lens. The aspheric model of Lotmar was taken for the anterior corneal surface.[171] In the model both the pupil and the lens are centered, and the diameter of the pupil is defined as the diameter of the magnified image of the anatomic pupil. With an apparent magnification of 13%, an entrance pupil of 3.0 mm corresponds to a physical pupil of 2.66 mm, and an entrance pupil of 7.0 mm corresponds to an anatomic pupil of approximately 6.2 mm. The angle of incidence ø is defined as the angle between the direction of the sun and the optical axis of the eye.

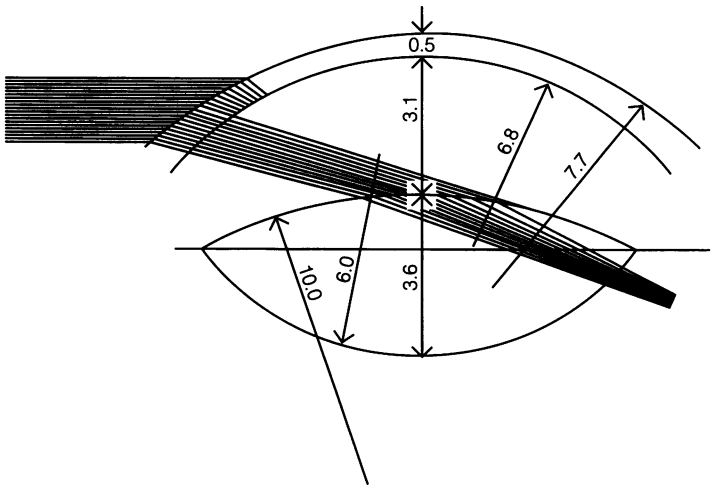

FIGURE 4
Dimensions of eye model used for ray tracing.

A number of simplifications have been made in the calculations. The sun has an angular diameter of 32 minutes of arc, but in the diagrams that follow, the relative size of the sun is so small that it is assumed to be a point source. The sky, reflected light from clouds, and reflection from the ground contribute to total irradiance, but with clear skies the sun is the brightest object in the sky. The contribution of reflected light to total irradiance is ignored in these calculations. Most important, irradiance is dependent on transmission, and transmission varies with tissue, age, wavelength and path through a tissue. Transmittance at a particular wavelength may be calculated when both path length and absorption coefficients are known:

$$T = e^{-al} \quad (1)$$

In equation 1, *a* is the absorption coefficient of the tissue of interest and l is the path length. Absorption of light by the lens is a complex function of wavelength, path through the lens, and age. The central part of the lens tends to become brunescent before such change is seen in the more peripheral cortex. Therefore, light passing along the visual axis may be attenuated differently than oblique light passing toward the periphery of the lens. Absorption tends to increase with age but may increase at different rates within the lens. If transmittance were known, irradiance then could be estimated more precisely as the product of transmittance and maximum irradiance. These complex variables have been ignored in order to determine maximum potential irradiance.

The relation of irradiance at sea level to solar wavelength and azimuth is shown in Fig V for a solar constant (total power measured at the earth's surface) of 1,322 W/m^2.[172] Spectral irradiance is a function of wavelength. To estimate power at a specific wavelength in Fig V, the value of E_λ or $[W/(m^2)(\text{Angstrom})]$ is read from the appropriate curve and multiplied by bandwidth. For example, for wavelength 400 nm (or 0.40 μm) and a zenith angle of 0° (sun directly overhead), the power of a 40-nm (or 400 angstrom) bandwidth may be estimated as:

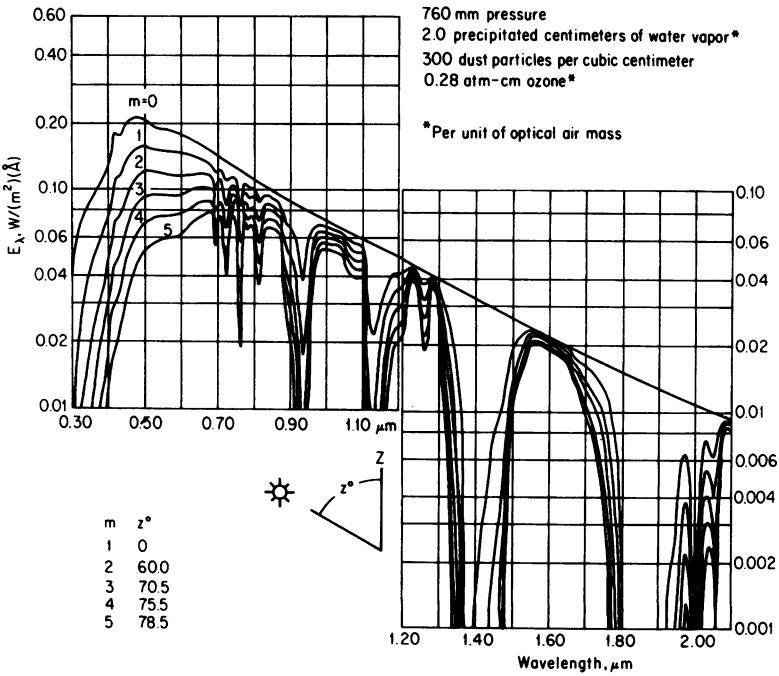

FIGURE 5
Solar spectral irradiance curves at sea level for various optical air masses. Value of solar constant is 1,322 W/m² (reproduced, with permission, from Zissis and Larocca[172]).

(2) $P=E_\lambda$ x Bandwidth = 0.074 W/m² x 400= 29.6 W/m² = 0.0296 mW/mm²

To determine irradiance of a wide bandwidth, it may be necessary to divide it into smaller intervals. In this section a constant bandwidth of 40 nm is assumed. Irradiance also is dependent on solar azimuth relative to zenith. For a wavelength of 320 nm, Fig V shows irradiance only for zenith angles of 0° and 60° (or solar elevation angles of 90° and 30°). To obtain irradiance for intermediate angles, the data from Fig V were replotted on a larger scale. More data points are available for 400 nm for solar elevation angles of 0° to 78°, and these were plotted as a guide for the curve for 320 nm. An additional point for a solar elevation angle of 15° was taken from another source to help to complete the curve for 320 nm. These data were recorded at Golden, Colo, and are therefore somewhat higher than sea level values.[173] The curve for 320 nm was constructed with considerable care, but the irradiance values are estimates. When more precise data for specific wavelengths and solar elevations are available, they can be substi-

tuted in the calculations of irradiance of the lens.

To estimate irradiance at the plane of the posterior capsule, ray tracing software (OSLO [Optical System Layout and Optimization], Sinclair Optics, Fairport, NY) was used to generate diagrams showing the pattern of light within the eye (Figs 6 through 19). The diagrams do not show rays that are blocked by the limbus or the iris or that miss the anterior surface of the lens. Prior to entering the eye, the arrangement of light rays is regular, and the rays are spaced evenly 0.1 mm apart. Using the equation shown previously, the power in a cross section of 0.01 mm^2 may be estimated as:

(3) $p = 0.01\ mm^2 \times 0.0296\ mW/mm^2 = 0.000296\ mw = 0.296\ \mu W$

As the angle of incidence increases, fewer rays enter the pupil, and they become more concentrated. In the model, the greatest angle at which a single light ray enters the lens is approximately 97.5° for the 3-mm pupil and 98° for the 7-mm pupil. Spot diagrams for angles of incidence of 0° to 97° illustrate the pattern of a light bundle at the plane of the pupil, at the equator of the lens, and at a plane perpendicular to the path of light at the posterior capsule (Figs 6 through 19, diagrams A,B, and C).

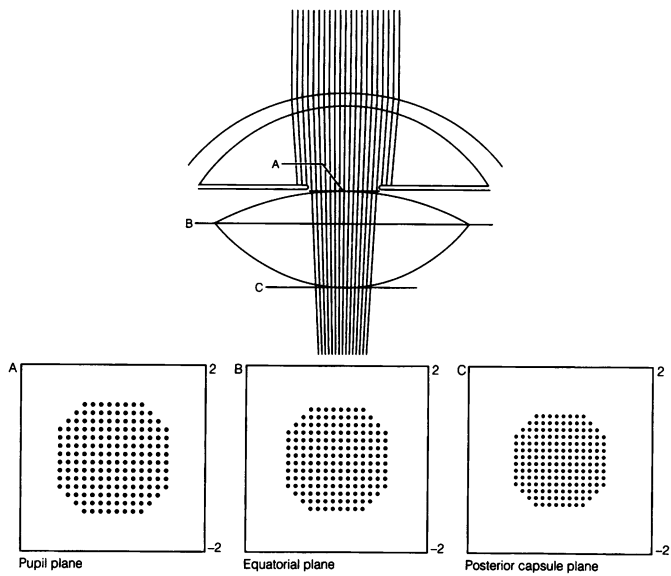

FIGURE 6
Ray tracing and spot diagrams for 3-mm pupil and 0° angle of incidence, 320-nm wavelength.

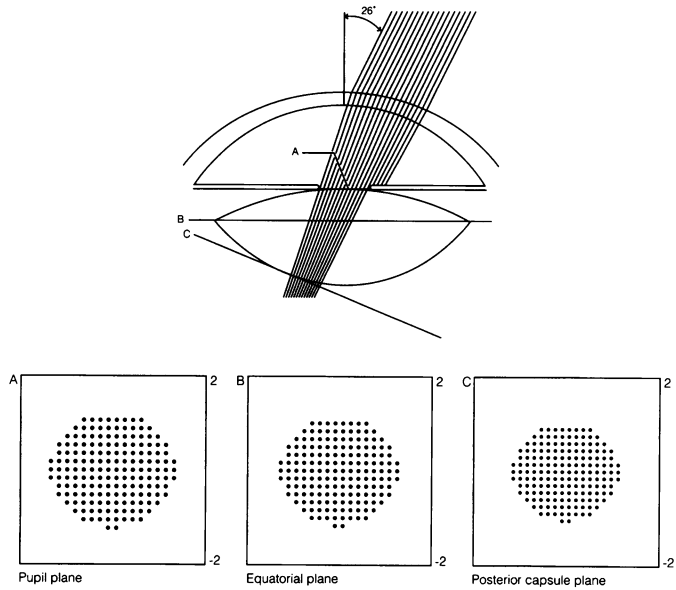

FIGURE 7

Ray tracing and spot diagrams for 3-mm pupil and 26° angle of incidence, 320-nm wavelength.

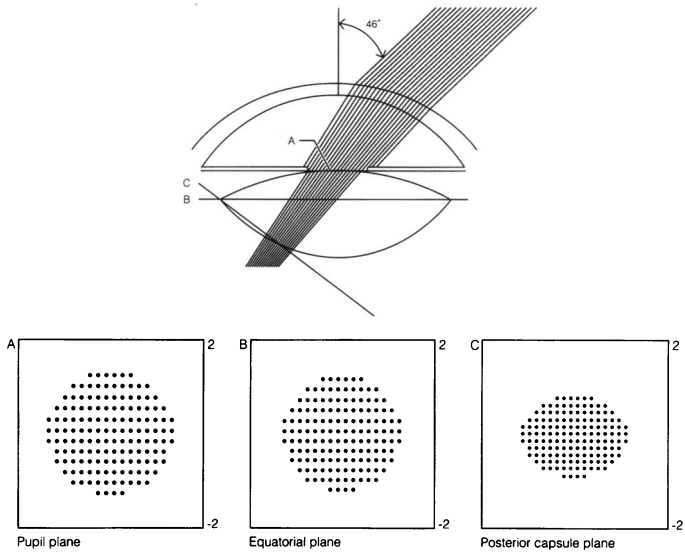

FIGURE 8

Ray tracing and spot diagrams for 3-mm pupil and 46° angle of incidence, 320-nm wavelength.

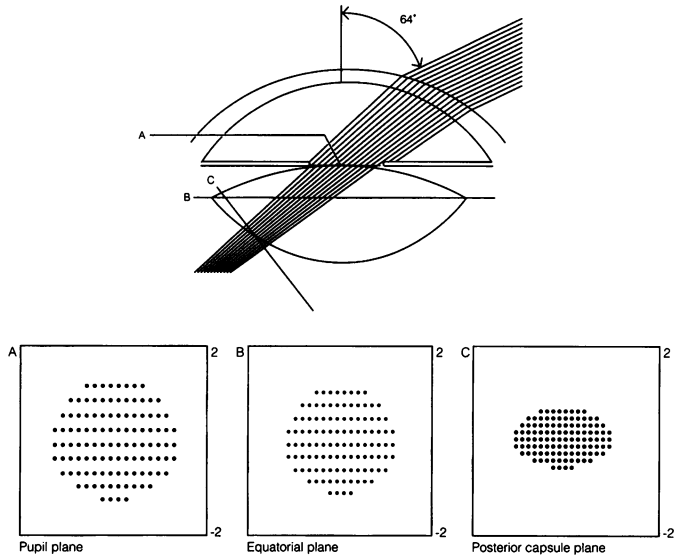

FIGURE 9

Ray tracing and spot diagrams for 3-mm pupil and 64° angle of incidence, 320-nm wavelength.

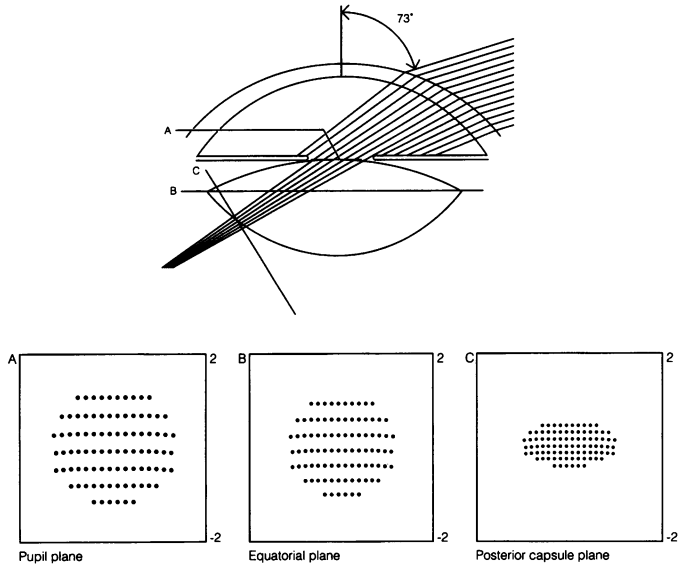

FIGURE 10

Ray tracing and spot diagrams for 3-mm pupil and 73° angle of incidence, 320-nm wavelength.

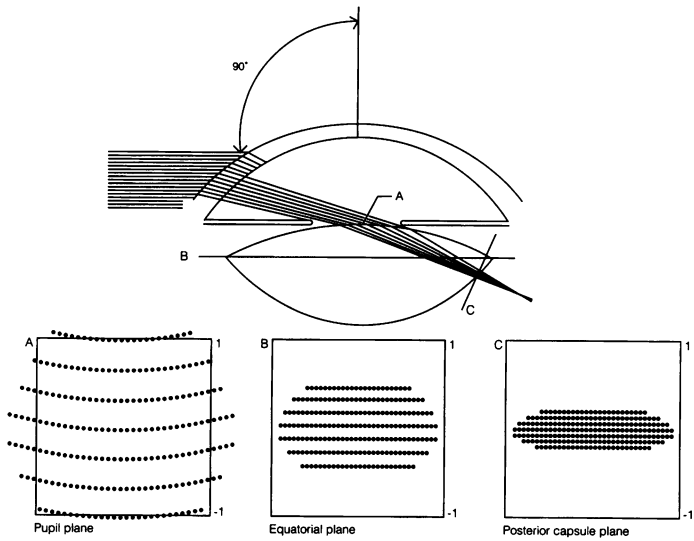

FIGURE 11

Ray tracing and spot diagrams for 3-mm pupil and 90° angle of incidence, 320-nm wavelength.

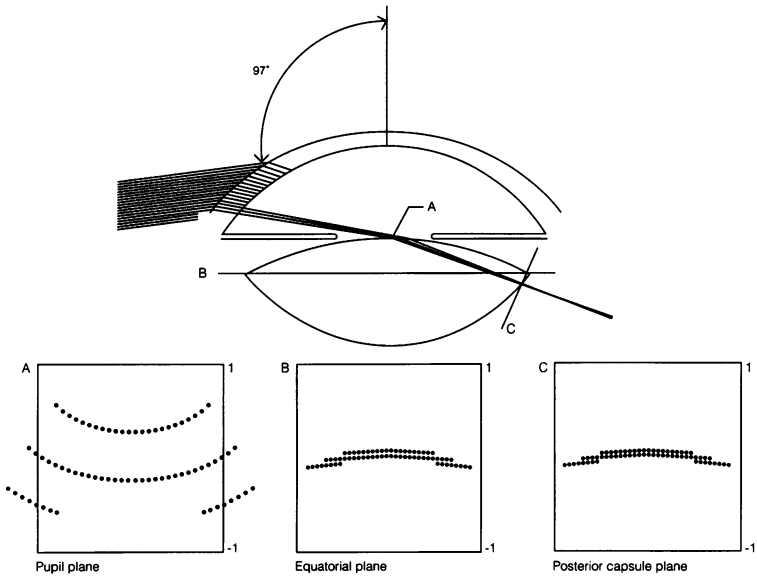

FIGURE 12

Ray tracing and spot diagrams for 3-mm pupil and 97° angle of incidence, 320-nm wavelength.

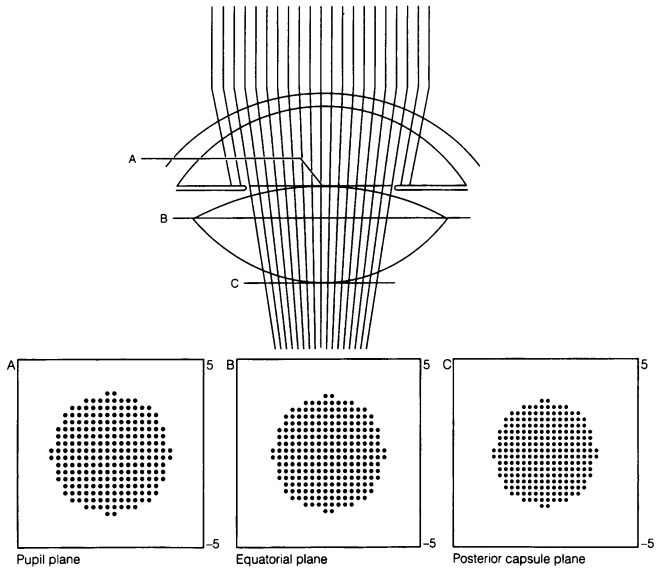

FIGURE 13
Ray tracing and spot diagrams for 7-mm pupil and 0° angle of incidence, 320-nm wavelength.

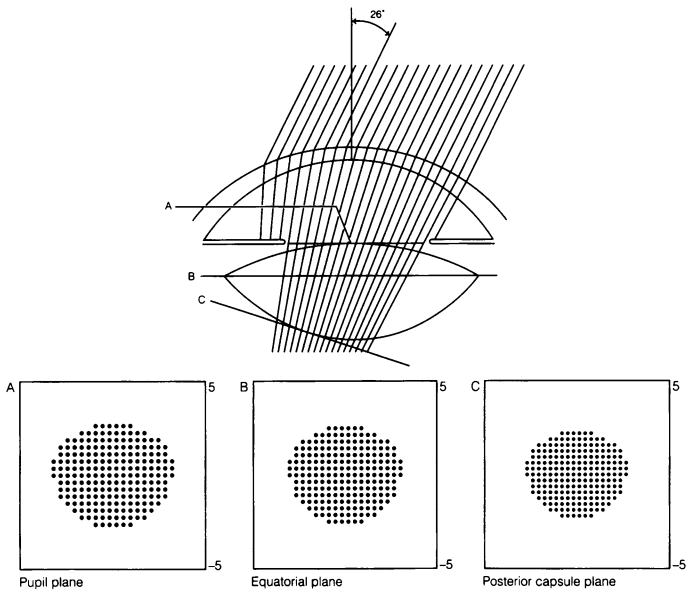

FIGURE 14
Ray tracing and spot diagrams for 7-mm pupil and 26° angle of incidence, 320-nm wavelength.

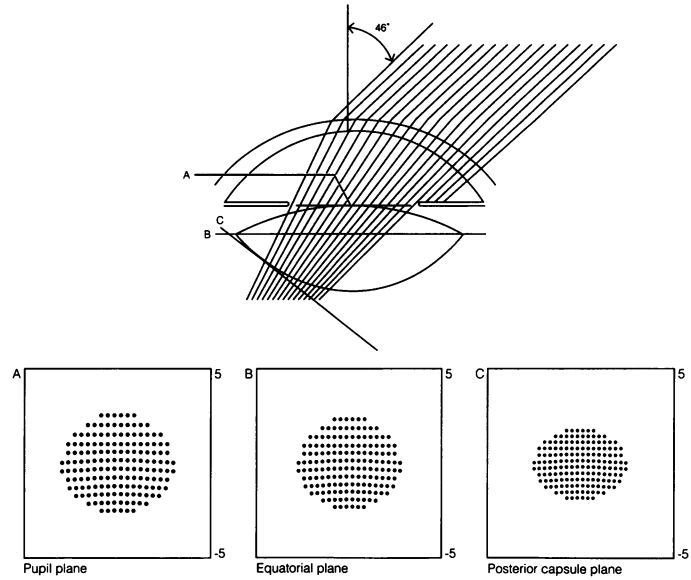

FIGURE 15

Ray tracing and spot diagrams for 7-mm pupil and 46° angle of incidence, 320-nm wavelength.

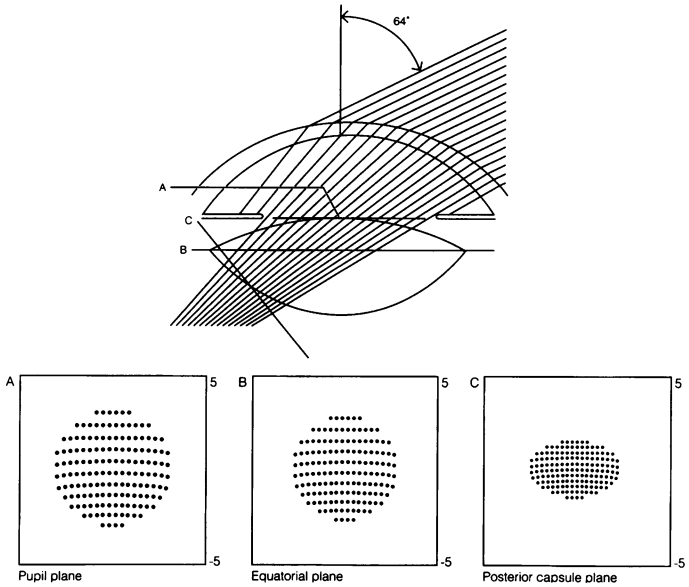

FIGURE 16

Ray tracing and spot diagrams for 7-mm pupil and 64° angle of incidence, 320-nm wavelength.

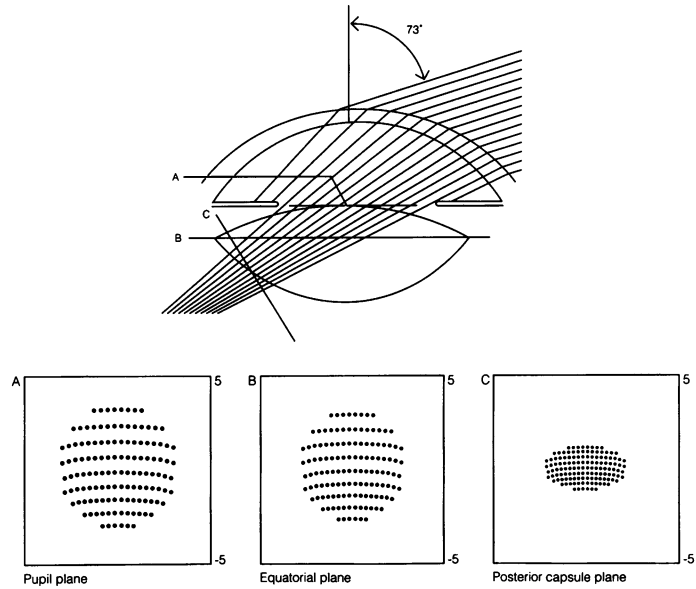

FIGURE 17

Ray tracing and spot diagrams for 7-mm pupil and 73° angle of incidence, 320-nm wavelength.

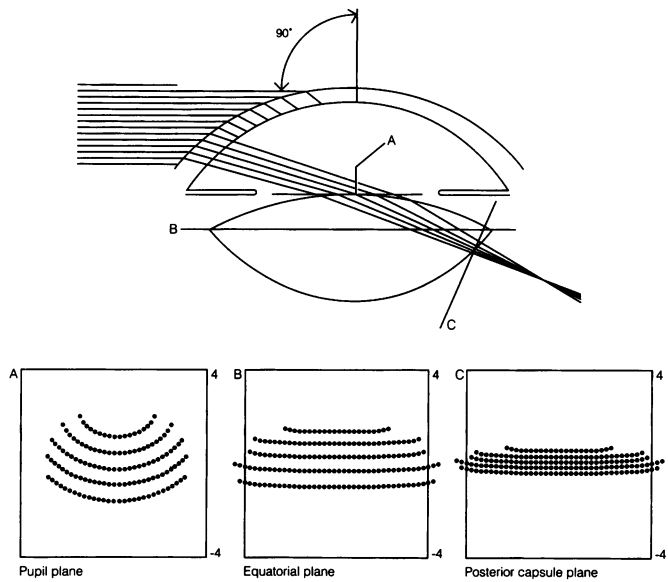

FIGURE 18

Ray tracing and spot diagrams for 7-mm pupil and 90° angle of incidence, 320-nm wavelength.

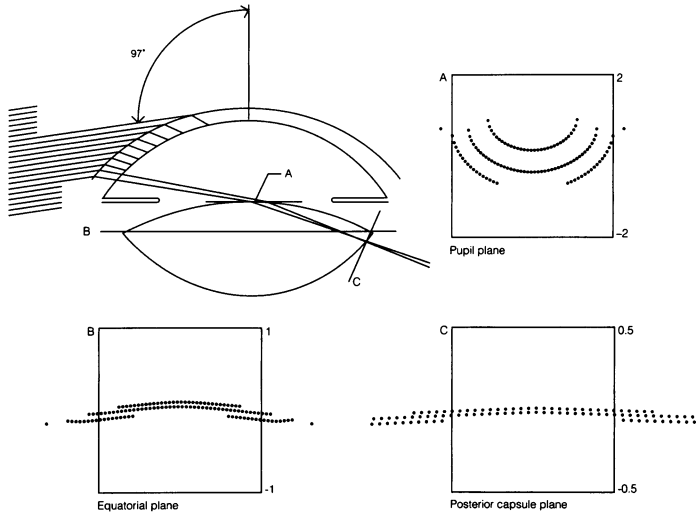

FIGURE 19
Ray tracing and spot diagrams for 7-mm pupil and 97° angle of incidence, 320-nm wavelength.

Assuming no loss of power from absorption or internal reflection, each ray retains within the eye the power that it had on entering the eye. In the center of the astigmatic image at the posterior capsule, the spacing of the rays is relatively regular and can be measured (Δx and Δy). The irradiance in the area occupied by one ray of wavelength λ is:

$$(4) \qquad \text{Irradiance}_{\lambda} = p/(\Delta x)(\Delta y).$$

At oblique angles of incidence the pupil is effectively narrowed along the axis of the direction of gaze, and diffraction in that direction will be increased. The effect of diffraction was estimated for the maximum angle in these calculations, 69° from the optical axis. The diffraction half angle from maximum to first minimum is 1.4 minutes of arc, which corresponds to a distance of only 0.0025 mm at the plane of the posterior capsule. This is significantly smaller than the estimated radius of the image of the sun. Diffraction therefore may be ignored in the center of the pattern; it will lead to a decrease in irradiance at the edge of the image.

Irradiance at the posterior capsule was estimated for fixed solar elevation of 90° and for varying solar elevation. A wavelength of 320 nm and a

bandwidth of 40 nm were used in all calculations. First, sun elevation was kept constant and maximum (zenith angle 0° in Fig 5) to illustrate the maximum irradiance that might occur as the angle of incidence varies (Table IV). For instance, an angle of 90° might occur if one were lying on one's side on a tropical beach and looking toward the horizon with the sun directly overhead.

Second, head position was kept constant with gaze toward the horizon in the direction of the sun, and the elevation of the sun was varied (Table V) to illustrate the change in irradiance over the course of a day as well as seasonal change in maximum potential irradiance. The angles in Table V were chosen to demonstrate the effect of:

90° - Sun directly overhead
73° - Elevation of the sun at noon in New York City on June 21
64° - Maximum angle at which rays clear the brow of the model skull, enter the model eye, and fill a 7-mm pupil
46° - Altitude of the sun over New York City at noon on September 30
26° - Altitude of the sun over New York City at noon on December 15
0° - Setting sun

Note that for elevation of 0°, the energy is too low to read a reliable E_λ from Fig 5.

The calculations for constant maximum irradiance and varying angle of incidence are summarized in Table IV, and those for constant gaze position and varying solar elevation are summarized in Table V. The value of irradiance in column C was taken from Fig 5. Incident power P (column D) is the product of a 40-nm bandwidth and the solar irradiance. The spacing of rays outside the eye is shown in column E. Columns F and G list the spacing between rays in the x and y directions at the plane of the posterior capsule measured on the spot diagrams. These values may be converted to millimeters within the eye by dividing by 31 (scale of one on the spot diagram is 31 mm) and multiplying by the scale of the diagram. The area associated with one ray in the image (column H) then was estimated by multiplying Δx and Δy, adjusted for scale:

$$(5)\ \text{Ray Area} = (\text{Scale})(\Delta x/31) \times (\text{Scale})(\Delta y/31) = (\text{Scale})^2(\Delta x)(\Delta y)/961$$

The power per ray (column I) is the product of incident power per square millimeter (column D) and area associated with each ray (column H). Column J lists the number of rays entering the lens for each angle of incidence. Total power in column K is the product of the number of rays and the power per ray (columns I and J). Maximum irradiance (column L) is the power per ray (column I) divided by the area per ray (column H) at

TABLE IV: ESTIMATION OF IRRADIANCE FOR SUN AT ZENITH, WAVELENGTH 320 NM, BANDWIDTH 40 NM

A	B	C	D	E	F	G	H	I	J	K	L	M	N
PUPIL	ANGLE OF SUN	IRRADIANCE ($\mu W/mm^2/Å$)	INCIDENT POWER (mW/mm^2)	RAY SPACING mm	ΔX (mm)	ΔY (mm)	RAY AREA (mm^2)	POWER PER RAY (MW)	RAYS	TOTAL POWER (MW)	IRRADIANCE (MW/mm^2)	CONCENTRATION ($E^2/_H$)	LENS PATH (mm)
3.0*	0°	0.0257	0.01028	0.2ᵛ	2.32	2.35	0.02269	0.0004112	172	0.071	0.0181	1.76	3.6
3.0*	26°	0.0257	0.01028	0.2ᵛ	2.27	2.30	0.02173	0.0004112	166	0.068	0.0189	1.84	3.65
3.0*	46°	0.0257	0.01028	0.2ᵛ	2.16	2.30	0.02068	0.0004112	144	0.059	0.0199	1.93	3.9
3.0*	64°	0.0257	0.01028	0.2ᵗ	4.00	4.50	0.01873	0.0004112	110	0.045	0.022	2.14	4.15
3.0*	73°	0.0257	0.01028	0.2ᵛ	1.94	2.26	0.01825	0.0004112	90	0.037	0.0225	2.19	4.2
3.0*	90°	0.0257	0.01028	0.1ᵗ	1.67	1.74	0.00302	0.0001028	204	0.021	0.034	3.31	4.6
3.0*	97°	0.0257	0.01028	0.1ᵗ	1.52	0.60	0.00095	0.0001028	72	0.007	0.108	10.54	4.25
7.0†	0°	0.0257	0.01028	0.4ⁿ	1.90	1.88	0.09292	0.0016448	232	0.382	0.0177	1.72	3.6
7.0†	26°	0.0257	0.01028	0.4ⁿ	1.84	1.88	0.08999	0.0016448	206	0.339	0.0183	1.78	3.65
7.0†	46°	0.0257	0.01028	0.4ⁿ	1.73	1.86	0.08371	0.0016448	160	0.263	0.0196	1.91	3.9
7.0†	64°	0.0257	0.01028	0.4ⁿ	1.58	1.80	0.07399	0.0016448	150	0.247	0.0222	2.16	4.15
7.0†	73°	0.0257	0.01028	0.4ⁿ	1.50	1.84	0.07180	0.0016448	128	0.211	0.0229	2.23	4.2
7.0†	90°	0.0257	0.01028	0.2ᵛ	1.68	1.6	0.01119	0.0004112	172	0.071	0.037	3.57	4.4
7.0†	97°	0.0257	0.01028	0.1ᵛ	3.3	1.2	0.00103	0.0001028	66	0.007	0.100	9.71	4.2

*APPARENT PUPIL DIAMETR (ANANTOMIC DIAMETER, 2.66 MM).

†APPARENT PUPIL DIAMETER (ANATOMIC DIAMETER, 6.2 MM).

ᵛSCALE ON PLOT, 2 MM.

ᵗSCALE ON PLOT, 1MM.

ⁿSCALE ON PLOT, 5 MM.

ᵛSCALE ON PLOT, 0.5 MM.

TABLE V: ESTIMATION OF IRRADIANCE, VARYING SOLAR ELEVATION, WAVELENGTH 320 NM, BANDWIDTH 40 NM

A	B	C	D	E	F	G	H	I	J	K	L	M	N
PUPIL	ANGLE OF SUN	IRRADIANCE ($\mu W/mm^2/Å$)	INCIDENT POWER (mW/mm^2)	RAY SPACING (mm)	ΔX (mm)	ΔY (mm)	RAY AREA (mm^2)	POWER PER RAY (mW)	RAYS	TOTAL POWER (mW)	IRRADIANCE (mW/mm^2)	CONCENTRATION ($E^2/_H$)	LENS PATH (mm)
3.0*	0°	NEGLIGIBLE		0.2[v]	2.32	2.35	0.02269		172			1.76	3.6
3.0*	26°	0.0082	0.000328	0.2[v]	2.27	2.30	0.02173	0.0001312	166	0.0218	0.006	1.84	3.65
3.0*	46°	0.017	0.0068	0.2[v]	2.16	2.30	0.02068	0.000272	144	0.0392	0.0132	1.93	3.9
3.0*	64°	0.021	0.0084	0.2[v]	4.00	4.50	0.01873	0.000336	110	0.0370	0.0179	2.14	4.15
3.0*	73°	0.0224	0.00896	0.2[v]	1.94	2.26	0.01825	0.0003584	90	0.0323	0.0196	2.19	4.2
3.0*	90°	0.0257	0.01028	0.1[i]	1.67	1.74	0.00302	0.0001028	204	0.0210	0.034	3.31	4.6
7.0[!]	0°	NEGLIGIBLE		0.4[n]	1.9	1.88	0.09292		232			1.72	3.6
7.0[!]	26°	0.0082	0.000328	0.4[n]	1.84	1.88	0.08999	0.0005248	206	0.108	0.0058	1.78	3.65
7.0[!]	46°	0.017	0.0068	0.4[n]	1.73	1.86	0.08371	0.001088	160	0.174	0.013	1.91	3.9
7.0[!]	64°	0.021	0.0084	0.4[n]	1.58	1.80	0.07399	0.001344	150	0.202	0.0182	2.16	4.15
7.0[!]	73°	0.0224	0.00896	0.4[n]	1.5	1.84	0.07180	0.0014336	128	0.184	0.01997	2.23	4.2
70.[!]	90°	0.0257	0.01028	0.2[v]	1.68	1.6	0.01119	0.0004112	172	0.071	0.037	3.57	4.4

*APPARENT PUPIL DIAMETER (ANANTOMIC DIAMETER, 2.66 MM).

[!]APPARENT PUPIL DIAMETER (ANATOMIC DIAMETER, 6.2 MM).

[v]SCALE ON PLOT, 2 MM.

[i]SCALE ON PLOT, 1MM.

[n]SCALE ON PLOT, 5 MM.

the plane of the posterior capsule. Concentration (column M) is the ratio of ray area incident on the cornea (square of value in column E) to ray area at the plane of the posterior capsule (column H). Assuming no absorption within the eye, the concentration is independent of bandwidth and compares irradiance at the level of the tissue of interest with that of the surface. The average length of the path of light rays within the lens is listed in column N.

RESULTS

As the angle of incidence increases, the concentration of light rays for all pupil diameters increases (Figs 6 through 19), resulting in an increase in maximum irradiance (Tables IV and V), but the size of the ray bundle reaching the lens decreases. When the sun is at its zenith, total power therefore is greatest when maximum irradiance is least, and total power increases with pupil size (Table IV, Figs 20 and 21).

When sun elevation varies, the relationship between total power and angle of incidence is affected by pupil size and progressive attenuation of energy by the atmosphere as solar elevation decreases (Table V). With a 3-mm pupil, total power is greatest when the sun is approximately 40° to 50° above the horizon (Fig 22). With a 7-mm pupil, maximum total power is seen when the sun is approximately 60° to 70° above the horizon (Fig 23).

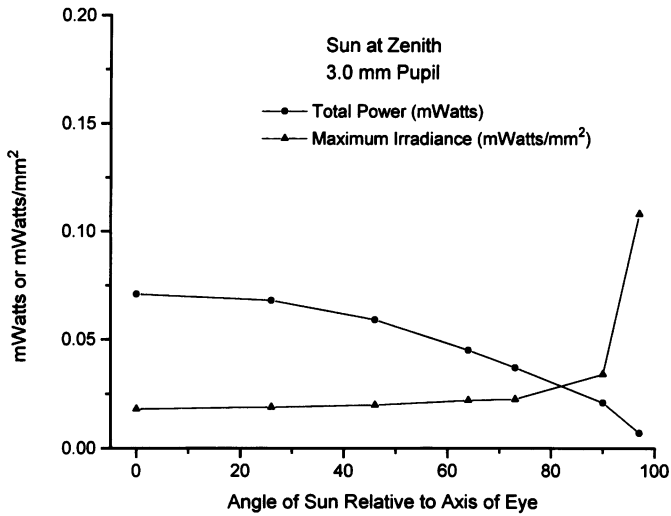

FIGURE 20

Relationship of total power and maximum potential irradiance at plane of posterior capsule for sun directly overhead and pupil diameter of 3-mm.

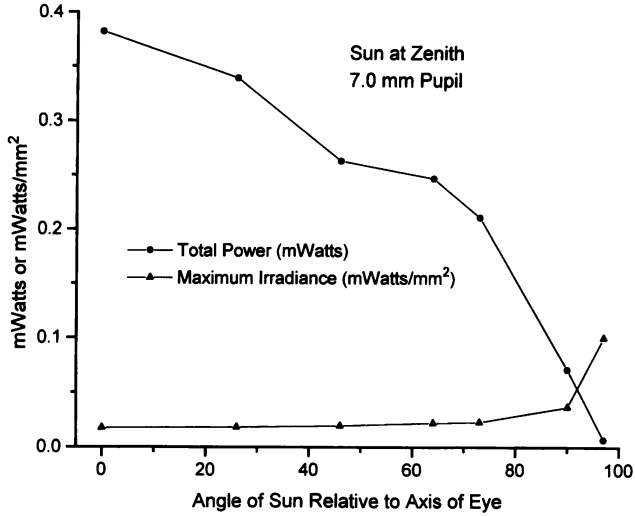

FIGURE 21

Relationship of total power and maximum potential irradiance at plane of posterior capsule for sun directly overhead and pupil diameter of 7-mm.

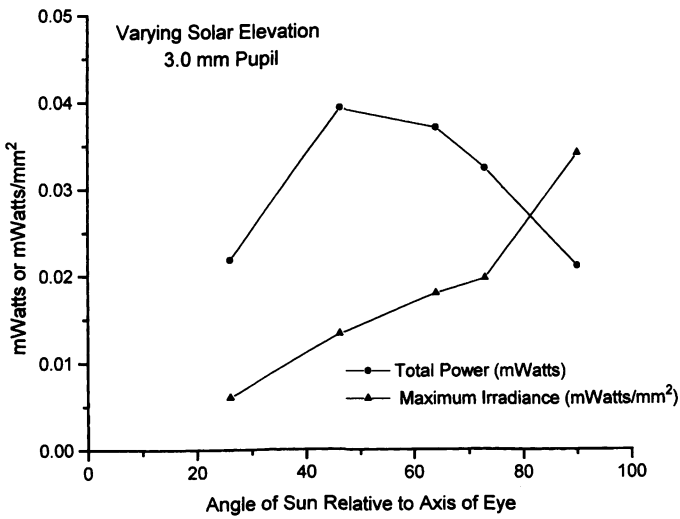

FIGURE 22

Relationship of total power and maximum potential irradiance at plane of posterior capsule for varying solar elevation and pupil diameter of 3-mm.

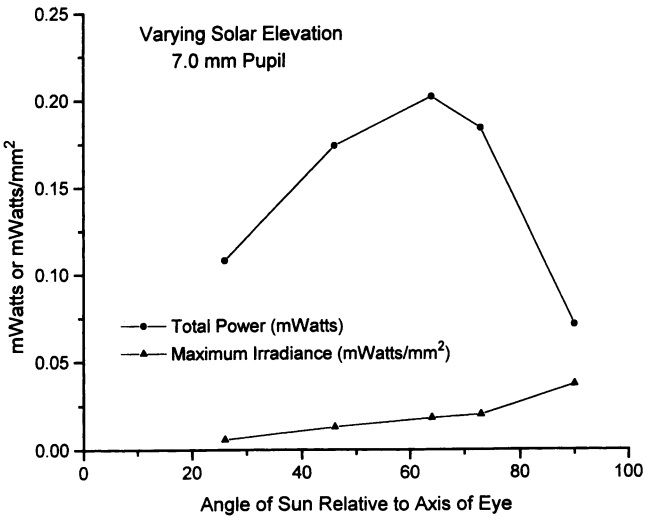

FIGURE 23

Relationship of total power and maximum potential irradiance at plane of posterior capsule for varying solar elevation and 7-mm pupil.

Estimates of maximum potential irradiance and total power were made for a limited number of angles of incidence and solar elevations; and with more data a more precise relationship between these parameters could be made. It is evident, however, that with fixed gaze toward the horizon, enlargement of the pupil permits more light of stronger energy to enter the lens. Normally, the brow blocks direct exposure of the eye and lens for high solar elevations. In the model described in the next section, the brow cut off at least part of direct radiation of the eye for solar angles greater than 64°. The precise "cutoff" for an individual depends on the shape of the orbit and nose, position of the globe within the orbit, position of the lid, curvature of the cornea, depth of the anterior chamber, and anterior radius of curvature of the lens. Detailed consideration of all these factors is beyond the scope of this analysis. It is evident, however, that for high solar elevations less direct light energy reaches the lens than is shown in Tables IV and V and Figs 20 through 23.

Another factor to be considered is time of exposure. The position of the areas on the posterior capsule irradiated by a point source at various angles of incidence is shown in Fig 24. Their position, size, and shape are approximately those that a viewer looking through the cornea and pupil

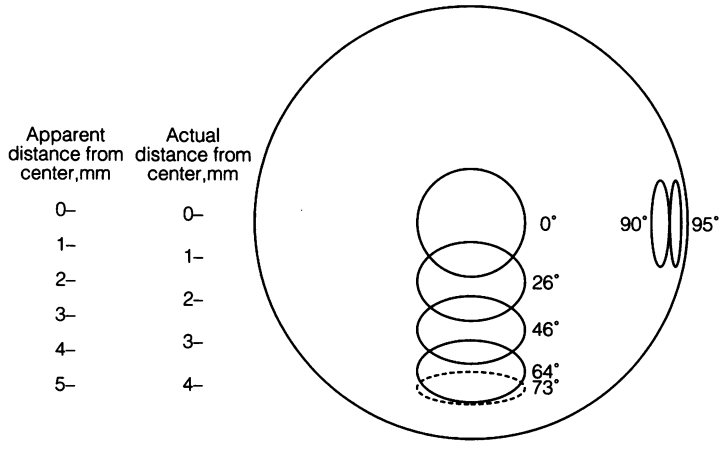

FIGURE 24

Front view of location, size, and shape of irradiated areas on posterior capsule for various solar elevations with 3-mm pupil. Compared with spot diagrams, ellipses are slightly shortened in radial direction owing to curvature of posterior capsule surface.

would observe. For angles of 0° to 73°, the sun is assumed to be straight ahead, and the individual is assumed to be erect. The ellipse for 73° is dashed to indicate that the eye would have to occupy a more forward position within the orbit than the model eye for direct sun to clear the brow. The highest sun elevation that permits a full bundle of rays to clear the brow of the skull used in the experiments is 64°. At even higher angles of 90° or 95°, the ellipse is shown in the midperiphery to suggest that the direction of the sun is approximately normal to the temple to permit light at these angles to enter the lens, although with movement of the eye or head relative to the sun, the angle of incidence may be greater than the solar elevation angle. Two scales are indicated on Fig 24. One shows actual distance from the center of the lens on the posterior capsule The other gives apparent distance and corrects for the approximately 25% magnification produced by the cornea and anterior surface of the lens. This scale reflects the distance a clinician might measure when viewing an opacity in the lens.

As the eye and head move from side to side, the angle between the axis of the eye and the sun may increase for constant solar elevation. The position and shape of the irradiated area will change and move away from the vertical meridian along a spiral path. When the solar elevation is 46°, the ellipse "A" in Fig 25 shows the shape and position of the irradiated area when the eye is looking toward the horizon in the direction of the sun.

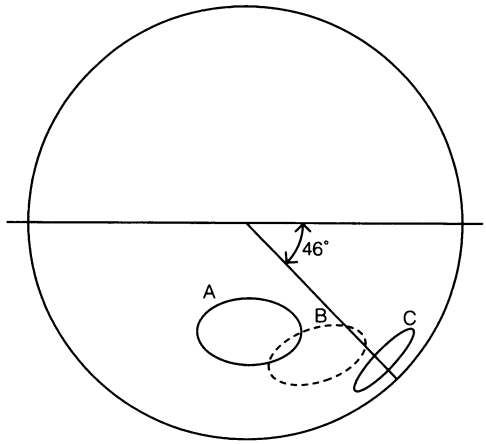

FIGURE 25

Movement of irradiated area on posterior capsule as head and eye direction change with solar elevation of 46°. A, Eye looks toward horizon in direction of sun. B, Eye has turned about 45° but still is fixated on horizon. C, Eye still is fixated on horizon but has turned about 90° to direction of sun. Light is incident on cornea at angle of 90° relative to axis of eye, forming quasi-astigmatic image at angle of 46° from center of lens.

Ellipse "C" is formed when the eye and head have turned 90° about the vertical axis, and ellipse "B" indicates the area of irradiance for an intermediate position. It is evident that the angle of incidence is a function of both solar elevation and eye position; and as the eye moves, the area of maximum irradiance sweeps a path on the posterior capsule. The pattern should be symmetric on each side of the vertical meridian, unless light is blocked by the brow, nose, or lid. Individual anatomy varies, but in general the nose and superonasal brow block light more effectively than the temporal and superotemporal rim of the orbit. Ray tracing thus suggests that the inferior portion of the lens receives significantly more light energy than the superior portion and that the inferonasal lens should be exposed to more light than the inferotemporal lens. As solar elevation increases, the brow blocks progressively more direct light, and part or all of the predicted area of maximum irradiance may not be exposed.

The preceding discussion concerns small bright sources such as the sun, which produce astigmatic and poorly focused images with reduced irradiance relative to a well-focused image of the same source. In contrast, a uniform field such as a blue sky is focused as an image with uniform irradiance that is not reduced by aberration of the optical system. The energy contribution of such sources as blue sky or brightly illuminated clouds may

be biologically significant, but analysis of their contribution is beyond the scope of this discussion.

It may be of interest to compare the irradiance of the lens with that of the retina. When the eye is looking in the direction of the sun the power of a 40-nm wavelength band at 400 nm through a 3-mm pupil is:

$$(6) \qquad \left(\frac{\pi 3^2}{4}\right) \times 0.0296 \text{ mW/mm}^2 = 0.209 \text{ mW}$$

The area of the image of the sun on the retina is:

$$(7) \quad \pi d^2/4 = \pi[(\text{minutes of arc}/\text{minutes/degree}/\text{degrees/radian}) \times \text{focal length}]^2$$
$$= \pi[(32/60/57.3) \times 17.1]^2/4 = 0.020 \text{ mm}^2$$

The irradiance then is:

$$(8) \qquad J_\lambda = 0.209/0.020 = 10.45 \text{ mW/mm}^2$$

This suggests that the power density of a 40-nm bandwidth of wavelength 400 nm at the plane of the retina is approximately 580 times greater than that of a 40-nm bandwidth of wavelength 320 nm at the posterior capsule for angle of incidence of 0°(see Table IV). The power density at the plane of the retina is much greater than at the posterior capsule because a good image is formed on the retina. If the entire visible spectrum had been included, the power density would be about tenfold greater. The potential for tissue damage depends on many factors, including absorption. The relative potential for damage of 320 nm versus 400 nm is not known with certainty, but it is thought that the shorter wavelength has greater potential to injure tissue. It is evident from these ray tracing studies that the inferior lens and, by extension, the inferior retina receive more light energy than the upper pole of the lens or retina. This may be relevant to the observation that glaucoma frequently leads to loss of the upper visual field before the lower visual field.

In the next section models of the anterior eye and a human skull are used to study the pattern and intensity of light concentration in the eye under various daylight conditions.

MODELS OF THE ANTERIOR SEGMENT OF THE EYE

MATERIALS AND METHODS

The First Model

The first model simulated the refraction of the cornea alone (cornea model) (Fig 26). A standard plano 12.0-mm diameter polymethyl-

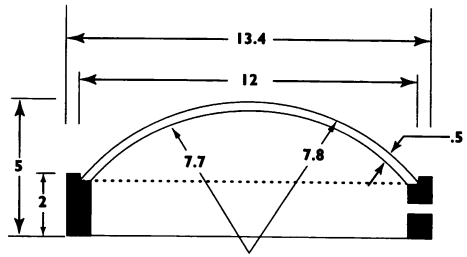

MODEL 1

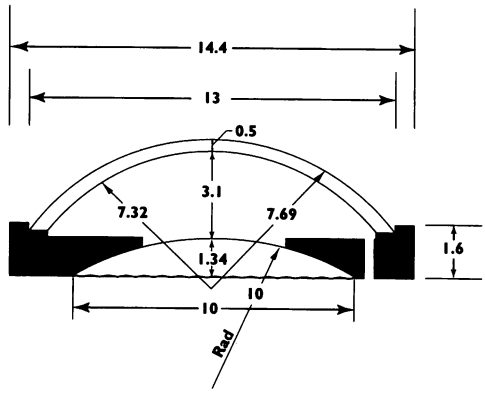

MODEL 2

FIGURE 26
Dimensions of first- and second- generation eye models. Dimensions in mm.

methacrylate (PMMA) contact lens of anterior and posterior radii of curvatures of 7.8 and 7.7 mm and uniform thickness of 0.5 mm was glued to a base of external diameter of 13.4 mm. The apex of the cornea was approximately 5.0 mm above a flat clear acrylic base. The model acted as a cutoff filter with 0% transmission at approximately 240 nm and 100% at 360 nm. The external surface of the clear circular sidewall was painted white to prevent light transmission. A single small hole in the side wall permitted the introduction of a 27-gauge cannula to fill the chamber with water (refractive index, 1.33) to simulate aqueous. This model and a disc of photosensitive paper (Gelatine Chloride Printing-out Paper, Chicago Albumen Works, Housatonic, MA 01236) were secured to a plastic cylindrical carrier, 14 mm wide and 15 mm long, with plastic tape. The carrier and model were supported by a moldable resin in the orbit of a human skull, used originally for radiation dosimetry, which was coated with a

mixture of paraffin and beeswax to simulate skin and subcutaneous tissue and approximate scatter from the skin.[174]

The initial model was useful to test the feasibility of modelling the path of light in the anterior segment but had limitations. The index of refraction of the PMMA cornea (1.473) differs from published figures for the index of refraction of the human cornea (1.377).[169] The model cornea has a uniform thickness of 0.5 mm, while the human cornea is approximately 0.6 mm centrally and nearly 1 mm thick peripherally. The plastic model also is spherical, while the human corneal diameter is greater horizontally than vertically. The model also did not transmit all wavelengths that the human cornea permits to reach the lens. Most significant, the model had no iris diaphragm or crystalline lens.

The Second Model

With ray tracing software (OSLO, Sinclair Optics, Fairport, NY) a second generation model was designed to model the anterior segment more closely. The second design included cornea, anterior chamber, iris diaphragm, and the anterior portion of the lens (Fig 26). The materials and surface curvatures were chosen to simulate the refraction of the human eye as closely as possible, and the radii of curvature of the anterior surface of the cornea and lens were chosen to match generally accepted norms for the human eye. Materials were used that transmit UV-B at least as well as the corresponding structures of the human eye. The human lens is biconvex, the posterior surface having a smaller radius of curvature than the anterior surface. Collecting and measuring light passing out the posterior curved surface of the lens poses particular problems. The photosensitive paper used in the initial experiments is suitable only with a flat transmitting surface. Other means of capturing light from a curved surface such as a fiberoptic field flattener or a CCD (charged coupled device) array were considered. While it is of interest to measure the flux of light through the whole lens, the apparatus to do this had limitations and added to the complexity and cost of the model.

To keep the model simple and portable, we chose to study the distribution of light at the equatorial plane of the lens (Fig 26). UV-grade fused silica with high transmittance to 200 nm was used to fabricate the cornea and crystalline lens with a surface quality of 60 to 40 (Twin State Optical, Keene, NH) (Fig 27). The high transmittance of short wavelengths means that the atmosphere alone determines the wavelengths to which the lens is exposed in this model, while in the human eye the cornea shields the lens from wavelengths below about 300 nm. However, this appears to simulate the exposure of the lens more closely than the original model.

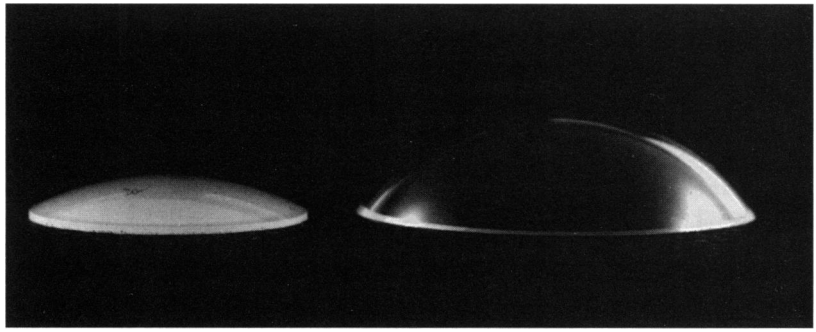

FIGURE 27
Model lens and cornea made from UV-grade silica. Plano back surface of model lens is rough-ground, making it appear more white than model cornea.

The index of refraction of fused silica (1.458) is closer to the indices of the human cornea and lens than many optical materials. The anterior radii of curvature of the model cornea and lens are 7.69 and 10.0 mm, respectively, as in the Helmholtz eye.[175] The posterior radius of curvature of the cornea (7.32 mm) was chosen so that the path of light rays in the anterior chamber approximates the path of light rays in the human eye, especially for high angles of incidence at the corneal surface. The corneal thickness is 0.5 mm centrally and slightly greater peripherally.

Because the refractive index of fused silica is higher than the human lens, the refraction of rays entering the model lens is greater than in the human lens. An anterior radius of curvature of the model lens might have been chosen to provide the same dioptric power as that of the human lens. This design would affect the distance at which rays are focused but would not alter significantly the refraction angle at which rays traverse the lens, as this angle depends primarily on the index of refraction. For very oblique angles of incidence the shape of the anterior lens affects the quantity of light rays captured by the lens. As it was considered important to try to model the contribution of oblique light to energy exposure, the model was designed to simulate the shape of the human lens as closely as possible. The posterior surface of the model lens is at the equatorial plane of the crystalline lens, based on the 10-mm anterior radius of curvature and a lens diameter of 10 mm. The central thickness of the model lens is 1.34 mm. The back surface was rough ground because computer ray tracings indicated that light passing through the pupil at high angles of incidence relative to the visual axis would be reflected by a polished rear surface. The coarse ground posterior surface of the model lens attenuated light trans-

mission. Therefore, the energy measured at the equatorial plane may be underestimated.

The corneal dome was glued to a black plastic base, with a peripheral lip of approximately 0.7-mm height to stabilize the cornea. The external lip and glue reduced the effective diameter of the model cornea from 13.0 to approximately 12.0 mm. The base has a round central aperture to simulate the pupil, and the convex-plano lens was glued to the base on the anterior periphery of the lens. Three models with fixed pupils of diameters of 2.5, 5.0, and 7.5 mm in air were made (Fig 28). The depth of the anterior chamber was kept constant at 3.1 mm centrally. A tiny hole on the posterior surface of the base at the edge of the lens permitted the introduction of a 30-gauge cannula to fill the chamber with water. This hole was sealed with a small piece of plastic tape. With the anterior chamber filled with water, the apparent pupil size is magnified by approximately 13%, resulting in apparent pupil sizes of 2.83, 5.65, and 8.48 mm. After several hours of continuous use, an air bubble often formed, and the anterior chamber was refilled as needed.

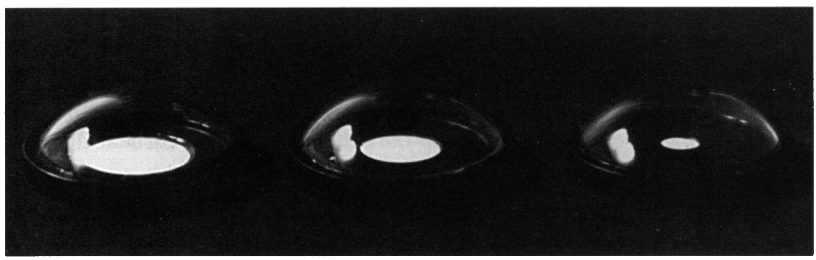

FIGURE 28
Second-generation eye models with pupil diameters in air of 7.5, 5.0, and 2.5 mm.

An aluminum cylindrical carrier with an external diameter of 16 mm and length of 18 mm was fabricated to support the model eyes (Fig 29). The anterior surface has a central recession with a diameter of 14.6 mm and depth of 1 mm. A central island of diameter 9 mm holds the photosensitive discs against the posterior surface of the lens of the model eye. A thin piece of adhesive tape was used to secure the model on the carrier. At the posterior end of the carrier, a 6-mm diameter screw projected approximately 9 mm. The screw fit a hole in the wax at the apex of the orbit and helped to stabilize the model in the orbit. The eye model was covered while the carrier and model were placed in the orbit.

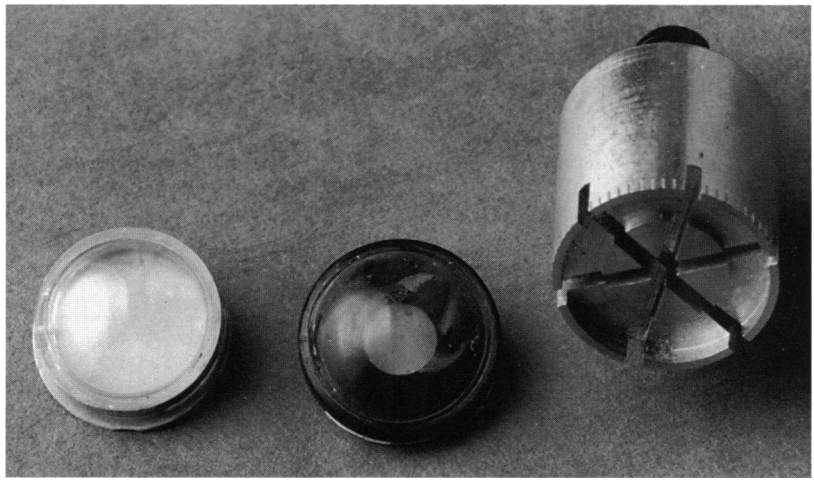

FIGURE 29
First- and second-generation eye models and aluminum carrier.

The Model Skull

From the medial to lateral rim, the margin of the orbit curves gently posteriorly. The most anterior projection of the superior orbital margin is approximately 6.25 mm anterior to the apex of the model cornea (Fig 30). The midpoint of the cornea is approximately 13 mm below the anterior projection of the superior rim and 10 mm below the overlying orbital roof. The maximum angle at which rays clear the brow of the model skull, enter the model eye, and fill a 7.0-mm pupil was calculated to be approximately 64°. The temporal rim of the orbit curves gently posteriorly and inferiorly, and the midtemporal rim is approximately 11 mm posterior to the apex of the cornea (Fig 31). At a base of 102 mm, the Hertel reading for the second-generation model in the left orbit was 13. The nasal superior orbital rim is slightly more prominent than the superior-temporal rim. The nasal bridge below the glabella is recessed relative to the brow and the lower portion of the nose. This portion of the bridge subtends an angle of about 20° from the apex of the cornea and is approximately 5 mm anterior to the corneal apex. The midline of the nose is about 30 mm from the midpoint of the cornea and 25 mm from the lateral orbital rim. (Fig 32).

Measurement of Ultraviolet

All experiments were performed on the roof of the Eye Institute (40°47′ N, 73°59′ W) at an elevation of approximately 200 ft above sea level. Ambient

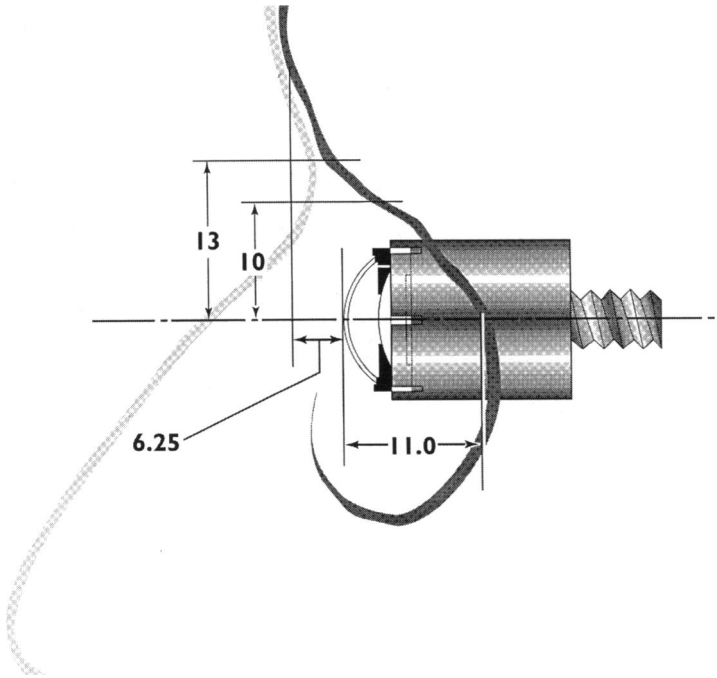

FIGURE 30
Relation of model cornea to brow of model skull. Dimensions in mm.

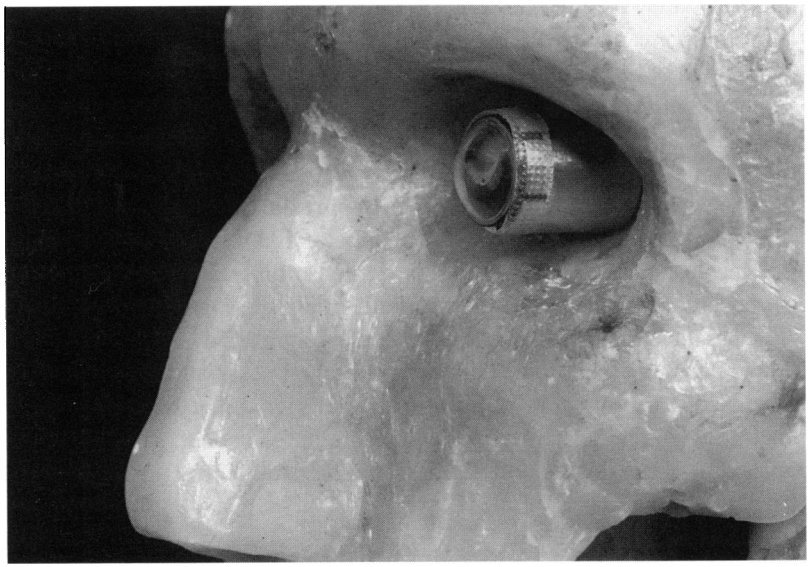

FIGURE 31
Lateral view of model eye and carrier in left orbit.

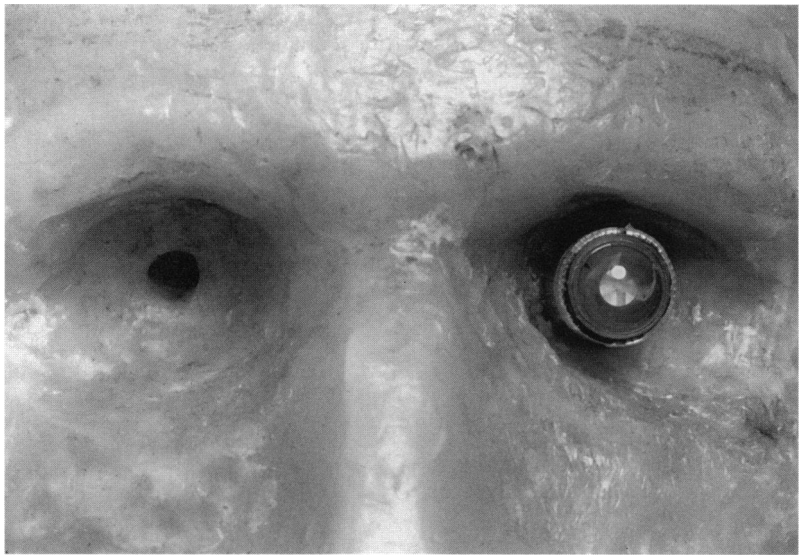

FIGURE 32
Model eye in left orbit. Center of cornea is approximately 30 mm from midline of nose and 25 mm from lateral orbital rim.

and cumulative UV-A (320 to 400 nm) and UV-B (290 to 320 nm) were measured simultaneously with the Personal Measurement Assistant (PMA) Model 2100 (Solar Light Co, Philadelphia, PA 19126-3342), which has an internal timer and records from two sensors simultaneously.[176] The UV-A and UV-B sensors attached to the PMA 2100 were placed on the concrete wall on the roof of the Eye Institute, next to the skull and eye model (Fig 33). The domed ultraviolet sensors thus looked up to the sky, while the eye model looked toward the horizon. In each series, the head and model were oriented with a compass to ensure uniform position.

According to the manufacturer, the photosensitive paper is maximally sensitive to ultraviolet and blue light. Exposure to light causes the off-white paper to become purple, and the color deepens with increasing dose. The intensity of color change of the discs is a function of energy, and the rate of color change varied with altitude of the sun and atmospheric conditions. Various exposure times were tested to obtain optimum contrast of color of the discs. In most cases an exposure of 2 minutes was adequate.

Because of the movement of the sun and momentary changes in atmospheric conditions, each exposed disc is unique. To prepare data for statistical comparison and to minimize the effect of brief changes in ambi-

FIGURE 33
Model eye in left orbit of skull next to UV-A and UV-B measuring devices on roof of Eye Institute.

ent lighting conditions, serial exposures were made in each study group. A series of four exposures of 2 minutes each with two eye models (eight discs) required approximately 25 minutes. In most series the pattern of exposure of the discs appeared uniform. At midday when the sun passed across the local meridian, the most intense concentration of light shifted from inferonasal to inferotemporal. The significance of this shift is discussed with the results.

To ensure uniform energy within each series, cumulative UV-A and UV-B energy were calculated for each series. Early and late in the day, when the energy of the sun changed relatively rapidly, it was difficult to obtain series of exposures of comparable energy. In nearly all cases the cumulative energy of compared series differs by less than 5%, and statistical comparison is not made if the cumulative UV-A or UV-B energy of compared series differs by more than 10%.

Data Acquisition and Analysis

A Scanjet 3C Scanner (Hewlett-Packard, Palo Alto, Calif) was used to scan exposed discs at 300 dpi and uniform acquisition parameters (black-and-white photo, brightness 125, contrast 125) to a personal computer with a

100-mHZ 486 microprocessor (Precision Computer, Fort Lee, NJ) and Windows 3.1 (Microsoft Corp, Redmond Wash). The color density of each disc was analyzed with image analysis software (Sigma Scan/Image, Jandel Scientific, San Rafael, Calif) which permits a number of techniques for analyzing image intensity. In initial experiments with the cornea model, the density of the digitized images was analyzed along two meridians normal to one another, inferonasal to superotemporal and inferotemporal to superonasal.[177] The pattern of exposure of discs with the second-generation model was different, and scanning along two axes at 90° to each other did not appear to be as useful. The images produced by the second-generation models were analyzed by sampling the intensity in each quadrant. For the small images produced by the 2.5-mm pupil, a 3x3 pixel cursor was used. For the images produced by the 5.0-mm pupil, a 5x5 round cursor was used, and for the images produced by the 7.5-mm pupil and the cornea model, a 7x7 round cursor was used. Generally, three or four discs were exposed in each group. A template was superimposed on each image to ensure consistent placement of the cursor. However, the images varied slightly in shape within each group, and judgment was used when the intensity of each image was sampled.

The system reports color intensity in gray scale units of 0 (exposed) to 250 (nonexposed). The off-white color of nonexposed paper registered about 220 U, while the deepest purple color produced by midday sun was about 50 U. Thus, as energy exposure increased, the intensity reading decreased. For each series, the mean and standard deviation of the gray scale readings of intensity from comparable locations in each disc were computed; and from these data, bar graphs were prepared (Origin 3.5, Microcal, Northampton, Mass). The *t*-test was used to assess the hypothesis that two means are different at the 95% confidence level.

The images of the discs were sampled in a counterclockwise direction, beginning in the superonasal quadrant. Hence, the order of the columns of the bar graphs is superonasal (1), superotemporal (2), inferotemporal (3), and inferonasal (4). The notch seen in each disc marks the 12-o'clock meridian. The areas sampled in each quadrant do not represent an integration of a complete quadrant, and the interpretation of the results of this sampling technique should be tempered by the pattern of exposure seen on the discs. In the Results and Discussion sections, the sampled areas in each quadrant may be referred to as the "samples," "sampled areas," "quadrants," or "areas."

Sunglasses

To attenuate light intensity and to test the effect of a temporal shield,

three pairs of sunglasses were compared under various conditions (Fig 34). The Hobie Woody has a standard black plastic frame with thin temple and is referred to as the standard or regular sunglasses. The Hobie Sportsman has a side shield made of the same material as the spectacle lens and is referred to as sport glasses. Hobie glasses were donated by the manufacturer (Hobie Sunglasses, San Clemente, CA 92673). UV Shield glasses (NoIR Medical Technologies, South Lyon, Mich) often are used after eye surgery, have a broad temple, and are referred to as wraparound glasses. During each experiment the sunglass frame was held as tightly against the forehead as the frame permitted.

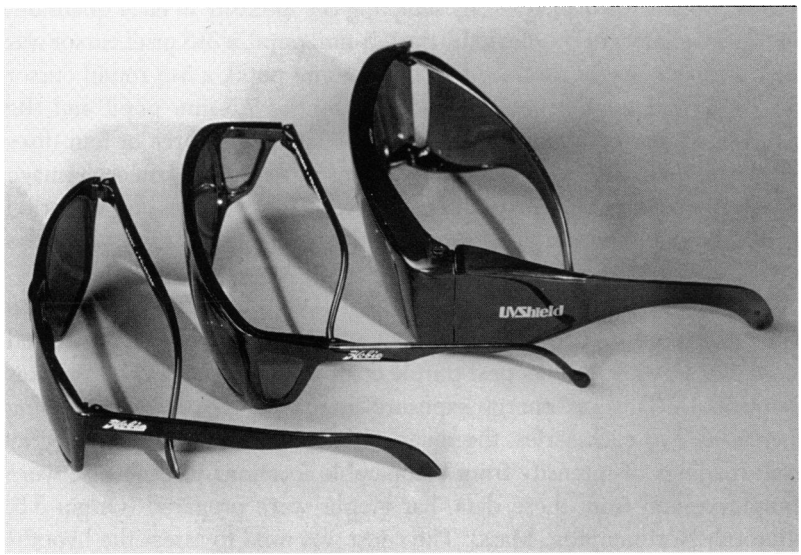

FIGURE 34
Three pairs of sunglasses used in studies with eye models.

The transmission spectra of all lenses and side shields were measured with a Varian DMS 100 Spectrophotometer. Transmission of all lenses was essentially identical and above about 415 nm was approximately 10% (Fig 35). The printouts from the spectrophotometer were scanned to the PC, and these images were digitized (UN-SCAN-IT 3.0 for Windows, Silk Scientific Corporation, Orem, Utah) for plotting and printing (Origin).

Eyelids

Masks to simulate eyelids were cut from black felt and pinned to the orbital rim in a constant position to approximate both a normal inter-

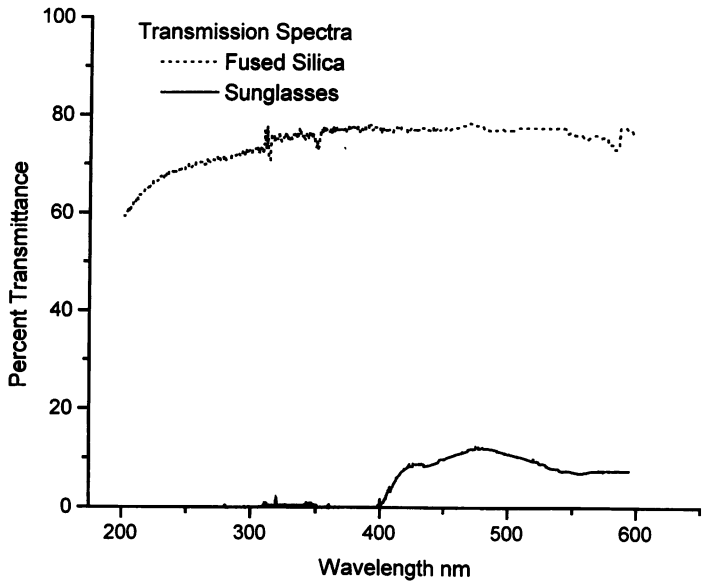

FIGURE 35
Transmission spectra of UV-grade silica and sunglass lenses.

palpebral fissure (Fig 36) and the effect of squinting (Fig 37). The normal aperture was 11 mm vertically and 28 mm horizontally and was positioned so that the upper margin overlapped the cornea for 1 to 2 mm, and the lower margin rested at the lower corneal "limbus." The squinting aperture measured 25 mm horizontally and 3 mm vertically and was positioned in the middle of the cornea. The mask could be molded to the curvature of the eye model but did not drape itself to the model quite as tightly as a normal eyelid.

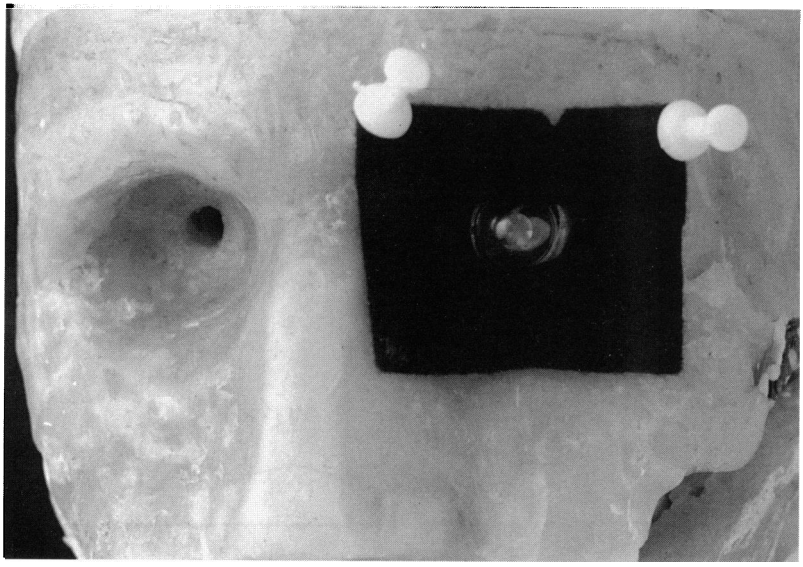

FIGURE 36
"Normal" lid mask.

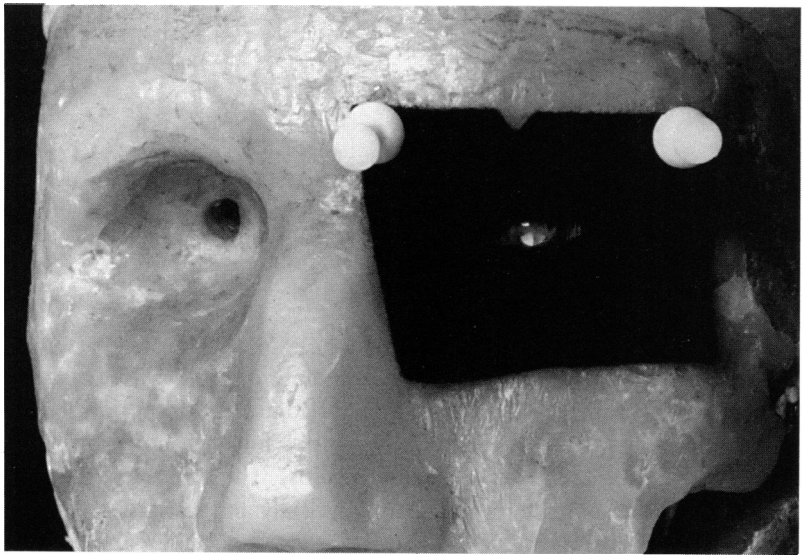

FIGURE 37
"Squinting" lid mask.

Calibration of Dose of UV-A and UV-B

To calibrate the intensity of the color change in various parts of each disc to UV-A and UV-B energy, strips of photosensitive paper were exposed in 10-second increments at various times of the day, producing stripes of increasing color intensity (Fig 38). With the PMA cumulative UV-A or UV-B energy was recorded for each 10-second increment. Depending on the elevation of the sun the strips reached maximal darkness after 60 to 100

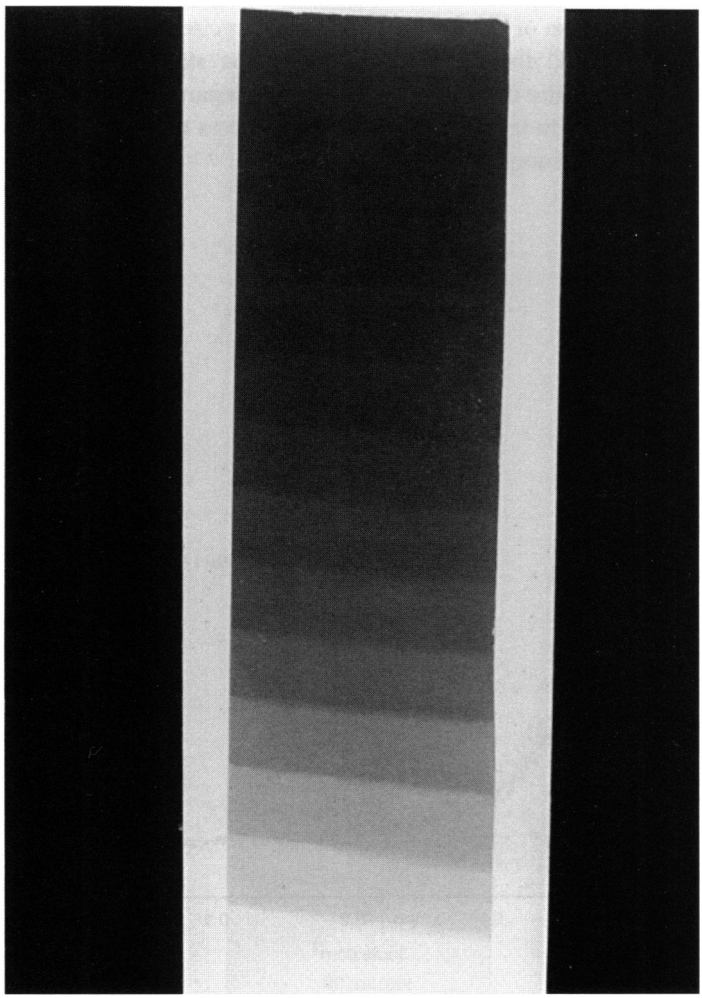

FIGURE 38

Sample calibration strip of photosensitive paper, exposed in 10-second increments. Darkest stripes are at top of strip.

seconds. The strips were scanned for image analysis, and the color intensity of each stripe was correlated with the cumulative energy recorded for that stripe. The relationship of color change to energy was plotted (Origin, Microcal), and a first-degree exponential decay used to fit a curve to the data. Separate curves were prepared for UV-A and UV-B (Figs 39 through 45) energy, and these curves then were used to estimate energy dose based on color change in various parts of the exposed discs. UV-A and UV-B exposure have been calculated for exposures with sunglasses, although they eliminated all light below 400 nm in wavelength passing through the spectacle lens. None of the frames conformed precisely to the sku11, and some light reached the model eye around the sides of each frame. However, because the calibration curves were prepared from photosensitive paper exposed to unfiltered sunlight, the curves may be less accurate for exposures with sunglasses.

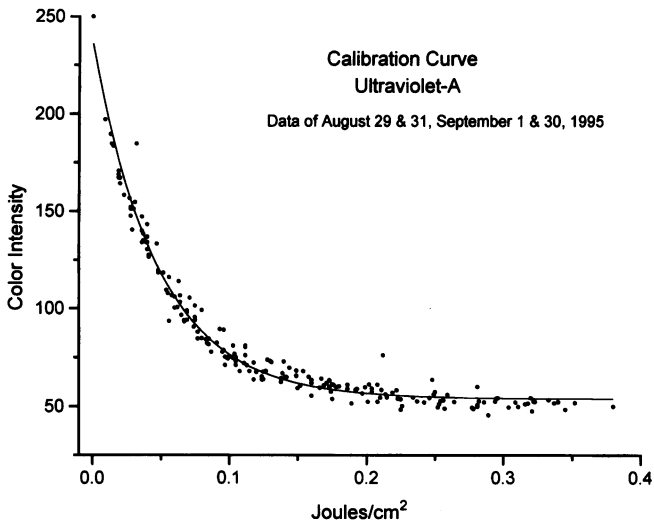

FIGURE 39

Calibration curve for UV-A prepared from strips of photosensitive paper exposed on Aug 29 and 31 and Sept 1 and 30, 1995.

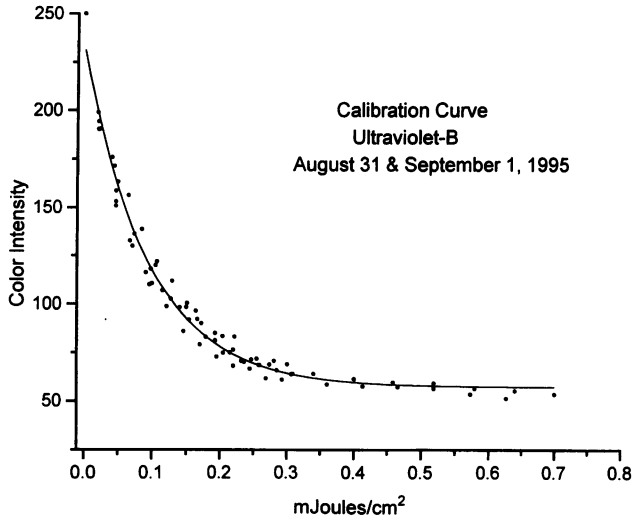

FIGURE 40

Calibration curve for UV-B prepared from strips of photosensitive paper exposed on Aug 31 and Sept 1, 1995.

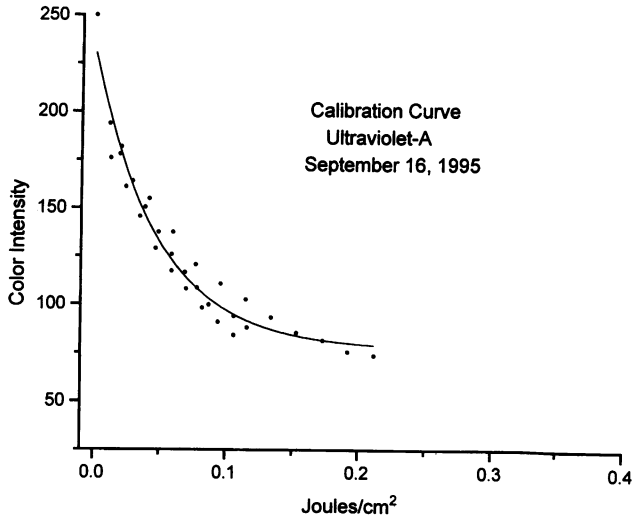

FIGURE 41

Calibration curve for UV-A prepared from strips of photosensitive paper exposed on Sept 16, 1995.

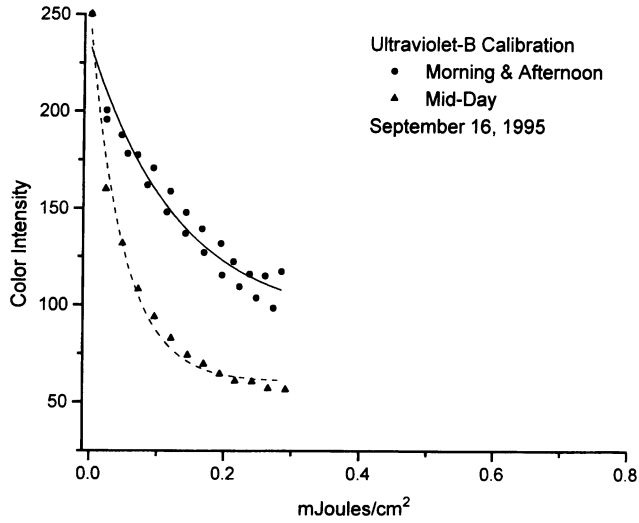

FIGURE 42

Calibration curve for UV-B prepared from strips of photosensitive paper exposed on Sept 16, 1995.

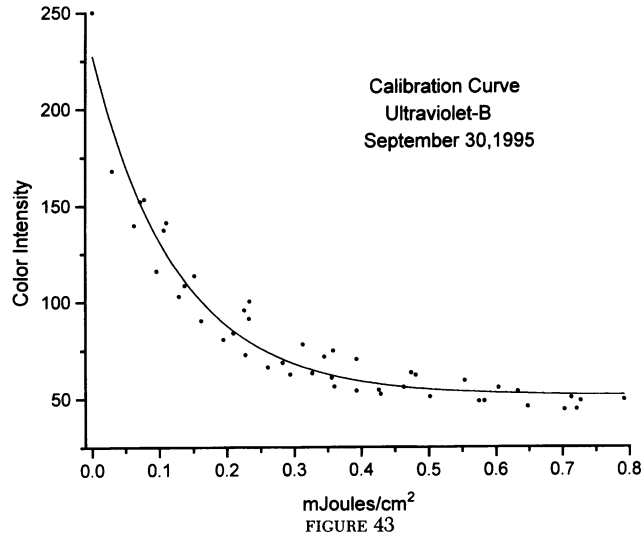

FIGURE 43

Calibration curve for UV-B prepared from strips of photosensitive paper exposed on Sept 30, 1995.

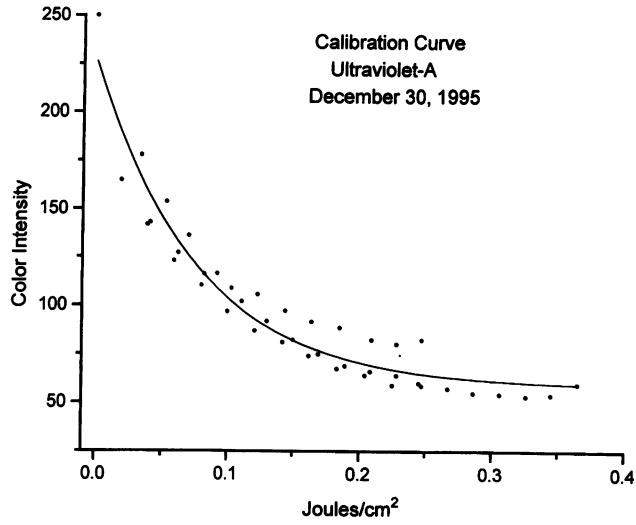

FIGURE 44

Calibration curve for UV-A prepared from strips of photosensitive paper exposed on Dec 30, 1995.

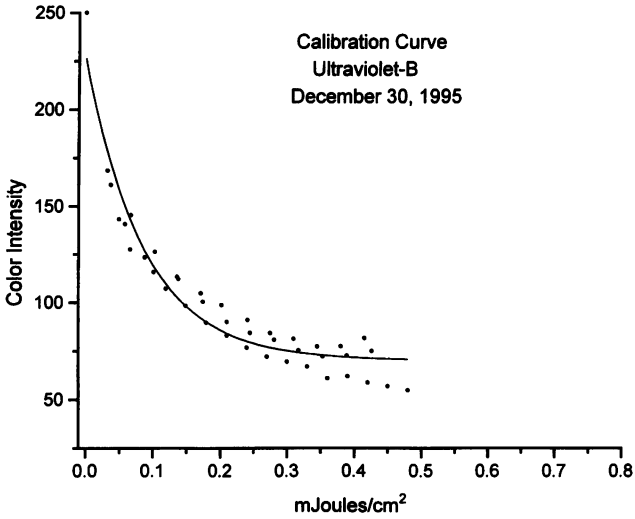

FIGURE 45

Calibration curve for UV-B prepared from strips of photosensitive paper exposed on Dec 30, 1995.

RESULTS

Unless otherwise stated, the sky was clear throughout the day, and each disc was exposed for 2 minutes in the left orbit with the head oriented to magnetic south by compass. The position of the sun is reported as altitude in degrees above the horizon and position along the horizon relative to true north, or azimuth. The position of true north is 0°, true east is 90°, true south is 180°, and true west is 270°. Time is always Eastern Standard Time (EST). To compare the position of the sun over New York at various times, consult Tables I and III.

Data are tabulated for experiments with the eye models conducted on Aug 19 and 20, Sept 11,16, and 30, and Dec 30, 1995. Bar graphs of illustrative patterns and photographs of representative exposures are included.

Ambient UV-A and UV-B and Calibration Curves

On Aug 19, 20, 29, and 31, Sept 1, 11, and 30, and Dec 30, clear skies prevailed, and ambient UV-A and UV-B energy plotted to a relatively uniform gaussian distribution (Figs 46 and 47). Calibration curves were prepared on Aug 29 and 31, Sept 1 and 30; and the calibration data for UV-A for these dates plot to a uniform curve (Fig 39). Insufficient UV-B data were recorded on Aug 29; the UV-B data from Aug 31 and Sept 1 plot to a uni-

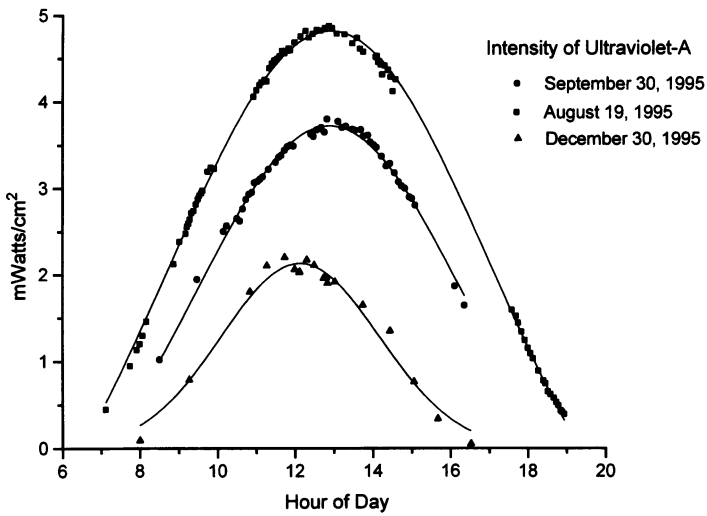

FIGURE 46

Intensity of ambient UV-A on Aug 19, Sept 30, and Dec 30, 1995, when sky was clear.

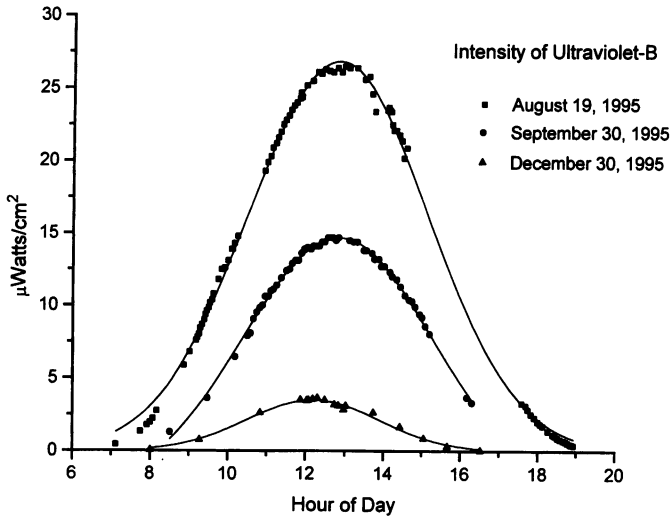

FIGURE 47
Intensity of ambient UV-B on Aug 19, Sept 30, and Dec 30, 1995, when sky was clear.

form curve (Fig 40). The plot of UV-B data from Sept 30 (Fig 43) is very close to that for Aug 31 and Sept 1 but is shifted slightly to the right, resulting in slightly higher energy levels at some values of color intensity. As noted previously, UV-B is more sensitive to changes in atmospheric conditions than UV-A. Data analysis for Sept 30 was performed using the pooled calibration data for UV-A (Fig 39) and the UV-B curve from Sept 30 (Fig 43). Separate calibration curves were prepared on Dec 30, 1995 (Figs 44 and 45)

On Sept 16 the sky was overcast, and ambient UV-A and UV B fluctuated (Figs 48 and 49). Despite this fluctuation, calibration data for UV-A plot to a relatively uniform curve (Fig 41), which is shifted to the right relative to the clear sky data (Fig 39). Calibration data for UV-B appear to separate into two curves: one for morning and afternoon and one for midday (Fig 42). Only estimates of UV-A energy have been made for Sept 16, and these data may be less reliable because of the fluctuation in ambient energy.

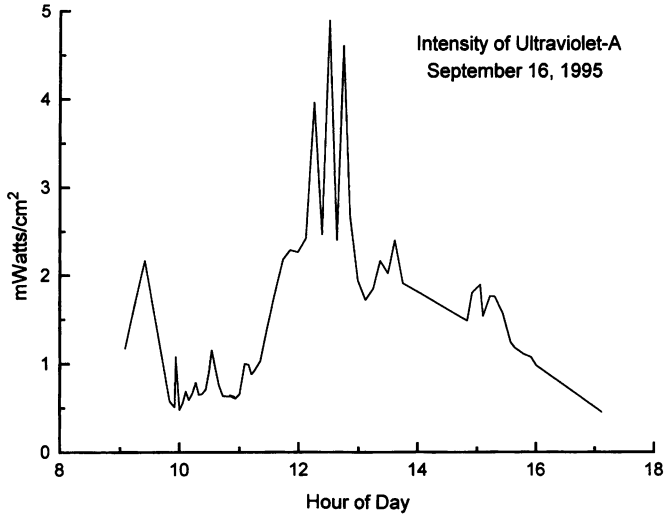

FIGURE 48
Intensity of ambient UV-A on Sept 16, 1995, when sun was obscured by thick clouds.

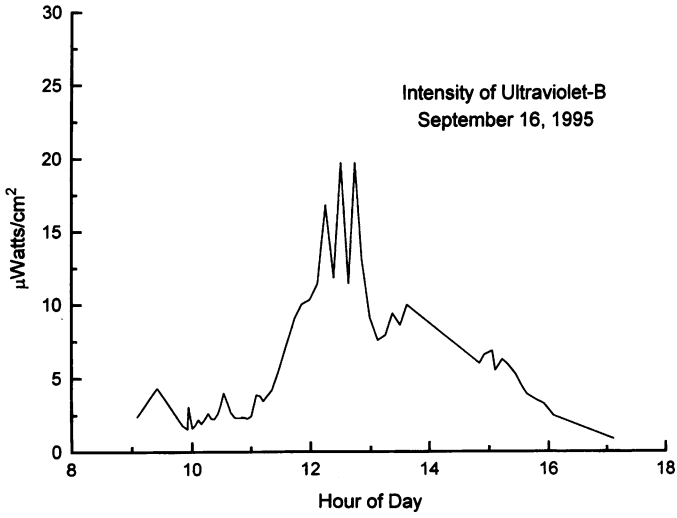

FIGURE 49
Intensity of ambient UV-B on Sept 16, 1995, when sun was obscured by thick clouds.

All the calibration curves reach an asymptote. The most intense color change has a gray scale level of just above 50. As this level is approached, relatively more light energy is required for small changes in color intensity. It appears that the calibration curves are most valid when color change and energy have a nearly linear relationship. For Figs 39, 40, 43, and 44 it has been assumed arbitrarily that color intensities of 75 and above are acceptable. For the UV-A calibration curve of Sept 16 (Fig 41) and the UV-B calibration curve of Dec 30 (Fig 45), this level is assumed to be 100. The most intense color change recorded on the discs often falls within the "nonlinear" portion of the calibration curves, especially for summer sunlight with no filter. These data are shown in the Tables but are flagged with an asterisk. Ratios of energy exposure in different quadrants also are shown in the Tables. The validity of these ratios are limited by the variables affecting the recording and estimation of energy described above.

Clear skies prevailed for the initial experiments on Aug 19 and 20. No calibration strips were recorded on those days. Because the ambient UV-A and UV-B energy levels for these days plot to a uniform gaussian distribution, it is assumed that the calibration curves prepared later (Figs 39 and 40) are valid.

Set One: Aug 19, 1995 (Clear Sky)

Experiment 1. A comparison of the exposure patterns of the 7.5-and 5.0-mm pupils was made from 8:11 to 8:37 AM. The pattern of light exposure is similar for the two pupil sizes (Fig 50, Table VI), although the inferior portion of the disc received more light with the larger pupil. With both the 7.5-mm and the 5.0-mm pupils, the intensity of exposure is significantly greater in the inferonasal and inferotemporal areas than both superior quadrants, and the inferonasal sample is significantly darker than any of the three other samples.

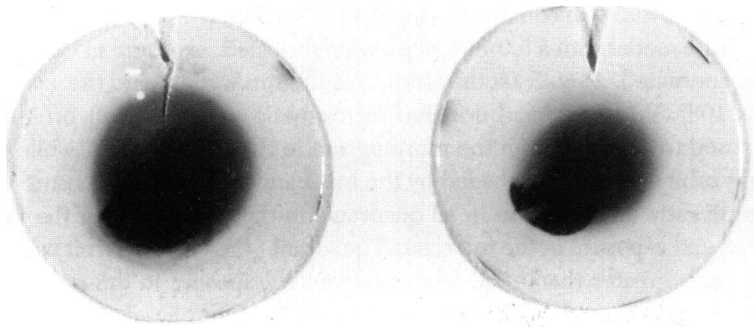

FIGURE 50

Experiment 1. Disc exposed in left orbit with 7.5-mm pupil (left), and disc exposed with 5-mm pupil (right). Intense focus of light from sun is seen inferonasally.

TABLE VIA: 7.5-MM PUPIL

QUADRANT	INTENSITY/STD DEV		UV-A J/CM²	UV-B MJ/CM²	UV-A RATIO 4/1	UV-B RATIO 4/1
1	101.39	8.34	0.0650	0.130	2.3	2.6
2	99.77	5.95	0.0656	0.133		
3	78.59	1.4	0.0950	0.196	UV-A RATIO 4/3	UV-B RATIO 4/3
4°	61.21°	3.17	0.1517°	0.343°	1.6	1.75

°DATA ON NONLINEAR PORTION OF CALIBRATION CURVES.

TABLE VIB: 5-MM PUPIL

QUADRANT	INTENSITY/STD DEV		UV-A J/CM²	UV-B MJ/CM²	UV-A RATIO 4/1	UV-B RATIO 4/1
1	96.24	5.36	0.0690	0.140	1.75	1.8
2	100.27	3.35	0.0653	0.1312		
3	89.19	2.63	0.0786	0.159	UV-B RATIO 4/3	UV-B RATIO 4/3
4°	68.83°	5.62	0.120°	0.255°	1.5	1.6

°DATA ON NONLINEAR PORTION OF CALIBRATION CURVES.

Experiment 2. With the 5.0-mm pupil model, light exposure of the left and right orbits was compared from 8:45 to 9:15 AM (Fig 51, Table VII). As only one model with a 5.0-mm pupil was fabricated, exposure in the orbits was alternated. At 8:45 AM the altitude of the sun was 39° and the azimuth was 108°. With the head oriented to magnetic south, the left orbit was exposed to full light from the morning sun in the southeast sky, while the right orbit was partially shaded by the brow and nose. Light exposure was significantly more intense in all quadrants in the left orbit than the right orbit, and exposure in the inferonasal quadrant (4) of the left orbit was significantly greater than in all other quadrants. Exposure in the right orbit was less intense and more uniform, although the inferonasal sample is significantly darker than the other three samples, and the inferotemporal sample is significantly darker than the superonasal sample.

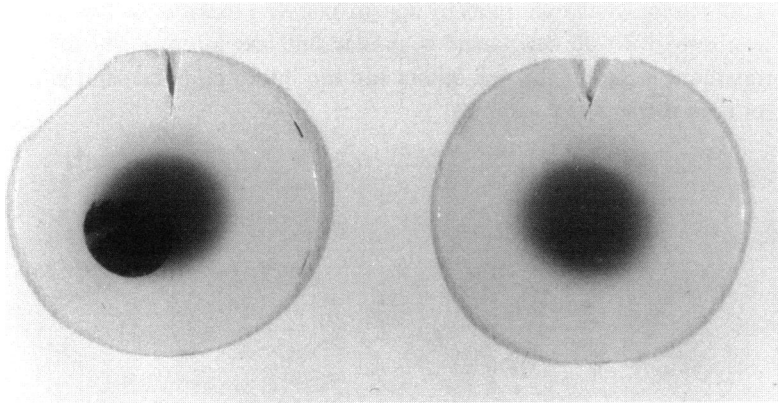

FIGURE 51
Experiment 2. Pattern of exposure from left orbit (left disc) and right orbit (right disc) with 5-mm pupil. Left orbit was exposed to more light, especially inferonasally.

TABLE VIIA: RIGHT ORBIT 5-MM PUPIL

QUADRANT	INTENSITY/STD DEV		UV-A J/CM²	UV-B MJ/CM²	UV-A RATIO 4/1	UV-B RATIO 4/1
1	110.98	2.27	0.0549	0.1118	1.25	1.23
2	106.97	1.98	0.060	0.118		
3	104	2.16	0.0624	0.126		
4	97.23	0.83	0.0689	0.138		

TABLE VIIB: LEFT ORBIT 5-MM PUPIL

QUADRANT	INTENSITY/STD DEV		UV-A J/CM²	UV-B MJ/CM²	UV-A RATIO 4/1	UV-B RATIO 4/1
1	97.09	1.4	0.0689	0.138	1.8	1.9
2	95.80	2.35	0.0698	0.143		
3	95.84	0.93	0.0695	0.142		
4°	67.37°	2.42	0.1237°	0.269°		

°DATA ON NONLINEAR PORTION OF CALIBRATION CURVES.

Experiment 3. The effect of three styles of sunglasses was studied with the 5.0-mm pupil from 9:56 to 10:50 AM.(Figs 52 and 53, Table VIII). The inferonasal area of the control discs exposed without sunglasses was significantly darker than all other samples, and the inferotemporal sample of controls was darker than both superior samples. Each of the sunglasses—standard frame, frame with side shields, and wraparound—attenuated

light energy in all quadrants by approximately a factor of 6. The pattern of exposure with all sunglasses is similar but less intense: the inferonasal quadrant is darker than all others and the inferotemporal sample is darker than the superior samples.

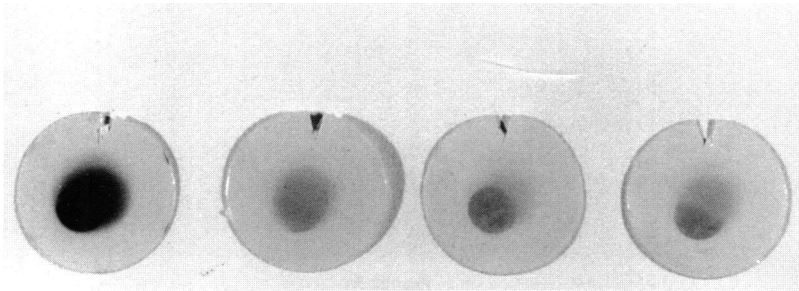

FIGURE 52

Experiment 3. Left to right, pattern of exposure with 5-mm pupil and no glasses, regular sunglasses, sport sunglasses, and wrap-around sunglasses. Inferonasal concentration is evident in all.

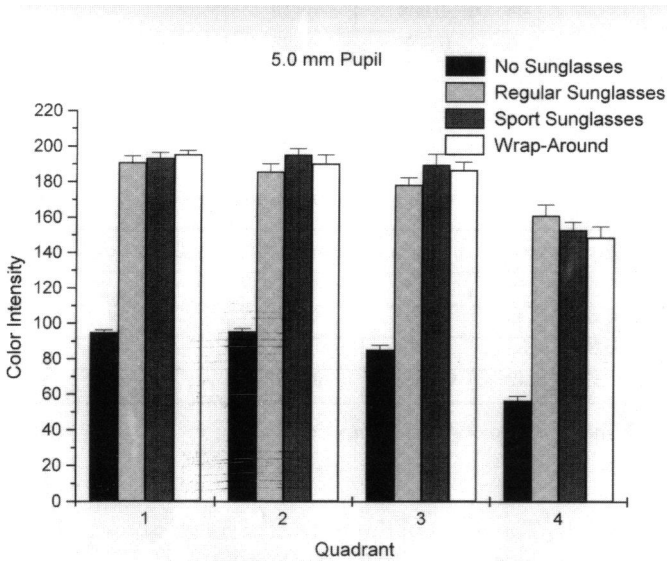

FIGURE 53

Experiment 3. Mean color intensity (5-mm pupil) from superonasal (1), superotemporal (2), inferotemporal (3), and inferonasal (4) quadrants.

TABLE VIIIA: NO GLASSES, 5-MM PUPIL

QUADRANT	INTENSITY/STD DEV		UV-A J/CM²	UV-B MJ/CM²	UV-A RATIO 4/1	UV-B RATIO 4/1
1	94.98	1.43	0.0721	0.146	2.75	3.6
2	95.45	1.8	0.07	0.145		
3	85.22	2.73	0.085	0.172	UV-A RATIO 4/3	UV-B RATIO 4/3
4°	56.53°	2.65	0.198°	0.519°	2.3	3.0

°DATA ON NONLINEAR PORTION OF CALIBRATION CURVES.

TABLE VIIIB REGULAR GLASSES, 5-MM PUPIL

QUADRANT	INTENSITY/STD DEV		UV-A J/CM²	UV-B MJ/CM²	UV-A RATIO 4/1	UV-B RATIO 4/1
1	190.89	3.7	0.0138	0.025	1.8	2.4
2	185.73	4.4	0.0152	0.028		
3	178.35	4.13	0.0181	0.0365	UV-A RATIO 4/3	UV-B RATIO 4/3
4	161.02	6.33	0.025	0.0494	1.38	1.35

TABLE VIIIC: SPORT GLASSES, 5-MM PUPIL

QUADRANT	INTENSITY/STD DEV		UV-A J/CM²	UV-B MJ/CM²	UV-A RATIO 4/1	UV-B RATIO 4/1
1	193.26	3.24	0.0126	0.023	2.4	2.4
2	195.06	3.67	0.0121	0.0217		
3	189.55	6.18	0.0142	0.0254	UV-A RATIO 4/3	UV-B RATIO 4/3
4	152.9	4.66	0.03	0.0557	2.1	2.2

TABLE VIIID WRAP-AROUND GLASSES, 5-MM PUPIL

QUADRANT	INTENSITY/STD DEV		UV-A J/CM²	UV-B MJ/CM²	UV-A RATIO 4/1	UV-B RATIO 4/1
1	195.43	2.23	0.0118	0.0210	2.7	2.9
2	190.29	4.92	0.0138	0.0253		
3	186.76	4.45	0.0149	0.0276	UV-A RATIO 4/3	UV-B RATIO 4/3
4	148.87	6.14	0.0320	0.0610	2.1	2.2

Experiment 4. The effect of a baseball cap with and without wraparound sunglasses was studied with the 5.0-mm pupil in the left orbit from 1:06 to 1:54 PM (Figs 54 and 55, Table IX). The inferior half of control discs was more intensely exposed than the upper half, and the inferotemporal sample was significantly darker than the inferonasal sample. A hat with brim did not protect the upper half of the disc as well as wraparound sunglasses alone, and the combination of hat and sunglasses was no better at shielding the upper half of the lens than the sunglasses alone. The hat and sunglasses each provided comparable protection to the inferotemporal area, but at this time of day the sunglasses were more effective in shielding the inferonasal sample. The combination of hat and sunglasses provided better protection to the inferior portion of the lens than either hat or glasses alone. With hat and glasses, the inferior half of the disc still received slightly more light exposure than the upper half, but this difference was not statistically significant.

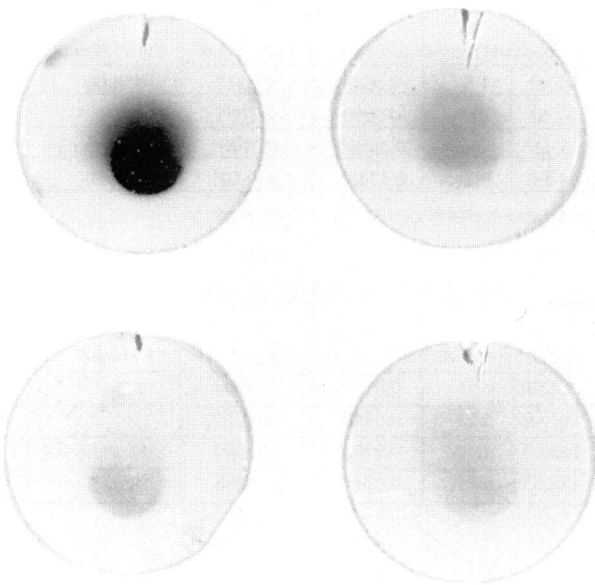

FIGURE 54
Experiment 4. Pattern of exposure of discs with the 5-mm pupil: control (upper left), hat alone (upper right), wraparound glasses (lower left), hat and sunglasses (lower right).

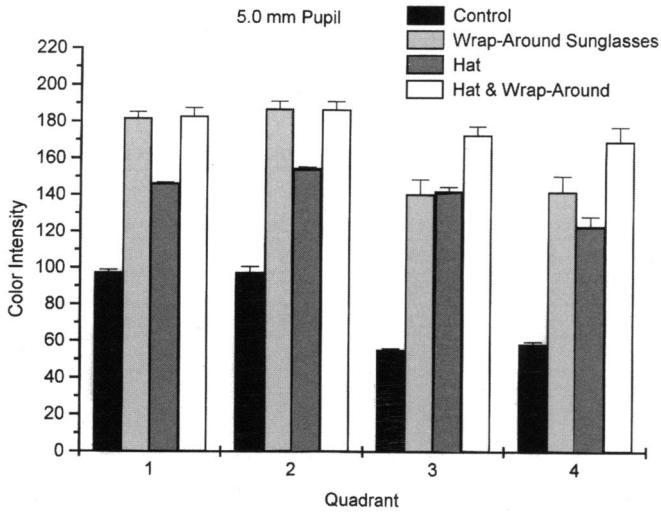

FIGURE 55
Experiment 4. Mean color intensity (5-mm pupil) from superonasal (1), superotemporal (2), inferotemporal (3), and inferonasal (4) quadrants.

TABLE IXA: CONTROLS, 5-MM PUPIL

QUADRANT	INTENSITY/STD DEV		UV-A J/CM^2	UV-B MJ/CM^2	UV-A RATIO 3/2	UV-B RATIO 3/2
1	97.49	1.5	0.0688	0.1377	3.06	4.15
2	97.57	3.12	0.0680	0.1375		
3°	55.41°	0.62	0.2080°	0.5700°	UV-A RATIO 3/4	UV-B RATIO 3/4
4°	58.48°	1.32	0.1746°	0.4480°	1.19	1.27

°DATA ON NONLINEAR PORTION OF CALIBRATION CURVES.

TABLE IXB: WRAP-AROUND GLASSES, 5-MM PUPIL

QUADRANT	INTENSITY/STD DEV		UV-A J/CM^2	UV-B MJ/CM^2	UV-A RATIO 3/2	UV-B RATIO 3/2
1	181.81	3.51	0.0170	0.0300	2.37	2.53
2	187.00	4.19	0.0148	0.0273		
3	140.62	8.14	0.0350	0.0690	UV-A RATIO 3/4	UV-B RATIO 3/4
4	142.05	8.71	0.0344	0.0688	1.02	1.004

TABLE IXC: HAT, 5-MM PUPIL

QUADRANT	INTENSITY/STD DEV		UV-A J/CM^2	UV-B MJ/CM^2	UV-A RATIO 4/2	UV-B RATIO 4/2
1	146.36	0.6	0.0332	0.0630	1.64	1.71
2	154.70	0.72	0.0280	0.0540		
3	142.30	2.34	0.0343	0.0686	UV-A RATIO 4/3	UV-B RATIO 4/3
4	123.24	5.3	0.0460	0.0925	1.34	1.35

TABLE IXD: HAT AND WRAPAROUND GLASSES, 5-MM PUPIL

QUADRANT	INTENSITY/STD DEV		UV-A J/CM^2	UV-B MJ/CM^2	UV-A RATIO 4/2	UV-B RATIO 4/2
1	183.00	4.51	0.0159	0.0295	1.43	1.54
2	186.65	4.44	0.0150	0.0277		
3	172.84	4.85	0.0202	0.0405	UV-A RATIO 4/3	UV-B RATIO 4/3
4	169.48	7.8	0.0214	0.0427	1.06	1.05

Experiment 5. The effect of two types of sunglasses on the pattern of light passing through the original cornea model was studied. The exposures were made in the late afternoon (4:35 to 5:47 PM) with the model in the left orbit (Table X). The altitude of the sun at 4:30 PM was 25° and its azimuth 265°. Without glasses, the greatest exposure was found in the inferotemporal portion of the disc. The intensity of exposure inferonasally appeared to be somewhat greater than in the upper half of control discs, but the difference was not statistically significant. Either type of sunglass attenuated light in all quadrants, and no significant difference in energy level was recorded between samples. At this time of day, the sun was in the southwestern sky. With the head facing south, the left orbit was partially shielded by the right side of the head and the nose, resulting in the inferotemporal concentration.

TABLE XA: NO GLASSES, CORNEA MODEL

QUADRANT	INTENSITY/STD DEV		UV-A J/CM²	UV-B MJ/CM²	UV-A RATIO 3/2	UV-B RATIO 3/2
1	127.14	11.02	0.0435	0.0870	2.53	2.69
2	133.64	10.51	0.0400	0.0785		
3	76.58	6.33	0.101	0.2110	UV-A RATIO 3/4	UV-B RATIO 3/4
4	114.32	10.61	0.053	0.1053	1.91	2.0

TABLE XB: REGULAR GLASSES, CORNEA MODEL

QUADRANT	INTENSITY/STD DEV		UV-A J/CM²	UV-B MJ/CM²	UV-A RATIO 3/2	UV-B RATIO 3/2
1	194.85	15.73	0.0125	0.0225	1.32	1.35
2	195.14	15.44	0.0120	0.0215		
3	183.62	23.89	0.0158	0.0290	UV-A RATIO 3/4	UV-B RATIO 3/4
4	197.74	10.27	0.0116	0.0189	1.29	1.53

TABLE XC: SPORT SUNGLASSES, CORNEA MODEL

QUADRANT	INTENSITY/STD DEV		UV-A J/CM²	UV-B MJ/CM²	UV-A RATIO 3/2	UV-B RATIO 3/2
1	197.15	5.21	0.0117	0.0190	1.05	1.13
2	196.83	3.06	0.0118	0.0194		
3	194.99	12.58	0.0124	0.0220	UV-A RATIO 3/4	UV-B RATIO 3/4
4	201.86	7.43	0.0094	0.0174	1.32	1.26

Experiment 6. The effect of sunglasses on the pattern of exposure of the 5.0-mm pupil model in the left orbit was studied from 4:45 to 5:56 PM (Table XI) The elevation of the sun at 4:30 PM was 25° and at 6 PM only 8°, and its azimuth at these times was 265° and 279°. In the late afternoon the light was relatively weak, and the exposure of the discs after 2 minutes was light. In the late afternoon, the intensity of exposure changes rapidly, resulting in a large standard deviation of mean color. The right side of the head was exposed directly to the setting sun while the nasal side of the left orbit was partially shaded by the nose and brow. Without glasses the inferotemporal exposure was significantly greater than the others. With either pair of sunglasses, no significant difference in exposure was detected in any quadrant.

TABLE XIA: NO GLASSES, 5-MM PUPIL

QUADRANT	INTENSITY/STD DEV		UV-A J/CM²	UV-B MJ/CM²	UV-A RATIO 3/1	UV-B RATIO 3/1
1	136.65	13.07	0.038	0.075	1.97	2.06
2	136.78	9.1	0.038	0.075		
3	91.78	19.93	0.075	0.1549	UV-A RATIO 3/4	UV-B RATIO 3/4
4	109.95	28.17	0.0555	0.1137	1.35	1.36

TABLE XIB: REGULAR GLASSES, 5-MM PUPIL

QUADRANT	INTENSITY/STD DEV		UV-A J/CM²	UV-B MJ/CM²	UV-A RATIO 3/1	UV-B RATIO 3/1
1	202.08	7.02	0.0094	0.017	1.34	1.38
2	199.16	7.53	0.0105	0.0188		
3	192.98	12.34	0.0126	0.0234	UV-A RATIO 3/4	UV-B RATIO 3/4
4	200.88	8.13	0.01	0.018	1.26	1.3

TABLE XIC: SPORT SUNGLASSES, 5-MM PUPIL

QUADRANT	INTENSITY/STD DEV		UV-A J/CM²	UV-B MJ/CM²	UV-A RATIO 3/1	UV-B RATIO 3/1
1	199.75	6.55	0.0105	0.0187	1.11	1.02
2	198.83	9.77	0.0110	0.0188		
3	197.15	11.76	0.0117	0.0190	UV-A RATIO 3/4	UV-B RATIO 3/4
4	199.99	7.87	0.0105	0.0186	1.11	1.02

Set Two: Aug 20, 1995 (Clear Sky)

Experiment 7. The effect of the two black felt lid masks was studied with the original cornea model and the 5.0-and 7.5-mm pupil models from 10:01 AM to 12:29 PM. The pattern of exposure with the normal lid mask is statistically indistinguishable from control discs with all eye models (Figs 56 through 59, Table XII), although the superior portion of some discs appeared slightly lighter with the normal lid mask than without. With each model the inferonasal area received the most intense exposure, and the exposure of the inferonasal and inferotemporal quadrants is significantly greater than both upper quadrants.

The squint mask attenuated light exposure in the upper and inferotemporal areas with all eye models. The inferonasal intensity remains greater than all other areas, although the difference between the inferonasal quadrant and the other quadrants is less marked with the 5.0-mm pupil model than with either the cornea or 7.5-mm pupil models. Squinting appears to protect the lens more effectively as pupil size decreases.

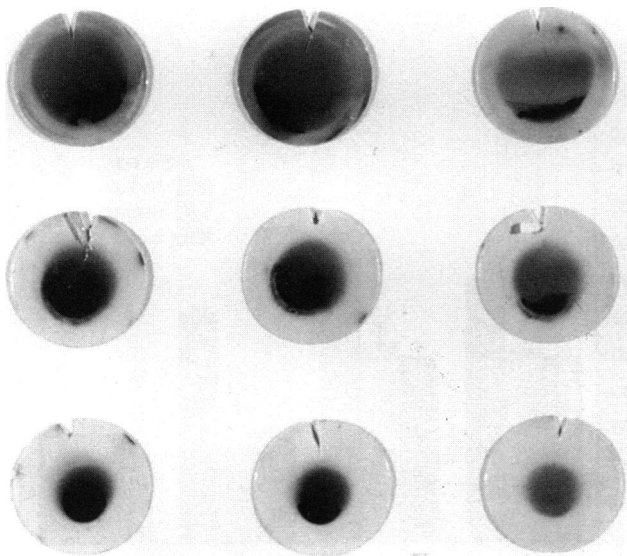

FIGURE 56

Experiment 7. Pattern of exposure with original cornea model, 7.5-mm pupil, and 5-mm pupil. Left to right: control, normal lid mask, squint lid mask. Change in pattern of exposure with cornea model (top row) is explained in text.

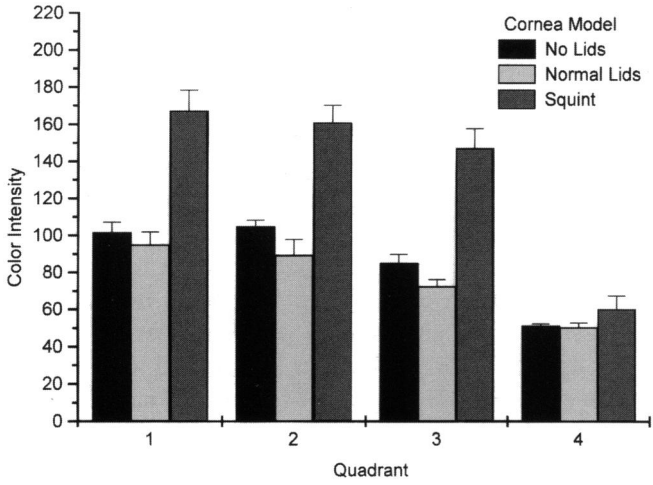

FIGURE 57

Experiment 7. Mean color intensity (corneal model) in superonasal (1), superotemporal (2), inferotemporal (3), and inferonasal (4) quadrants.

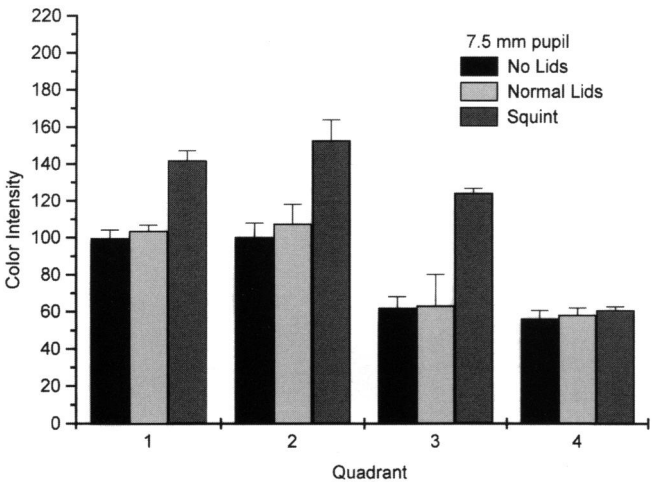

FIGURE 58

Experiment 7. Mean color intensity (7.5-mm pupil) in superonasal (1), superotemporal (2), inferotemporal (3), and inferonasal (4) quadrants.

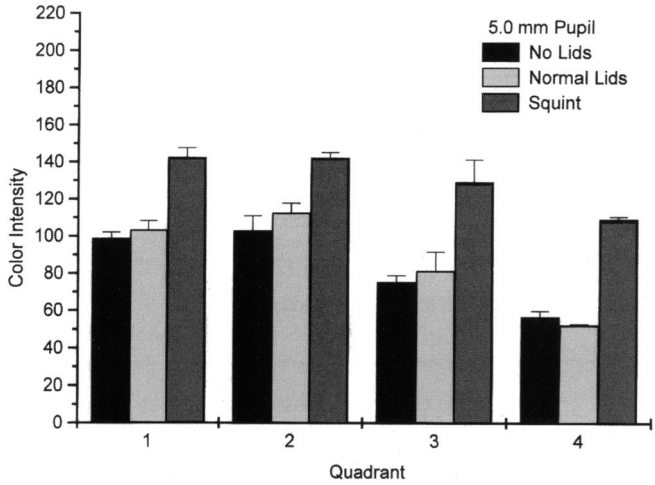

FIGURE 59

Experiment 7. Mean color intensity (5-mm pupil) in superonasal (1), superotemporal (2), inferotemporal (3), and inferonasal (4) quadrants.

TABLE XIIA: CONTROLS, CORNEA MODEL

QUADRANT	INTENSITY/STD DEV		UV-A J/CM²	UV-B MJ/CM²	UV-A RATIO 4/1	UV-B RATIO 4/1
1	101.77	5.5	0.0644	0.128	3.68	4.78
2	104.847	3.44	0.061	0.1246		
3	85.163	4.73	0.085	0.173	UV-A RATIO 4/3	UV-B RATIO 4/3
4°	51.26°	1.08	0.237°	0.612°	2.79	3.54

°DATA ON NONLINEAR PORTION OF CALIBRATION CURVES.

TABLE XIIB NORMAL LID MASK, CORNEA MODEL

QUADRANT	INTENSITY/STD DEV		UV-A J/CM²	UV-B MJ/CM²	UV-A RATIO 4/1	UV-B RATIO 4/1
1	95.04	7.0	0.071	0.1455	3.44	4.3
2	89.30	8.61	0.077	0.159		
3°	72.59°	3.7	0.1087°	0.266°	UV-A RATIO 4/3	UV-B RATIO 4/3
4°	50.37°	2.53	0.244°	0.625°	2.24	2.77

°DATA ON NONLINEAR PORTION OF CALIBRATION CURVES.

TABLE XIIC: SQUINT LID MASK, CORNEA MODEL

QUADRANT	INTENSITY/STD DEV		UV-A J/CM²	UV-B MJ/CM²	UV-A RATIO 4/1	UV-B RATIO 4/1
1	167.14	11.29	0.0224	0.0435	7.12	8.85
2	160.81	9.57	0.0252	0.04936		
3	147.20	10.68	0.0327	0.0623	UV-A RATIO 4/3	UV-B RATIO 4/3
4*	60.16*	7.46	0.1593	0.385	4.87	6.18

*DATA ON NONLINEAR PORTION OF CALIBRATION CURVES.

TABLE XIID: CONTROLS, 7.5-MM PUPIL MODEL

QUADRANT	INTENSITY/STD DEV		UV-A J/CM²	UV-B MJ/CM²	UV-A RATIO 4/1	UV-B RATIO 4/1
1	99.58	4.65	0.0666	0.134	3.11	4.15
2	100.22	7.8	0.0655	0.132		
3*	62.04*	6.14	0.149	0.314	UV-A RATIO 4/3	UV-B RATIO 4/3
4*	56.19*	4.62	0.207*	0.556*	1.39	1.77

*DATA ON NONLINEAR PORTION OF CALIBRATION CURVES.

TABLE XIIE: NORMAL LID MASK, 7.5-MM PUPIL MODEL

QUADRANT	INTENSITY/STD DEV		UV-A J/CM²	UV-B MJ/CM²	UV-A RATIO 4/1	UV-B RATIO 4/1
1	103.54	3.36	0.0625	0.1265	2.88	3.66
2	107.40	10.75	0.0592	0.116		
3*	63.19*	17.13	0.141*	0.312*	UV-A RATIO 4/3	UV-B RATIO 4/3
4*	58.19*	3.84	0.1798*	0.463*	1.28	1.48

*DATA ON NONLINEAR PORTION OF CALIBRATION CURVES.

TABLE XIIF: SQUINT LID MASK, 7.5-MM PUPIL MODEL

QUADRANT	INTENSITY/STD DEV		UV-A J/CM²	UV-B MJ/CM²	UV-A RATIO 4/1	UV-B RATIO 4/1
1	141.85	5.42	0.0344	0.0688	4.62	5.45
2	152.70	11.2	0.0302	0.0558		
3	124.19	2.79	0.0454	0.092	UV-A RATIO 4/3	UV-B RATIO 4/3
4*	60.66*	2.11	0.159*	0.375*	3.5	4.08

*DATA ON NONLINEAR PORTION OF CALIBRATION CURVES.

TABLE XIIG: CONTROLS, 5-MM PUPIL MODEL

QUADRANT	INTENSITY/STD DEV		UV-A J/CM²	UV-B MJ/CM²	UV-A RATIO 4/1	UV-B RATIO 4/1
1	98.72	3.51	0.067	0.135	2.91	3.83
2	102.86	8.08	0.063	0.127		
3°	70.2475°	3.79	0.102°	0.2132°	UV-A RATIO 4/3	UV-B RATIO 4/3
4°	56.61°	3.37	0.195°	0.517°	1.91	2.43

°DATA ON NONLINEAR PORTION OF CALIBRATION CURVES.

TABLE XIIH: NORMAL LID MASK, 5-MM PUPIL MODEL

QUADRANT	INTENSITY/STD DEV		UV-A J/CM²	UV-B MJ/CM²	UV-A RATIO 4/1	UV-B RATIO 4/1
1	103.25	5.06	0.0627	0.1267	3.72	4.82
2	112.5	5.39	0.0546	0.110		
3	81.445	10.24	0.0892	0.1831	UV-A RATIO 4/3	UV-B RATIO 4/3
4°	52.53°	0.50	0.233°	0.610°	2.61	3.33

°DATA ON NONLINEAR PORTION OF CALIBRATION CURVES.

TABLE XII I: SQUINT LID MASK, 5-MM PUPIL MODEL

QUADRANT	INTENSITY/STD DEV		UV-A J/CM²	UV-B MJ/CM²	UV-A RATIO 4/1	UV-B RATIO 4/1
1	142.41	5.31	0.0343	0.0685	1.66	1.68
2	142.15	3.06	0.0344	0.0687		
3	129.23	12.02	0.0419	0.084	UV-A RATIO 4/3	UV-B RATIO 4/3
4	109.30	1.39	0.0569	0.115	1.36	1.36

°DATA ON NONLINEAR PORTION OF CALIBRATION CURVES.

The discs exposed with the cornea model (top row, Fig 56) illustrate the visible shift in the most intense focus from movement of the sun. The control disc was exposed at 11:42 AM, the middle disc was exposed with the normal lid mask at 10:05 AM, and the right disc was exposed with the squint lid mask at 11:50 AM. The most intense concentration in the middle disc is inferonasal; in the later exposures the greatest concentration is more inferotemporal. The discs exposed with the 7.5-mm pupil were exposed at 10:13, 10:18, and 10:23 AM. The discs exposed with the 5-mm

pupil were exposed at 11:05, 11:34, and 11:38 AM. The pattern of light exposure clearly shows the effect of the model lens. With the original cornea model, the intense focus is an arc of denser color. With the pupil models, a smaller image of the sun is evident.

Experiment 8. The effect of head orientation was tested with the 5.0-mm pupil model and the cornea model from 12:35 to 2:10 PM when the sun was in the southwestern sky (Table XIII). The eye models were placed in the left orbit. With the head facing south, the right side of the skull received more light than the left side of the skull. With the head facing west, the left side of the skull received more direct light than the right. With the head facing north, the back of skull received direct light, and both orbits were in the shade.

With the head facing north, no significant difference in light exposure was evident in any quadrant with either model. With the head facing south, the inferior quadrants received more light than the superior quadrants, and the inferotemporal quadrant received more light than the inferonasal quadrant. The difference between the inferonasal and the inferotemporal samples was statistically significant with the cornea model but was not significantly different for the 5.0-mm pupil model.

With the head facing west, the inferonasal quadrant received significantly more light than the inferotemporal quadrant. With the 5-mm pupil, the inferotemporal sample was slightly but significantly darker than both superior samples. With the cornea model no difference was detected between the inferotemporal and superior samples.

The reversal of location of the most intense focus, from inferotemporal to inferonasal, with change in orientation from south to west indicates that the orientation of the sun to the head determines the location of the greatest exposure.

TABLE XIIIA: SOUTH GAZE, CORNEA MODEL

QUADRANT	INTENSITY/STD DEV		UV-A J/CM²	UV-B MJ/CM²	UV-A RATIO 3/1	UV-B RATIO 3/1
1	104.67	4.85	0.0612	0.1248	2.57	2.80
2	95.76	8.21	0.0699	0.144		
3°	60.94°	4.68	0.157°	0.35°	UV-A RATIO 3/4	UV-B RATIO 3/4
4	81.046	6.82	0.0915	0.1896	1.72	1.85

°DATA ON NONLINEAR PORTION OF CALIBRATION CURVES.

TABLE XIIIB: NORTH GAZE, CORNEA MODEL

QUADRANT	INTENSITY/STD DEV		UV-A J/CM²	UV-B MJ/CM²	UV-A RATIO 3/1	UV-B RATIO 3/1
1	123.53	3.71	0.0457	0.0924	1.12	1.11
2	118.81	4.83	0.0503	0.0988		
3	116.19	5.38	0.051	0.103	UV-A RATIO 3/4	UV-B RATIO 3/4
4	125.68	10.62	0.045	0.09	1.13	1.14

°DATA ON NONLINEAR PORTION OF CALIBRATION CURVES.

TABLE XIIIC: WEST GAZE, CORNEA MODEL

QUADRANT	INTENSITY/STD DEV		UV-A J/CM²	UV-B MJ/CM²	UV-A RATIO 4/1	UV-B RATIO 4/1
1	90.92	6.22	0.0763	0.157	2.26	2.69
2	88.48	3.39	0.0806	0.1614		
3	88.59	5.39	0.0795	0.161	UV-A RATIO 4/3	UV-B RATIO 4/3
4°	58.59°	2.02	0.1723°	0.4223°	2.17	2.62

°DATA ON NONLINEAR PORTION OF CALIBRATION CURVES.

TABLE XIIID: SOUTH GAZE, 5-MM PUPIL MODEL

QUADRANT	INTENSITY/STD DEV		UV-A J/CM²	UV-B MJ/CM²	UV-A RATIO 3/1	UV-B RATIO 3/1
1	103.51	9.15	0.0625	0.1265	1.60	1.62
2	102.70	4.78	0.0634	0.127		
3	77.35	12.59	0.10	0.2044	UV-A RATIO 3/4	UV-B RATIO 3/4
4	84.88	16.64	0.0851	0.174	1.18	1.17

TABLE XIIIE: NORTH GAZE, 5-MM PUPIL MODEL

QUADRANT	INTENSITY/STD DEV		UV-A J/CM²	UV-B MJ/CM²	UV-A RATIO 3/1	UV-B RATIO 3/1
1	128.18	8.42	0.0428	0.0856	0.90	0.91
2	129.77	6.96	0.0417	0.0836		
3	134.72	8.67	0.0386	0.0777	UV-A RATIO 3/4	UV-B RATIO 3/4
4	130.44	8.78	0.041	0.0813	0.94	0.95

TABLE XIIIF: WEST GAZE, 5-MM PUPIL MODEL

QUADRANT	INTENSITY/STD DEV		UV-A J/CM²	UV-B MJ/CM²	UV-A RATIO 4/2	UV-B RATIO 4/2
1	98.48	1.59	0.0675	0.136	2.66	2.8
2	114.40	1.22	0.0526	0.1053		
3	93.54	8.27	0.0742	0.148	UV-A RATIO 4/3	UV-B RATIO 4/3
4*	63.933*	3.98	0.14*	0.295*	1.89	1.99

*DATA ON NONLINEAR PORTION OF CALIBRATION CURVES.

Set Three: Sept 11, 1995 (Clear Sky)

Experiment 9. Experiment 9 was performed on Sept 11, 1995, from 2:56 to 3:22 PM with the head oriented northwest so that the left temple was normal to the direction of the sun (Table XIV). The pattern of light exposure for both the 2.5-mm and 5.0-mm pupil models was similar, although the area of exposure was smaller with the smaller pupil and the intensity in each sample is less with the smaller pupil. The greatest concentration of light was seen inferonasally. No significant difference in intensity was detected between the other three quadrants with each pupil.

TABLE XIVA: 5-MM PUPIL MODEL

QUADRANT	INTENSITY/STD DEV		UV-A J/CM²	UV-B MJ/CM²	UV-A RATIO 4/2	UV-B RATIO 4/2
1	134.31	6.53	0.0396	0.0775	2.97	3.1
2	142.19	7.41	0.0343	0.0687		
3	124.40	4.81	0.0452	0.0914	UV-A RATIO 4/3	UV-B RATIO 4/3
4*	75.56*	1.91	0.102*	0.213*	2.26	2.33

*DATA ON NONLINEAR PORTION OF CALIBRATION CURVES.

TABLE XIVB: 2.5-MM PUPIL MODEL

QUADRANT	INTENSITY/STD DEV		UV-A J/CM²	UV-B MJ/CM²	UV-A RATIO 4/2	UV-B RATIO 4/2
1	142.67	3.35	0.034	0.0684	2.37	2.53
2	145.64	11.23	0.0335	0.0638		
3	151.06	4.82	0.0311	0.0577	UV-A RATIO 4/3	UV-B RATIO 4/3
4	88.5	5.59	0.0795	0.1614	2.56	2.8

*DATA ON NONLINEAR PORTION OF CALIBRATION CURVES.

Set Four: Sept 16, 1995 (Overcast Sky)

Experiment 10. On Sept 16, 1995, the effect of head orientation was tested with 5.0- and 2.5-mm pupil models from 8:55 to 10:15 AM (Fig 60, Table XV). The model was oriented in a southeast direction facing the sun, and in a southwest direction so that the left temple was roughly 90° to the direction of the sun. The sun was obscured by thick clouds, and no significant difference was detected in the intensity of any quadrant in either

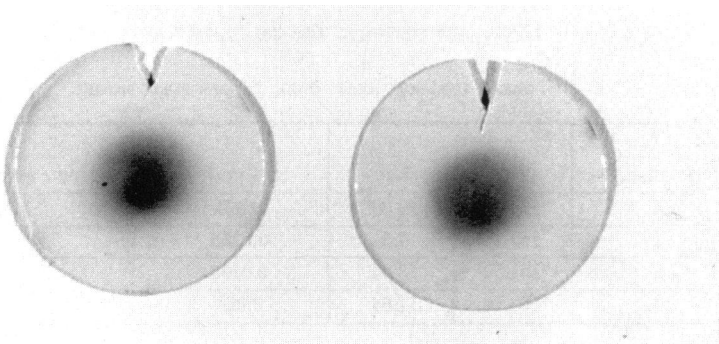

FIGURE 60
Experiment 10. Pattern of exposure with 5-mm pupil facing southwest (left) and southeast (right).

TABLE XVA: SOUTHWEST GAZE, 5-MM PUPIL MODEL*

QUADRANT	INTENSITY/STD DEV		UV-A J/CM²	UV-A RATIO 4/2
1	154.14	8.38	0.034	1.32
2	156.66	8.57	0.0325	
3	149.33	11.54	0.0365	uv-a ratio 4/3
4	140.39	8.65	0.043	1.18

*NO UV-B ENERGY LEVELS ARE SHOWN, AS THE CALIBRATION DATA WERE TOO VARIABLE.

TABLE XVB: SOUTHWEST GAZE, 5-MM PUPIL MODEL*

QUADRANT	INTENSITY/STD DEV		UV-A J/CM²	UV-A RATIO 4/2
1	152.39	10.90	0.035	1.17
2	151.18	7.20	0.036	
3	142.64	10.51	0.041	
4	141.95	13.76	0.042	

*NO UV-B ENERGY LEVELS ARE SHOWN, AS THE CALIBRATION DATA WERE TOO VARIABLE.

TABLE XVC: SOUTHWEST GAZE, 2.5-MM PUPIL MODEL*

QUADRANT	INTENSITY/STD DEV		UV-A J/CM²	UV-A RATIO 4/1
1	169.39	8.05	0.025	1.16
2	166.57	8.29	0.026	
3	164.00	11.27	0.028	
4	161.65	10.01	0.029	

*NO UV-B ENERGY LEVELS ARE SHOWN, AS THE CALIBRATION DATA WERE TOO VARIABLE.

TABLE XVD: SOUTHEAST GAZE, 2.5-MM PUPIL MODEL*

QUADRANT	INTENSITY/STD DEV		UV-A J/CM²	UV-A RATIO 3/1
1	171.87	10.39	0.024	1.23
2	167.71	7.5	0.0255	
3	161.59	13.94	0.0294	
4	163.70	17.64	0.028	

*NO UV-B ENERGY LEVELS ARE SHOWN, AS THE CALIBRATION DATA WERE TOO VARIABLE.

head position. The lower portion of some discs is slightly darker than the upper portion, and the sum of the intensities of the lower samples is slightly but significantly greater than that of the upper samples.

Experiment 11. The effect of head orientation was tested with two styles of sunglass and the 5.0-mm pupil from 10:21 AM to 12:37 PM (Table XVI). The head was oriented in a southeast direction facing the sun and southwest, normal to the position of the sun. The sun was obscured by thick clouds. The pattern of light exposure on some discs shows a concentration inferiorly, but the pattern is variable due to the cloud cover, resulting in a large standard deviation. No statistically significant difference is detected in the samples from the four quadrants with either type of sunglass.

TABLE XVIA: SOUTHWEST GAZE, REGULAR GLASSES*

QUADRANT	INTENSITY/STD DEV		UV-A J/CM²	UV-A RATIO 4/1
1	160.03	8.61	0.0297	1.22
2	159.25	9.65	0.03	
3	152.62	19.68	0.035	UV-A RATIO 4/3
4	150.69	22.49	0.0363	1.04

*NO UV-B ENERGY LEVELS ARE SHOWN, AS THE CALIBRATION DATA WERE TOO VARIABLE.

TABLE XVIB: SOUTHEAST GAZE, REGULAR GLASSES*

QUADRANT	INTENSITY/STD DEV		UV-A J/CM²	UV-A RATIO 4/1
1	160.64	9.1	0.0296	1.59
2	160.93	12.75	0.0295	
3	146.28	16.81	0.0385	UV-A RATIO 4/3
4	135.56	20.71	0.047	1.22

*NO UV-B ENERGY LEVELS ARE SHOWN, AS THE CALIBRATION DATA WERE TOO VARIABLE.

TABLE XVIC: SOUTHWEST GAZE, SPORT SUNGLASSES*

QUADRANT	INTENSITY/STD DEV		UV-A J/CM²	UV-A RATIO 4/1
1	163.34	10.07	0.028	1.45
2	159.36	11.78	0.03	
3	144.38	23.52	0.04	UV-A RATIO 4/3
4	143.86	20.02	0.0405	1.01

*NO UV-B ENERGY LEVELS ARE SHOWN, AS THE CALIBRATION DATA WERE TOO VARIABLE.

TABLE XVID: SOUTHEAST GAZE, SPORT SUNGLASSES*

QUADRANT	INTENSITY/STD DEV		UV-A J/CM²	UV-A RATIO 4/1
1	165.16	10.89	0.0267	1.42
2	165.05	10.17	0.0275	
3	161.11	11.39	0.0294	UV-A RATIO 4/3
4	147.99	28.29	0.0378	1.29

*NO UV-B ENERGY LEVELS ARE SHOWN, AS THE CALIBRATION DATA WERE TOO VARIABLE.

Experiment 12. To maximize exposure of the temporal side of the head, the skull was oriented north-northwest when the sun direction was approximately south-southwest and then tilted approximately 30° from the vertical. Two types of sunglasses were used with the 5.0-mm pupil to determine which protected the temporal eye more effectively. Because the sky was overcast from 1:50 to 2:55 PM, exposures were 6 minutes with sunglasses and 3 minutes without sunglasses. To measure color intensity six sampling sites were used. As with other discs, sampling began in the upper left of each disc image and moved clockwise. This corresponds to beginning in the superonasal area (1), moving to the superotemporal (2), midtemporal (3), inferotemporal (4), inferonasal (5), and midnasal areas (6) (Table XVI1, Figs 61 and 62). Tilting the head so that the direction of the sun was roughly normal to the temple shifted the focus of light, best seen with control discs, to an intermediate nasal position (section 6), roughly midway between the upper and lower boundaries of exposure. Because of the overcast sky, the focus nasally is not as clear as that produced on clear days. Without sunglasses the middle nasal (sample 6) area had the highest concentration of light, followed by nearly equal exposure of the superior and inferior nasal samples (1 and 5) and the midtemporal

TABLE XVIIA: NO GLASSES, 5-MM PUPIL*

SECTION	INTENSITY/STD DEV		UV-A J/CM²	UV-A RATIO 6/2
1	143.63	7.39	0.0405	2.85
2	166.30	13.69	0.0267	UV-A RATIO 6/4
3	140.52	9.13	0.043	2.84
4	166.02	5.27	0.0267	
5	141.10	9.17	0.0422	UV-A RATIO 6/3
6	109.37	1.27	0.076	1.77

*NO ESTIMATES OF UV-B ENERGY ARE SHOWN, AS THE CALIBRATION DATA WERE TOO VARIABLE.

TABLE XVIIB: REGULAR GLASSES, 5-MM PUPIL*

SECTION	INTENSITY/STD DEV		UV-A J/CM²	UV-A RATIO 6/2
1	198.73	1.01	0.0118	1.6
2	206.98	0.89	0.0084	UV-A RATIO 6/4
3	203.11	1.14	0.0092	2.06
4	211.01	2.43	0.0065	
5	206.22	3.94	0.0085	UV-A RATIO 6/3
6	194.25	6.5	0.0134	1.46

*NO ESTIMATES OF UV-B ENERGY ARE SHOWN, AS THE CALIBRATION DATA WERE TOO VARIABLE.

TABLE XVIIC: SPORT SUNGLASSES, 5-MM PUPIL*

SECTION	INTENSITY/STD DEV		UV-A J/CM²	UV-A RATIO 6/2
1	195.35	4.06	0.0126	1.81
2	201.08	1.24	0.0105	UV-A RATIO 6/4
3	192.76	4.17	0.014	1.80
4	200.59	2.46	0.0106	
5	192.38	1.3	0.014	UV-A RATIO 6/3
6	182.22	5.7	0.019	1.36

*NO ESTIMATES OF UV-B ENERGY ARE SHOWN, AS THE CALIBRATION DATA WERE TOO VARIABLE.

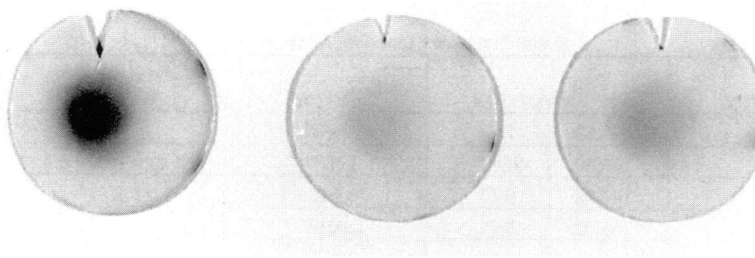

FIGURE 61
Experiment 12. Pattern of exposure with 5-mm pupil: control (left), regular sunglasses (center), sport sunglasses (right).

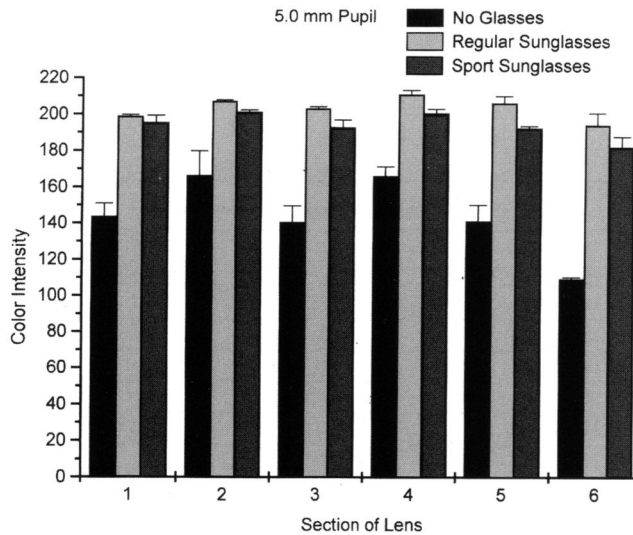

FIGURE 62
Experiment 12. Mean color intensity (5-mm pupil) for superonasal (1), superotemporal (2), midtemporal (3), inferotemporal (4), inferonasal (5), and midnasal (6) samples.

sample (area 3). The superotemporal (area 2) and inferotemporal (area 4) samples were significantly less intense than all others.

After 6 minutes of exposure with regular sunglasses, the pattern of exposure was similar. The greatest exposure was found in the mid-nasal (6) and superonasal (1) areas, followed by the midtemporal sample. The intensity measurements with the sport sunglasses with side shields were generally slightly higher than those obtained with the regular glasses, although the difference was significant only for areas 2, 3, 4, and 5. With the sport frames the superonasal and midnasal areas also were significantly darker than all other areas. No statistically significant difference was noted with the two frames in the exposure of the superonasal and midnasal areas (1 and 6).

Set Five: Sept 30, 1995 (Clear Sky)

Experiment 13. The 5.0- and 2.5-mm pupil models were compared from 9:30 to 10:15 AM (Table XVIII, Fig 63). The sun was in the southeast sky, and the head looked south. The pattern produced by the two pupil sizes is similar, although the area of exposure is smaller with the smaller pupil. The most intense concentration is found inferonasally, but the intensity of each sample is significantly less with the 2.5-mm pupil than with the 5.0-mm pupil model.

TABLE XVIIIA: 5-MM PUPIL MODEL

QUADRANT	INTENSITY/STD DEV		UV-A J/CM²	UV-B MJ/CM²	UV-A RATIO 4/2	UV-B RATIO 4/2
1	111.35	8.9	0.0547	0.1312	2.91	2.7
2	114.82	4.55	0.0515	0.125		
3	94.18	6.35	0.0735	0.1785	UV-A RATIO 4/3	UV-B RATIO 4/3
4°	61.48°	1.54	0.15°	0.338°	2.04	1.89

°DATA ON NONLINEAR PORTION OF CALIBRATION CURVES.

TABLE XVIIIB 2.5-MM PUPIL MODEL

QUADRANT	INTENSITY/STD DEV		UV-A J/CM²	UV-B MJ/CM²	UV-A RATIO 4/2	UV-B RATIO 4/2
1	128.67	7.59	0.042	0.103	3.52	3.54
2	135.69	2.85	0.0385	0.0901		
3	122.31	7.15	0.0464	0.1136	UV-A RATIO 4/3	UV-B RATIO 4/3
4°	64.29°	0.96	0.1356°	0.3188°	2.92	2.8

°DATA ON NONLINEAR PORTION OF CALIBRATION CURVES.

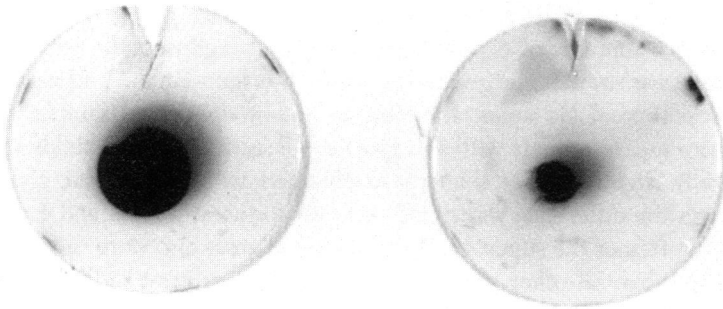

FIGURE 63
Experiment 13. Pattern of exposure with 5-mm pupil (left) and 2.5-mm pupil (right).

Experiment 14. The effect of regular sunglasses was tested with the 2.5-mm pupil from 10:30 AM to 1:01 PM on Sept 30, 1995 (Table XIX, Fig 64). The head was directed south in the direction of the sun or west (approximately 90° to the direction of the sun) to maximize exposure of the temporal side of the left orbit. Without sunglasses the inferior areas received more light than the upper areas in both positions, but the intensity of exposure of all areas is greater in gaze south than gaze west. In gaze

TABLE XIXA: GAZE SOUTH, CONTROLS (2.5-MM PUPIL)

QUADRANT	INTENSITY/STD DEV		UV-A J/CM²	UV-B MJ/CM²	UV-A RATIO 4/2	UV-B RATIO 4/2
1	121.85	2.9	0.0467	0.116	3.93	3.87
2	132.22	3.67	0.0402	0.0955		
3	84.11	20.68	0.086	0.212	UV-A RATIO 4/3	UV-A RATIO 4/3
4°	60.85°	1.61	0.158°	0.37	1.84	1.75

°DATA ON NONLINEAR PORTION OF CALIBRATION CURVES.

TABLE XIXB: GAZE WEST, CONTROLS (2.5-MM PUPIL)

QUADRANT	INTENSITY/STD DEV		UV-A J/CM²	UV-B MJ/CM²	UV-A RATIO 4/2	UV-B RATIO 4/2
1	177.36	7.91	0.0182	0.0426	2.19	2.36
2	177.00	6.13	0.0191	0.0428		
3	149.34	5.55	0.0317	0.0726	UV-A RATIO 4/3	UV-B RATIO 4/3
4	129.50	1.17	0.0418	0.1011	1.32	1.39

TABLE XIXC: GAZE SOUTH, REGULAR GLASSES (2.5-MM PUPIL)

QUADRANT	INTENSITY/STD DEV		UV-A J/CM²	UV-B MJ/CM²	UV-A RATIO 4/2	UV-B RATIO 4/2
1	200.14	4.76	0.0105	0.02115	2.74	2.93
2	200.81	5.7	0.0105	0.02115		
3	175.83	8.84	0.0195	0.0427	UV-A RATIO 4/3	UV-B RATIO 4/3
4	154.23	5.56	0.0288	0.0665	1.48	1.56

TABLE XIXD: GAZE WEST, REGULAR GLASSES (2.5-MM PUPIL)

QUADRANT	INTENSITY/STD DEV		UV-A J/CM²	UV-B MJ/CM²	UV-A RATIO 3/1	UV-B RATIO 3/1
1	218.64	6.17	0.0052	0.0082	1.17	1.28
2	214.58	1.24	0.0061	0.0104		
3	213.64	2.79	0.0061	0.0105		
4	214.19	3.51	0.0061	0.01047		

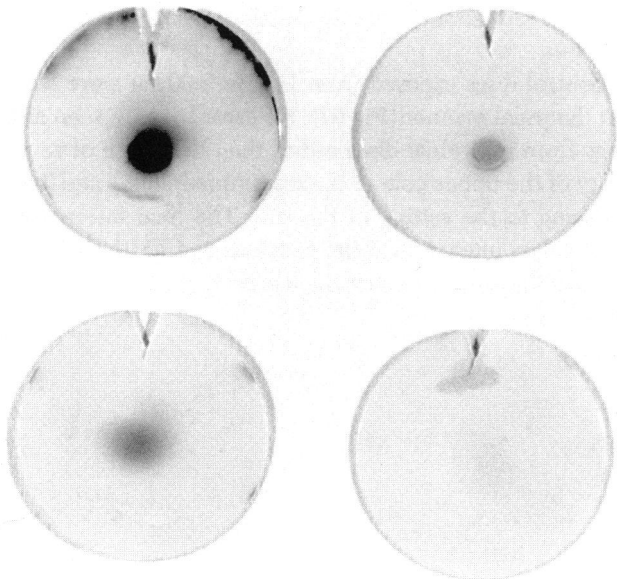

FIGURE 64

Experiment 14. Pattern of exposure with 2.5-mm pupil model oriented south toward sun without sunglasses (upper left) and with sunglasses (upper right), and west without sunglasses (lower left) and with sunglasses (lower right).

south the superonasal sample is significantly darker than the superotemporal sample, and the inferonasal sample is darker than the inferotemporal sample. In gaze west no difference is detected in the intensity of exposure of the superonasal and superotemporal samples; the inferonasal area is significantly darker than the inferotemporal area.

Sunglasses reduced the intensity of exposure in all samples; the exposures in gaze south remain significantly darker than in gaze west. When looking south toward the sun the inferonasal sample is significantly darker than all others, and the inferotemporal sample is darker than both superior samples. In gaze west, the intensity of exposure is uniformly light.

Experiment 15. The effect of the lid masks was studied with the 2.5-mm pupil model in the left orbit from 12:06 to 1:01 PM on Sept 30, 1995. The head was oriented south. The pattern of exposure with no lids and the regular lid mask was similar (Table XX, Figs 65 and 66). There was no significant difference between the intensity of the inferotemporal and inferonasal areas. The squint mask attenuated light intensity in all samples. The inferior samples remain significantly darker than the superior samples. As in experiment 16, rather large standard deviations are noted on the inferotemporal and inferonasal bar graphs (sections 3 and 4), due to the movement of the sun.

Three control discs exposed from 1:15 to 2:00 PM were scanned and analyzed in the usual manner (Fig 67). No error bars are seen as these are the readings from individual discs rather than the mean of several discs. The intensity of the upper pole of the discs (quadrants 1 and 2) decreases with time owing to the setting of the sun. The final inferonasal sample (quadrant 4) is less intense than the previous two. With westward movement of the sun the nasal aspect of the left orbit gradually was thrown into shadow from the nose.

TABLE XXA: CONTROLS (2.5-MM PUPIL)

QUADRANT	INTENSITY/STD DEV		UV-A J/CM²	UV-B MJ/CM²	UV-A RATIO 3/1	UV-B RATIO 3/1
1	121.52	13.78	0.0471	0.116	2.81	2.72
2	139.22	10.7	0.0365	0.088		
3°	65.52°	2.34	0.1325°	0.315°	UV-A RATIO 3/4	UV-B RATIO 3/4
4	91.04	29.33	0.0757	0.189	1.75	1.67

°DATA ON NONLINEAR PORTION OF CALIBRATION CURVES.

TABLE XXB: NORMAL LID (2.5-MM PUPIL)

QUADRANT	INTENSITY/STD DEV		UV-A J/CM²	UV-B MJ/CM²	UV-A RATIO 3/1	UV-B RATIO 3/1
1	122.78	16.34	0.0462	0.113	2.52	2.39
2	141.34	2.2	0.0346	0.084		
3°	70.23°	16.19	0.1163°	0.27°	UV-A RATIO 3/4	UV-B RATIO 3/4
4	86.67	12.25	0.0826	0.20	1.41	1.35

°DATA ON NONLINEAR PORTION OF CALIBRATION CURVES.

TABLE XXC: SQUINT LID MAST (2.5-MM PUPIL)

QUADRANT	INTENSITY/STD DEV		UV-A J/CM²	UV-B MJ/CM²	UV-A RATIO 4/1	UV-B RATIO 4/1
1	167.00	6.32	0.0224	0.0512	1.47	1.50
2	169.82	14.24	0.021	0.048		
3	155.07	8.76	0.0279	0.0643	UV-A RATIO 4/3	UV-B RATIO 4/3
4	146.93	5.77	0.033	0.077	1.18	1.20

°DATA ON NONLINEAR PORTION OF CALIBRATION CURVES.

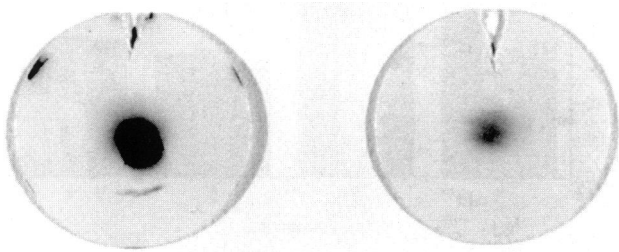

FIGURE 65

Experiment 15. Pattern of exposure with 2.5-mm pupil and normal lid mask (left) and squint lid mask (right). Pattern of control discs was similar to that with normal lid mask.

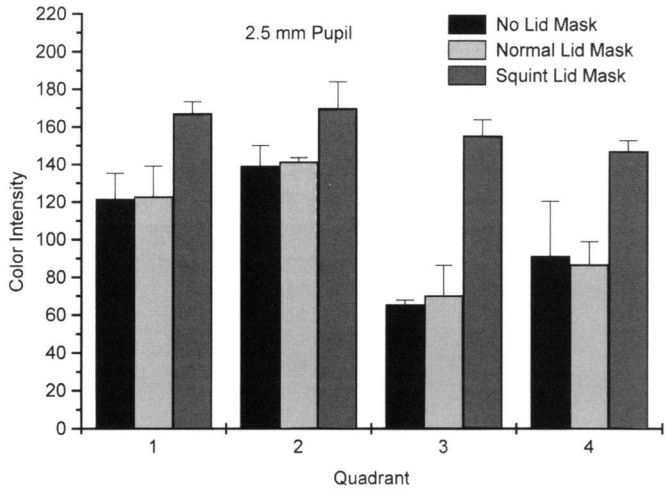

FIGURE 66

Experiment 15. Mean color intensity (2.5-mm pupil) in superonasal (1), superotemporal (2), inferotemporal (3), and inferonasal (4) quadrants.

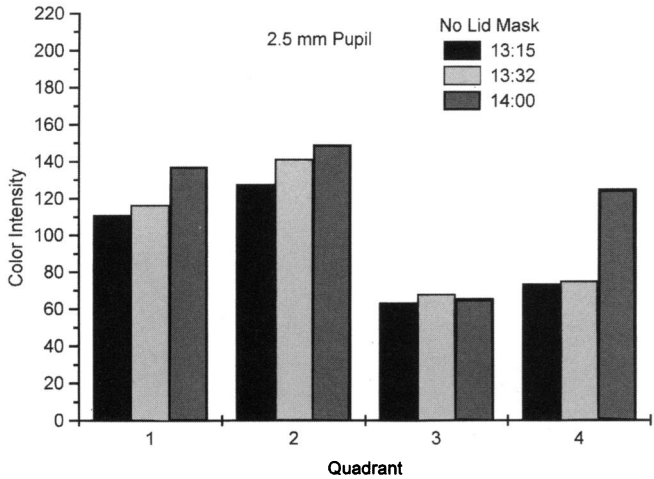

FIGURE 67

Experiment 15. Pattern of three control discs (2.5-mm pupil) to illustrate change in intensity of exposure with movement of sun. Third inferonasal sample (4) is lighter than first two owing to shadow cast by nose and superonasal brow.

Experiment 16. With the normal and squint lid masks and the 2.5-mm pupil model, the head was turned to the west-northwest so that it was 90° to the sun to maximize exposure of the temporal side of the skull from 1:13 to 2:05 PM (Table XXI, Fig 68). The inferior portion of the discs received more light than the upper portion of the discs with both lid masks; the squint mask attenuated the intensity of exposure.

Set 6: Dec 30, 1995 (Clear Sky)

TABLE XXIA: NORMAL LID MASK (2.5-MM PUPIL)

QUADRANT	INTENSITY/STD DEV		UV-A J/CM²	UV-B MJ/CM²	UV-A RATIO 4/1	UV-B RATIO 4/1
1	197.75	2.91	0.0116	0.0234	2.80	3.2
2	192.78	7.95	0.0127	0.0253		
3	167.44	14.39	0.0224	0.0493	UV-A RATIO 4/3	UV-B RATIO 4/3
4	147.42	6.63	0.0325	0.075	1.45	1.52

TABLE XXIB: SQUINT LID MASK (2.5-MM PUPIL)

QUADRANT	INTENSITY/STD DEV		UV-A J/CM²	UV-B MJ/CM²	UV-A RATIO 4/1	UV-B RATIO 4/1
1	209.86	5.644	0.0073	0.0123	2.79	3.66
2	208.17	6.0	0.00734	0.0146		
3	177.70	5.72	0.0181	0.0426	UV-A RATIO 4/3	UV-B RATIO 4/3
4	172.28	4.36	0.0204	0.045	1.13	1.06

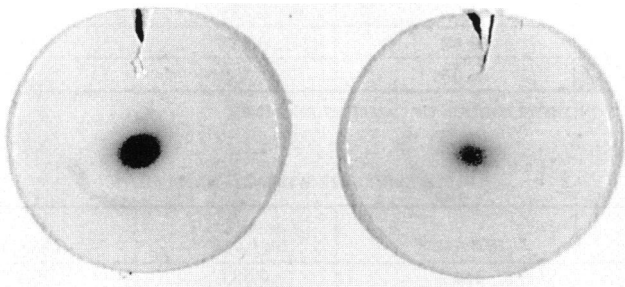

FIGURE 68

Experiment 16. Pattern of exposure with 2.5-mm pupil and normal lid mask (left) and squint lid mask (right).

Experiment 17. Our intention had been to do the final exposure on the shortest day of the year. However, persistent overcast conditions prevented conducting the experiment before Dec 30, when the sky was clear except for occasional high wispy clouds (Table XXII).

A single exposure with the 5.0-mm pupil was made with the head oriented south at 12:18 pm. With the 7.5-mm pupil, single exposures were recorded with the head oriented south at 12:29 PM and southwest at 12:50 PM. Calibration strips were prepared before and after the exposure of the models (Figs 44 and 45). At this time of day, the sun was nearly due south and near its maximum altitude for all exposures (Table I). When the head was oriented south, the eye was exposed to direct sun, and all quadrants were uniformly dark (Table XXII). When the head was turned to the west,

TABLE XXII: GAZE SOUTH, 5-MM PUPIL

QUADRANT	INTENSITY	UV-A J/CM²	UV-B J/CM²
1	57°	0.264	0.439
2	51.48°	0.338	0.48
3	51.19°	0.338	0.48
4	51.9°	0.338	0.48

°DATA ON NONLINEAR PORTION OF CALIBRATION CURVES.

TABLE XXII: GAZE SOUTH, 7.5-MM PUPIL

QUADRANT	INTENSITY	UV-A J/CM²	UV-B J/CM²
1	54.57°	0.290	0.467
2	51.33°	0.338	0.48
3	51.86°	0.338	0.48
4	51.38°	0.338	0.48

°DATA ON NONLINEAR PORTION OF CALIBRATION CURVES.

TABLE XXII: GAZE WEST, 7.5-MM PUPIL

QUADRANT	INTENSITY	UV-A J/CM²	UV-B J/CM²
1	114.9	0.083	0.107
2	121.38	0.075	0.096
3	103.62	0.099	0.131
4	76.29	0.167	0.271

°DATA ON NONLINEAR PORTION OF CALIBRATION CURVES.

the overall intensity in each quadrant was less than with gaze south, and the lower quadrants, especially the inferonasal quadrant, received more light than the upper quadrants. Statistical comparison is not possible, because only single exposures were recorded in each gaze position. With the head looking west, the intensity of UV-A exposure in the inferonasal sample is approximately 2.25 times greater than in the superotemporal area, and the intensity of UV-B exposure is approximately 2.8 times greater inferonasally than superotemporally.

DISCUSSION

MECHANISMS

How Does Light Damage the Lens?

The biological effects of ultraviolet radiation on the eye are complex and have been reviewed in detail.[107,178-185] Only major issues will be touched upon here.

The terrestrial intensity of solar ultraviolet increases approximately exponentially from 280 to 320 nm, while the sensitivity of tissue decreases approximately exponentially.[186,187] Wavelengths of 290 nm are estimated to be 1,000 to 10,000 times more effective in producing tissue injury than wavelengths above 330 nm.[133] The action spectrum for mammalian cells is similar to the DNA absorption spectrum over wavelengths 297 to 313 nm,[187-189] and wavelengths between 313 and 334 nm are most effective in producing cell inactivation, mutation, and DNA single strand breaks.[190-197] Animal studies suggest that X-irradiation produces cataract by damaging cell nuclei in the germinative zone of the lens epithelium,[198] and it is possible that UVR may injure the nuclear DNA of the lens epithelium.[199-201] However, the mitochondria and plasma membrane also have been shown to be injured by ultraviolet.[180,187,202,203]

UVR also may affect lens proteins,[204-210] enzyme systems,[211-215] and transmittance of light.[216-219] The two principal chromophores that absorb and dissipate radiant energy between 295 and 400 nm in the young human lens are tryptophan and 3-hydroxykynurenine.[220,221] The concentration of 3-hydroxykynurenine decreases with age while the concentration of yellow compounds increases, resulting in a progressive increase in light absorption with age.[220-225] Ultraviolet radiation is more potent in the presence of oxygen, indicating that the generation of free radicals may be a mechanism of tissue injury.

Within 6 hours of exposing Sprague-Dawley rats to 1.5 J/cm^2 of UV light (280 to 380 nm), Gillardon and colleagues[227] detected c-fos and c-Jun positive nuclei in the epithelium of the cornea and lens, prior to morphologic signs of tissue injury. They speculated that the appearance of these

transcription factors may be part of evoked apoptosis and that apoptosis may play a role in cataract formation.[228] Injury to lens sutures also may play a role in the development of opacities.[229,230]

Perhaps the most convincing experimental evidence that ultraviolet light is cataractogenic is the production of cataract in experimental animals. In 1907 Hess[231] used ultraviolet to produce cataracts in rabbits, and Duke-Elder[140,141] subsequently studied the effect of various wavelengths of light on the development of keratitis and cataract. Both broad-band and laser light have been used to produce lens opacities in a variety of species, including mice, rats, rabbits, squirrels, trout, and primates.[232-243]

What Else May Contribute to Cataractogenesis?

Fisher[244-248] has proposed that the increase in lens thickness and a decrease in elasticity of the anterior capsule account for the progressive loss of accommodation with age, and he further suggests that maximum accommodative stress occurs during the fifth decade of life. Thereafter, the strength of the ciliary muscle is thought to decline. Fisher has proposed that the "trauma of accommodation" injures the superficial cortical fibbers, leading to the appearance of cortical opacities. This hypothesis remains to be confirmed, and it may be significant that cortical opacities are not distributed uniformly around the equator of the lens.

An epidemiologic study in India suggested that the risk of blinding cataract was about three times higher among those exposed to severe dehydration.[249] A smaller study based on interviews of patients having cataract surgery at the Oxford Eye Hospital revealed that severe diarrhea was a "marginal" risk factor there. The investigators stated that the association was stronger among patients of 70 to 79 years old, which they attributed to military service in the Far East during World War II.[250-252] Cataract was not noted to be among the effects of slow starvation on English and Soviet POWs during World War II, although the time of follow-up was limited[253]; and other studies have failed to confirm the association of diarrhea with cataract.[254] Harding[252] has challenged the causal association of sunlight and cataract, and a survey of fishermen in Hong Kong in 1989 failed to find a statistically significant association of sun exposure or antioxidant status with cataract.[255] Harding has pointed out that pterygium, climatic droplet keratopathy, and cataract all are thought to be related to sun exposure, yet these conditions have not been proved to be associated with one another. The association of ultraviolet exposure and pterygium was confirmed by Darrell in 1963 in a large study of American veterans.[256] The Waterman study also confirmed the association of climatic droplet keratopathy and pterygium with ultraviolet exposure.[94] It seems likely that a

disorder of the cornea would reduce UVR dose to the lens.

The development of cataract is undoubtedly multifactorial.[257] Epidemiologic studies in Europe and North America have revealed some potential risk factors, although association does not necessarily imply causation. Variables associated with cataract in the Framingham Eye Study included education below the seventh grade, diabetes, hypertension, short stature, reduced vital capacity, elevated serum phospholipids, and reduced hand grip strength.[258] An epidemiologic study of 931 cataract patients in southeast Scotland revealed positive correlations with age-related macular degeneration; psychiatric illness; use of major tranquilizers; smoking; number of pregnancies; genetic eye disease; high serum bilirubin; heart disease; physical injury to the eye or eye surgery; use of diuretics, miotics, or corticosteroids; rural environment; high serum phosphate and creatinine; diabetes; hypertension; occupation involving exposure to animal infections; glaucoma; excess alcohol use; and high serum urea level.[259]

Risk factors also have been linked to type of cataract.[260] In one study the risk of all types of lens opacities increased with decreasing education and decreased with intake of multivitamins. Riboflavin and vitamins C, E, and carotene were protective for the development of cortical, nuclear, and mixed cataract. Use of oral steroids increased the risk of posterior subcapsular cataract, and diabetes increased the risk of posterior subcapsular and mixed cataract. The risk of nuclear cataract increased with nonprofessional occupation, smoking, body mass index, and occupational exposure to sunlight. The risk of mixed cataract increased with use of gout medications, family history, and myopia in youth. Increased intake of vitamin E has been claimed to decrease the risk of nuclear cataract and an increased intake of iron may lower the risk of cortical cataract.[261] Another study failed to find a protective effect of higher serum levels of carotenoids and tocopherols on nuclear and cortical cataract.[262]

Two studies have addressed the role of smoking in cataractogenesis.[263,264] Men who smoked more than 20 cigarettes per day at the time of the study had an increased risk of both nuclear and posterior subcapsular opacities, and men who had smoked more than 20 cigarettes per day in the past had only an increased risk of PSC cataract.[263] Among women cigarette smoking also was strongly associated with PSC cataract.[264] In the Beaver Dam Eye Study hypertension was associated with PSC cataract after adjustment for age, gender, and diabetes; diabetes was a risk factor for cortical cataract.[265]

The Physicians' Health Study of 17,764 male physicians 40 to 84 years old in the United States has reported that the leanest men had the lowest rates of cataract surgery, and higher body mass index was strongly associ-

ated with both PSC and nuclear cataract.[266] The study also found that users of a multivitamin had reduced rates of surgery, while current smokers and those who had a myocardial infarction before age 60 had a higher risk of surgery. It is difficult to compare studies involving different populations and data collection methods, but the epidemiologic evidence suggests that there are nutritional and socioeconomic influences on cataract development.[267] How these factors may interact with one another remains to be determined.

Heiba and colleagues[268] used sister-sister and brother-brother correlation of the percentage of the lens area involved with cortical cataract in 1,275 individuals in the Beaver Dam Eye Study to propose that a single major gene may account for 58% of the variability of cortical cataract. They suggest that this effect is independent of environmental influences and also that sex affects residual variance.

How Significant Is the Problem of Cataract Blindness?

The availability and accuracy of data on the causes of blindness vary, and estimates of the number of cataract blind in the world are only approximate. In the United States, blindness is defined legally as best corrected acuity less than 6/60. In contrast, the World Health Organization (WHO) criterion for blindness is best corrected acuity of less than 3/60. Using data from 1980 or earlier, Hyman[269] reported in 1987 that the number of blind in the world was about 42 million, of whom about 17 million were blind from cataract. Thirteen of these seventeen million were found in developing nations and four million in the developed countries. The 1987 figures of the WHO suggest that there are 27 to 35 million blind in the world and at least an equal number of persons with low vision. In 1993 the WHO estimated that more than 50 million people needed cataract surgery.[270]

The prevalence of blindness is linked to age. In nations that maintain registries, the blindness rate increases from approximately 0.5% to 10% between the ages of 65 and 90.[259] In the vicinity of Alexandria, Egypt, in 1970 the prevalence of cataract blindness (acuity less than 6/60) among men over age 60 was 60.9 per 1000 in urban areas and 150 per 1000 in rural communities. The comparable figures for women were significantly higher: 84.4 and 258.1 per 1000.[271] In Nepal the prevalence of blindness also is higher among women than men.[269] By the WHO criterion the prevalence of blindness in the total population in Saudi Arabia in 1986 was 15.1 per 1,000, but over age 60 the prevalence rose to 152.3 for men and 282.7 per 1,000 for women. Over 1.5% of the total population and over 20% of the population over age 60 were blind, and cataract accounted for more than half the cases of blindness. In contrast, by the American criterion only

0.2% of the population of the United States is considered blind.[272] The first epidemiologic study of cataract blindness in central India sampled 1,735 persons over age 30. Based on an estimated population of 827,152,000 people, the incidence rates of the survey projected a minimum of 3.8 million new cases of cataract blindness per year.[273]

Although the need for cataract surgery is greatest in the developing countries, where the number of people over age 55 may exceed 1.1 billion by 2025, the changing demography of Europe and North America indicate that the need will increase there as well.[274] As in the developing world, in Europe and North America visual acuity declines with age and the prevalence of cataract rises. WHO estimated that the population 60 years old and older in Europe will increase from about 14% in 1993 to 35% by the year 2050.[270] One third of the 601 inhabitants of Turku, Finland between the ages of 65 and 69 had a cataract in at least one eye; after age 85 this rose to 87%.[275] A survey in the Kuopio district of Finland in 1989 found that 41.7% of the population born in 1924 had cataract, while 91.1% of those born in 1914 had cataract.[276] Another Finnish survey, in Oulu County, found a prevalence of cataract of 44.6% at ages 70 to 74 and 97.6% at ages 85 to 89.[277] In the Melton Mowbray area of England, 46.1% of people over age 76 had vision worse than 6/9 due to cataract.[278]

In the United States in 1970, the prevalence of cataract blindness, defined as corrected acuity less than 6/60 in the better eye, was 13.5/100,000, and the incidence increased with age.[279] Between 1980 and 2030, the number of persons over age 55 may increase by 82%, and the number of people over age 85 may increase by 150%. More than a million cataract operations have been performed annually in the United States since 1987.[274] If the development of cataract could be delayed by 10 years, the number of operations might be halved.[280]

What Can Be Learned from the Global Distribution of Cataract?

The variation among the nations of the world in the collection and reporting of data on the prevalence and causes of blindness makes precise comparison of societies difficult. Nonetheless, differences in the global distribution of eye diseases may help to reveal the relation of diet, ethnicity, culture, heredity, and climate to various disorders.[281] Considerable effort is directed to controlling infectious causes of blindness, but efforts to delay the development of cataract may be limited by the perception that cataract is a normal and inevitable accompaniment of aging.[282] In the tropics the average lifespan is shorter than at northern latitudes, and shorter lifespan should lower the prevalence of disorders associated with aging, such as cataract. In the tropics infectious and nutritional diseases, such as tra-

choma, onchocerciasis, and vitamin A deficiency, account for much blindness. These problems, which are virtually nonexistent in the developed world, must lower the percentage of blindness due to cataract where they are prevalent. How can we account for the fact that the prevalence of blindness due to cataract is about five times greater in the tropics than at latitudes greater than 46°? The greater proportion of cataract blindness in the tropical zone appears to occur despite the reduction of lifespan and the prevalence of infectious and nutritional causes of blindness.[107,283]

Across societies, cultures, and races, the prevalence of cataract and cataract blindness increase consistently with two factors: age and decreasing latitude. The only variable yet known to be associated with latitude is solar radiation. In the course of a year at the equator the maximum angle of the sun above the horizon varies from 90° (directly overhead) to 66.5°. At midlatitudes the maximum angle varies from 73.5° to 26.5°, and in the Arctic from 47° to 0°. Radiation traversing the atmosphere loses energy from scatter and absorption, and energy loss thus increases as path length through the atmosphere increases. The annual direct and scattered radiation under a clear sky for wavelength 320 nm is about 3.8 times greater at the equator than at the Arctic or Antarctic Circles. At 330 nm the energy is three times greater; and at 340 nm, where ozone effects are minimal, it is 2.7 times greater.[107] The prevalence of cataract is clearly consistent with the increase in UVR with decreasing latitude, and epidemiologic studies also have shown that UVR specifically influences the development of cortical opacities. It may be significant that the controls for these studies were not individuals with no UVR exposure, but rather persons from the same geographic area with less UVR exposure. It seems likely that the association of UVR, especially UV-B, with cortical cataract would be shown more clearly if groups from widely varying latitudes and ambient UVR levels were compared. Such a study also might demonstrate more clearly the relationship of UVR to nuclear and PSC cataract. The mechanism of UVR cataractogenesis remains to be worked out, but the association of UVR, especially UV-B, with cataractogenesis has been established .

What Does This Study Show? Geometric optics and the eye models confirm that the position of the sun relative to the eye determines the area within the lens of greatest light exposure, and under normal daylight conditions the inferior lens receives a higher dose of UVR than the upper portion of the lens. With the models the area of greatest exposure can be moved predictably by changing the angle of the eye relative to the sun. The inferonasal lens receives more light energy than the inferotemporal lens because the superonasal orbital rim is more prominent than the superolateral orbital rim; and when the sun is low in the sky or the head is

turned 90° to the sun, the nose protects the eye more effectively than the temporal orbital rim.

Because the cornea and lens produce a converging ray bundle, irradiance is strongly dependent on position within the eye. The elevation of the sun ensures that the inferior lens receives more light energy than the superior lens. For the same reason, it is certain that the inferior retina receives more light energy than the superior retina, but the irradiance at the plane of the retina is much greater than at any plane within the lens. Whether the concentration of light on the inferior retina is clinically significant is not known but appears to warrant investigation.

To our knowledge, this is the first attempt to measure the energy flux through different regions of the lens. Using a mannequin with sensors on the vertex of the head and in the orbit, Rosenthal and colleagues[284,285] demonstrated that the dose to the orbit is about 20% of that to the top of the head and that glasses and a brimmed hat could further attenuate the exposure of the orbit. The development of a small dosimeter might provide more precise information on exposure of an individual under different conditions.[286] In this study calibrated exposure of photosensitive paper was used to estimate dose to the equator of the lens . The color of the paper is a function of incident energy, and the color reaches a maximum beyond which additional energy produces no color change. In many cases, after 2 minutes of exposure part of the disc reached the maximum or near-maximum color change. As the areas of most intense light exposure are those most likely to develop cataract, the UVR dose to these regions is of particular interest. Estimates of energy dose made from the nonlinear portions of the calibration curves, however, are uncertain. With shorter exposure times, the color change of the photosensitive discs may be kept on the linear or nearly linear portion of the calibration curves, permitting more accurate estimation of UVR dose to these regions of the lens.

Some of the exposures, however, permit an estimate of the relative energy dose to the lens equator. Table XXIII summarizes the ratios of maximum to minimum UV-A and UV-B recorded from the linear portion of the calibration curves. In these experiments, the ratio of the greatest exposure in the lower half of the disc to the least exposure in the upper pole of the disc was between 2 and 3. Attenuation of light by shadow, clouds, or the atmosphere lowers this ratio; it is possible that UVR exposure of the lower half of the lens in bright direct light is more than two or three times that of the upper portion of the lens. High scatter or albedo could lead to greater relative exposure of the upper portion of the lens than was noted in this study, and the pattern of light exposure on snow and white sand remains to be studied with the models.

TABLE XXIII: RATIO OF MAXIMUM/MINIMUM UVR

EXPERIMENT	MAX/MIN UV-A	MAX/MIN UV-B
3	1.8 - 2.7	2.4 - 2.9
4	2.37	2.53
5	2.53	2.69
6	1.97	2.06
9	2.56	2.8
14	2.74	2.93
17	2.25	2.8

Estimating dose to specific regions of the lens is complex because transmittance depends on both wavelength and path length, and the transmittance of the lens changes with age. With accurate data on transmittance and index of refraction in the UV, more precise estimates of potential energy dose will be possible.

Coroneo[114,115] has suggested that light entering the eye laterally strikes the cornea with a high angle of incidence and is concentrated to the opposite limbus and the inferonasal lens, accounting for the common location of pterygium and cortical cataract. To assess the effect of temporal oblique light on the lens, the eye models were exposed with three styles of sunglasses with different frames. The relation of the frame to the brow proved to be more significant than the size of the temple in determining exposure of the discs (Figs 69 through 71). The standard frame with a thin temple conformed best to the brow; and with the head in the general direction of the sun, the standard frame attenuated light in the lower portion of the lens at least as effectively as either frame with a wide temple (experiments 3, 5, 7, 11, and 12). A spectacle frame with a broad temple may be protective in some settings, although when the sun was obscured by clouds, no benefit of the side shields could be demonstrated even when the head was turned to maximize exposure of the temple (experiments 11 and 12). As the eyes move from side to side, light may strike the cornea obliquely (Fig 25) even if the sun is not high in the sky or the head turned so that the direction of the sun is roughly normal to the temple. Under most daylight conditions, it appears that the lens is better protected by shielding light from above than shielding light from the side. It is not surprising that sunglasses and a cap with a brim cut exposure of the inferior lens more effectively than sunglasses alone (experiment 4).

FIGURE 69
Standard frame conforms to brow of model skull.

FIGURE 70
Space is seen between brow and sport frame with side shields.

FIGURE 71
Gap is visible between wraparound frame and brow.

As the pupil enlarges, the eye models show that more of the lens is exposed to light, and the ray tracings show clearly that the total power entering the eye increases. The maximum potential irradiance through a 3-mm pupil is virtually the same as that of a 7-mm pupil, but the larger pupil admits more light at all angles of incidence. When the sun is at zenith, maximum potential total power incident on an eye with a 3-mm pupil looking directly at the sun is approximately equivalent to the power received by an eye with a 7-mm pupil turned so that the angle of incidence is 90° (Table IV). However, at the higher angle of incidence, maximum potential irradiance approximately doubles and the area of maximum exposure of the lens moves toward the periphery. Constriction of the pupil thus protects the lens by both decreasing the area of exposure and reducing the total power of light entering the lens (Tables IV and V, Figs 20 through 23).

The eyelids also help to protect the eye. With the normal lid mask, the upper pole of some discs appeared lighter than controls, although this effect was not demonstrated consistently. The squint lid mask attenuated overall levels of light (experiments 7, 15, 16, and 17) in all quadrants,

although the inferior lens still received more light than the superior lens.

When the sun is directly overhead, maximum potential irradiance increases as the angle of incidence increases, and the size of the ray bundle, or total power, decreases. However, maximum irradiance changes little until angles of incidence greater than about 80° are reached (Table III, Figs 20 and 21). As the brow blocks direct light above about 64°, the eye may not be exposed to such high angles of incidence frequently.

The sun is in constant motion, and the relation between total power and irradiance for varying solar elevation may describe exposure of the eye more realistically. With the 3-mm pupil maximum total power is reached when the solar elevation is between about 40° and 50°. With the 7-mm pupil, maximum potential total power is reached between approximately 60° and 70°. At 64°, the maximum elevation at which direct light clears the brow of the model, the total power received through the 7-mm pupil is about 5.5 times that received through the 3-mm pupil, with comparable irradiance (Table V).

Whether total power or maximum irradiance is more significant to the development of cataract must depend on the threshold of sensitivity of lens cells to UVR damage. If cataract is the result of injury to a small group of cells, maximum irradiance may be the most important factor. If the development of cataract is due to injury to a large number of cells at lower energy levels, then total power at lower irradiance may be the more important factor. Damage to cells undoubtedly also depends on time of exposure and the ability of cells to recover after exposure. It is certain that the inferior half of the lens receives a higher cumulative dose than the superior half of the lens, and the potential time of exposure to higher energy increases with decreasing latitude.

It is interesting to compare color intensity recorded in the quadrants of the discs to the prevalence of cortical cataract in the same quadrants (Fig 72). Exposures with sunglasses from experiment 3 were chosen, as these data all plot to the linear portion of the calibration curves. Mean color intensity in the four quadrants was plotted against the percent of cortical opacities noted by Schein and colleagues[103]: 6.4% superonasal (quadrant 1), 12.8% superotemporal (quadrant 2), 17% inferotemporal (quadrant 3), and 63.8% inferonasal (quadrant 4). The correlation is linear, and the plot helps to illustrate that cortical cataract is dose-dependent. Other data from the experiments can be plotted in this way, and the slopes vary somewhat. If data from the nonlinear portion of the calibration curves are included, the slope is less steep, suggesting that estimates taken from this portion of the calibration curves are low.

The distribution of cortical cataract has been documented since the

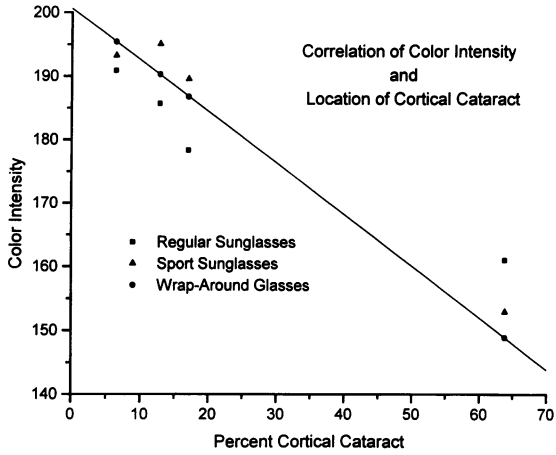

FIGURE 72

Correlation of reported prevalence of cortical cataract by quadrant with mean color intensity of same quadrants of photosensitive discs from experiment 3.

turn of the century, and the association of ultraviolet light with cataract has been suspected for nearly 100 years. In 1684 van Leeuwenhoek wrote:

> If we attentively look at the said crystalline body fresh from the eye, we still find that no glass exceeds it in transparency, although it consists of so many thousands of fibres; well may we say that it is a wonderful thing in our eye; the more so when we consider how closely and tightly these fibres must be conjoined in order that the light can go straight through it; for if this were not the case, the crystalline body would not appear to our eyes to be transparent but white.[32]

Cataract is due at least in part to dose-dependent UV exposure, and decreasing the cumulative exposure of UV may slow the progression of normal aging changes within this "wonderful thing in our eye."

ACKNOWLEDGEMENTS

The author is grateful to many people without whose interest and assistance this work would not have been possible. Dr. Charles Koester's expertise in physiological optics was essential to the design of the eye models and the computer ray tracings. Dr. James Dillon first suggested trying to model the anterior segment, and his encouragement is gratefully acknowledged. While a medical student, Dr. Priya Narayanan spent two summers assisting with the experiments described here, and her gracious

enthusiasm made the work a pleasure. Mr. Heinz Rosskothen constructed the eye models with care and precision. Dr. Lisa Tian, the librarian of the John S. Wheeler Library at the Edward S. Harkness Eye Institute, assisted with the bibliographic research for the paper, especially that involving the Institute's Rare Book collection. The Health Sciences Library of the College of Physicians and Surgeons, especially its Jerome P. Webster Collection of Rare Books, and the library of the New York Academy of Medicine also were valuable resources. Drs. Hindola Konrad and Herman Schubert assisted with the translation of articles from German. Ms. Amy Gallagher, Assistant Producer at the Hayden Planetarium of the American Museum of Natural History in New York, provided data on solar elevation and azimuth for different seasons and locations. Mr. Charles Manley and Mr. Stephen J. Douglas prepared the photographic illustrations, and Dr. Daniel Casper and Mr. Richard Harris prepared the line drawings. The author's secretaries, Ms. Theresa Conyers and Ann-Marie Kelly, helped in many ways with the preparation of the manuscript. The author also wishes to thank Drs. James Dillon, Charles Koester, Max Forbes, Robert Kennedy, and George R. Merriam, Jr., for reviewing portions of the manuscript.

REFERENCES

1. Atkinson DT. The evolution of cataract surgery. *J Ophthalmol Otolaryngol* 1926; 30:322-327.
2. Chance B. *Ophthalmology*. New York, Hafner Publishing, 1962.
3. Duke-Elder WS, Wybar KC. *The Anatomy of the Visual System*. In: Duke-Elder WS, ed. *System of Ophthalmology, Vol II*. London, Henry Klimpton, 1961.
4. Gordon BL. The problem of the crystalline lens. *Arch Ophthalmol* 1935; 14:774-788.
5. Gorin G. *History of Ophthalmology*. Wilmington, Delaware, Publish or Perish Inc, 1982.
6. Kirby DB. The early history of cataract surgery. *Surgery of Cataract*. Philadelphia, JB Lippincott, 1950, pp 3-18.
7. Kirby DB. The development of cataract extraction. *Surgery of Cataract*. Philadelphia, JB Lippincott, 1950, pp 19-35.
8. Lindberg DC. *Theories of Vision from Al-Kindi to Kepler*. Chicago, University of Chicago Press, 1976.
9. Siraisi NG. *Medieval and Early Renaissance Medicine: An Introduction to Knowledge and Practice*. Chicago, University of Chicago Press, 1990.
10. Sorsby A. *A Short History of Ophthalmology*. 2d ed. London, Staples Press, 1948.
11. Stricker L. A historical review of the development of the cataract operation. *J Ophthlalmol Otolaryngol* 1909; 3:403-413.
12. Siraisi NG,[9] p 108.
13. Elliot RH. The Indian operation of couching for cataract, incorporating the Hunterian Lectures. New York, PB Hoeber, 1918.
14. Snyder C. Aurelius Cornelius Celsus on cataracts. *Arch Ophthal* 1964; 71:144-146.
15. Sood NN, Ratnaraj A. Couching for cataract: Hazard and management. *Am J*

Ophthalmol 1968; 66:687-693.
16. Talbott JH. *A Biographical History of Medicine: Excerpts and Essays on The Men and their Work*. New York, Grune & Stratton, 1970.
17. Debus AG. The study of man. *Man and Nature in the Renaissance*. New York, Cambridge University Press, 1990, pp 54-73.
18. Schultz B. *Art and Anatomy in Renaissance Italy*. Ann Arbor, Mich, University of Michigan Research Press, 1985.
19. Roberts KB, Tomlinson JD. *The Fabric of the Body: European Traditions of Anatomical Illustration*. Oxford, Clarendon Press, 1992.
20. Benevenutus G; Wood CA, trans. *De Oculis*. Palo Alto, Calif, Stanford University Press, 1929.
21. Ibid, p 76.
22. O'Malley CD. *Andreas Vesalius of Brussels, 1514-1564*. Berkeley, Calif, University of Calif Press, 1964.
23. Ibid, p 82.
24. Vesalius A. *Humani Corpora Fabrica*. Basileae, Libri Septum, 1543.
25. Choulant L; Frank M, trans and ed. *History and Bibliography of Anatomic Illustration in Its Relation to Anatomic Science and the Graphic Arts*. Chicago, University of Chicago Press, 1920.
26. Castiglioni A; Krumbhaar EB, trans. *A History of Medicine*. New York, AA Knopf, 1941.
27. Hind AM. *A History of Engraving and Etching From the Fifteenth Century to the Year 1914*. New York, Dover Publications, 1963.
28. Bartisch G. *Das Ist Augendienst*. Dresden, M Stöckel, 1583.
29. Hirschberg J, Blodi FC, trans. *History of Ophthalmology, Vol II. The Middle Ages: The Sixteenth and Seventeenth Centuries*. Bonn, Verlag, 1985.
30. Fabricius H. *De Visione, Voce, Auditu*. Venice, Franciscum Bolzettam, 1600.
31. Van Leeuwenhoek A. Letter 11. *The Collected Letters of Antoni Van Leeuwenhoek. Vol I*. Amsterdam, Swets & Zeitlinger, 1939.
32. Van Leeuwenhoek A. Letter 80. *The Collected Letters of Antoni Van Leeuwenhoek. Vol VI*. Amsterdam, Swets & Zweitlinger, 1952.
33. Hubbell AA. Jacques Daviel and the beginnings of modern operation of extraction of cataracts. *JAMA* 1902; 39:177-185.
34. Maître-Jan A. *Traité des Maladies de l 'Oeil (et Des Rémedes Propres pour leur Guérison, Enrichy de plusieurs Experiences de Physique)*. Troyes, France, J LeFebure, 1707.
35. Zinn JG. *Descriptio Anatomica Oculi Humani*. Gottingen, Germany, A Vandenhoeck, 1755.
36. de Saint Yves C; Stockton J, trans. *A New Treatise of the Diseases of the Eyes*. London, Society of Booksellers, 1741, p 52.
37. DeWenzel M; Ware J, trans. *A Treatise on the Cataract; With Cases to Prove the Necessity of Dividing the Transparent Cornea, and the Capsule of the Crystalline Humor, Differently, the Different Species of the Disease*. London, C Dilly, 1791; Birmingham, England, Classics of Ophthalmology Library, Gryphon Editions, 1984.
38. Perera C. Albrecht von Graefe, founder of modern ophthalmology. *Arch Ophthalmol* 1935; 14:742-773.
39. Scarpa A; Briggs J, trans. *Practical Observations on the Diseases of the Eyes*. London, Cadell & Davies, 1806; Birmingham, England, Classics of Medicine Library, Gryphon Editions, 1980.
40. Frick G. *A Treatise on the Diseases of the Eye Including the Doctrines and Practice of the Most Eminent Modern Surgeons and Particularly Those of Professor Beer*. Baltimore, Fielding Lucces, 1823.

41. Dalrymple J. *The Anatomy of the Human Eye*. London, Longman, Rees, Orme, Brown & Greene, 1834.
42. Dalrymple J. *Pathology of the Human Eye*. London, J Churchill, 1852.
43. Von Ammon FA. *Klinische Darstellungen der Kraukheiten und Bildungsfehler des Menschlichen Auges, Vol I-III*. Berlin, G Reimer, 1838, 1841, 1847.
44. Sichel J. *Iconographie Ophthalmologique, ou Description, Aves Figures Coloriées, des Maladies de l'organe de la Vue Comprenant L' Anatomies Pathologique, La Pathologie et la Thérapeutique Medico-Chirurgicales*. Paris, J-B Bailliere et Fils, 1852-1859.
45. Wardrop J. *Essays on the Morbid Anatomy of the Human Eye*. 2d ed. London, J Churchill, 1839.
46. Jaeger E. *Beitrage zur Pathologie des Auges*. Vienna, Kaiserleich-Königlichen Hof und Staats Druckerei, 1855.
47. Ruete CG. *Lehrbuch der Ophthalmologie für Aerzte und Studirende*. Braunschweig, Friedrich Vieweg & Sohn, 1854.
48. Noyes HD. How to examine the eye. *A Text-Book on Diseases of the Eye*. 2d ed. New York, William Wood & Co, 1894, pp 35-38.
49. Ibid, pp 39-52.
50. Duke-Elder WS, ed. *The Foundations of Ophthalmology: Heredity, Pathology, Diagnosis, and Therapeutics. System of Ophthalmology. Vol VII*. St Louis, CV Mosby, 1962.
51. Haugwitz TV. Optical instruments. *Hirschberg's History of Ophthalmology, Vol XI*. Bonn, Verlag, 1986, pp A1-A185.
52. Bowman W. *Lectures on the Parts Concerned in the Operations on the Eye, and on the Structure of the Retina*. (Delivered at the Royal London Ophthalmic Hospital, Moorfields, June 1847.) London, Longman, Brown, Green, & Longman, 1849, p 72.
53. Magnus H. Pathologisch-anatomicshe Studien über die Anfänge des Altersstaares. *Archiv Ophthal* 1889; 35:57-92.
54. Brailey WA. On some points in the development of cataract. *Trans Ophthal Soc UK* 1891; 11:66-69.
55. Jackson E. *A Manual of the Diagnosis and Treatment of the Diseases of the Eye*. Philadelphia, WB Saunders, 1900, p 412.
56. Greene DW. The association of age and incipient cataract with normal and pathologic blood pressure. *J Am Med Assoc* 1908; 51:400-405.
57. Handmann M. Ueber den Beginn des altersstares in der unteren-linsenhalfte. Klinisch-statistische Studien an 845 Augen mit Cataracta senilis incipiens nebst Bemerkungen über die Cataracta glaukomatosa und diabetica. *Klin Monatsbl Augenheilkd* 1909; 47:692-720.
58. Schild H. Untersuchungen über die Häufigkeit der lamellären Zerklüftung, ihre Lage und Verlaufsrichtung in der vorderen und hinteren Linsenrinde an 218 Augen sonst gesunder Personen. *Arch Ophthalmol* 1922; 107:49-60.
59. Clapp CA. Senile cataract. *Cataract: Its Etiology and Treatment*. Philadelphia, Lea & Febiger, 1934, pp 127-134.
60. Berliner ML. Presenile and senile cataract. *Biomicroscopy of the Eye: Slit Lamp Microscopy of the Living Eye, Vol II*. New York, Hafner, 1949 (reprinted 1966), p 1121.
61. Kirby DB. Basic science applied to cataract surgery. *Surgery of Cataract* . Philadelphia, JB Lippincott, 1950, p 75.
62. Wright RE. The possible infuence of solar radiation on the production of cataract in certain districts of Southern India: A preliminary investigation. *Ind J Med Res* 1937; 24:917-920.
63. Dhir SP, Detels R, Alexander ER. The role of environmental factors in cataract, pterygium and trachoma. *Am J Ophthalmol* 1967; 64:128-135.
64. Van Heyningen R. The human lens: I. A comparison of cataracts extracted in Oxford

(England) and Shikarpur (W. Pakistan). *Exp Eye Res* 1972; 13:136-147.
65. Van Heyningen R. The human lens: II. Some observations on cataracts removed in Oxford, England. *Exp Eye Res* 1972; 13:148-154.
66. Zigman S, Datiles M, Torcyznski E. Sunlight and human cataracts. *Inves Ophthalmol Vis Sci* 1979; 18:462-467.
67. Chatterjee A, Rambo VC, Franken S. Vision survey in Himalayan area. *Am J Ophthalmol* 1968; 66:113-116.
68. Chatterjee A. Cataract in Punjab. *The Human Lens in Relation to Cataract*. New York, Elsevier (Excerpta Medica), 1973, pp 265-279. Ciba Foundation Symposium 19.
69. Kahn HA, Leibowitz HM, Ganley JP, et al. The Framingham eye study. I. Outline and major prevalence findings. *Am J Epidemiol* 1977; 106:17-32.
70. Chatterjee A, Milton RC, Thyle S. Prevalence and etiology of cataract in Punjab. *Br J Ophthalmol* 1982; 66:35-42.
71. Halevi HS, Landau J. Hospitalized senile cataract in different Jewish communities in Israel. *Br J Ophthalmol* 1962; 46:285-290.
72. Jamieson SW. Eye survey: Mrewa trust lands. *Postgrad Med J* 1970; 46:557-561.
73. Osuntokun O, Olurin O. Cataract and cataract extraction in Nigerians. *Br J Ophthalmol* 1973; 57:27-33.
74. Gregor Z, Joffe L. Senile macular changes in the black African. *Br J Ophthalmol* 1978; 62:547-550.
75. Marré E, Marré M. Epidemiological study of cataracts in Burma and Central Europe. *Dev Ophthalmol* 1989; 17:206-208.
76. Taylor HR. The environment and the lens. *Br J Ophthalmol* 1980; 64:303-310.
77. Hollows F, Moran D. Cataract: The ultraviolet risk factor. *Lancet* 1981; 2(Dec 5):1249-1250.
78. Cass E. A decade of northern ophthalmology. *Can J Ophthalmol* 1973; 8:210-217.
79. Wyatt HT. Abnormalities of cornea, lens, and retina: survey findings. *Can J Ophthalmol* 1973; 8:291-297.
80. Brilliant LB, Grasset NC, Pokhrel RP. Association among cataract prevalence, sunlight hours, and altitude in the Himalayas. *Am J Epidemiol* 1983; 118:250-264.
81. Wen-Shu M, Tian-sheng H. An epidemiologic survey of senile cataract in China. *Chin Med J* 1982; 95:813-818.
82. Hu T-S, Lao Y-X. An epidemiologic survey of senile cataract in China. *Dev Ophthalmol* 1987; 15:42-51.
83. Hu T-S, Zhen Q, Sperduto RD, et al. Age-related cataract in the Tibet Eye Study. *Arch Ophthalmol* 1989; 107:666-669.
84. Javitts JC, Taylor HR. Cataract and latitude. *Doc Ophthalmol* 1995; 88:307-325.
85. Hiller R, Giacometti L, Yuen K. Sunlight and cataract: an epidemiologic investigation. *Am J Epidemiol* 1977; 105:450-459.
86. Hiller R, Sperduto RD, Ederer F. Epidemiologic associations with cataract in the 1971-1972 national health and nutrition examination survey. *Am J Epidemiol* 1983; 118:239-249.
87. Hiller R, Sperduto RD, Ederer F. Epidemiologic associations with nuclear, cortical, and posterior subcapsular cataracts. *Am J Epidemiol* 1986; 124:916-925.
88. Collman GW, Shore DL, Shy CM, et al. Sunlight and other risk factors for cataracts: an epidemiologic study. *Am J Public Health* 1988; 78:1459-1462.
89. Taylor HR, West SK, Rosenthal FS, et al. Effect of ultraviolet radiation on cataract formation. *N Engl J Med* 1988; 319:1429-1433.
90. Taylor HR. Ultraviolet radiation and the eye. *Trans Am Ophthalmol Soc* 1989; 87:802-853.
91. Taylor HR. Ocular effects of UV-B exposure. *Doc Ophthalmol* 1995; 88:285-293.
92. Bochow TW, West SK, Azar A, et al. Ultraviolet light exposure and risk of posterior sub-

capsular cataracts. *Arch Ophthalmol* 1989; 107:369-372.
93. Taylor HR, West SK, Rosenthal FS, et al. Corneal changes associated with chronic UV irradiation. *Arch Ophthalmol* 1989; 107:1481-1484.
94. Taylor HR, West S, Munoz B, et al. The long-term effects of visible light on the eye. *Arch Ophthalmol* 1992; 110:99-104.
95. Ormerod LD, Dahan E, Hagele JE, et al. Serious occurrences in the natural history of advanced climatic keratopathy. *Ophthalmology* 1994; 101:448-453.
96. Coroneo MT. Pterygium as an early indicator of ultraviolet insolation: a hypothesis. *Br J Ophthalmol* 1993;77:734-739.
97. Cruickshanks KJ, Klein BE, et al. Ultraviolet light exposure and lens opacities: the Beaver Dam Eye Study. *Am J Pub Health* 1992; 82:1658-1662.
98. Klein BE, Klein R, Linton KL. Prevalence of age-related lens opacities in a population: the Beaver Dam Eye Study. *Ophthalmol* 1992; 99:546-552.
99. Klein BE, Cruickshanks KJ, Klein R. Leisure time, sunlight exposure and cataracts. *Doc Ophthalmol* 1995; 88:295-305
100. Rosmini F, Stazi MA, Milton RC, et al. Italian-American Cataract Study Group: a dose-reponse effect between a sunlight index and age-related cataracts. *Ann Epidemiol* 1994; 4:266-270.
101. Belpoliti M, Rosmini F, Carta A, et al. Distribution of cataract types in the Italian-American case-control study and at surgery in the Parma area. *Ophthalmol* 1995; 102:1594-1597.
102. Adamsons I, Munoz B, Enger C, et al. Prevalence of lens opacities in surgical and general populations. *Arch Ophthalmol* 1991; 109:993-997.
103. Schein OD, West S, Munoz B, et al. Cortical lenticular opacification: distribution and location in a longitudinal study. *Invest Ophthalmol Vis Sci* 1994; 35:363-366.
104. Mohan M, Sharma YR, Vajpayee RB, et al. Clinical evidence for light-induced thermal damage in cortical cataracts. *Dev Ophthalmol* 1989; 17:114-117.
105. Sharma YR, Vajpayee RB, Honavar SG. Sunlight and cortical cataract. *Arch Environ Health* 1994; 49:414-417.
106. Chylack LT, Wolf JK, Singer DM, et al. The lens opacities classification system III. *Arch Ophthalmol* 1993; 111:831-836.
107. Young R. *Age-Related Cataract*. New York, Oxford University Press, 1991.
108. Christen WG. Sunlight and age-related cataracts. *Ann Epidemiol* 1994; 4:338-339.
109. Dolin PJ. Ultraviolet radiation and cataract: a review of epidemiological evidence. *Br J Ophthalmol* 1994; 78:478-482.
110. Dolin PJ. Assessment of the epidemiological evidence that exposure to solar ultraviolet radiation causes cataract. *Doc Ophthalmol* 1995; 88:327-337.
111. van der Hoeve J. Eye lesions produced by light rich in ultraviolet rays: senile cataract, senile degeneration of macula. *Am J Ophthalmol* 1920; 3:178-194.
112. Southall JP, trans. *Helmholtz's Treatise on Physiological Optics, Vol I.* (Translated from the third German edition, 1909.) Menasha, Wis, G Barton, 1924.
113. Rizzutti AB. Diagnostic illumination test for keratoconus. *Am J Ophthalmol* 1970; 70:141-143.
114. Coroneo MT. Albedo concentration in the anterior eye: a phenomenon that locates some solar diseases. *Ophthalmic Surg* 1990; 21:60-66.
115. Coroneo MT, Muller-Stolzenburg NW, Ho A. Peripheral light focusing by the anterior eye in the ophthalmohelioses. *Ophthalmic Surg* 1991; 22:705-711.
116. Maloof AJ, Ho A, Coroneo MT. Influence of corneal shape on limbal light focusing. *Invest Ophthalmol Vis Sci* 1994; 35:2592-2598.
117. Frederick JE. Ultraviolet sunlight reaching the earth's surface: a review of recent research. *Photochem Photobiol* 1993; 57:175-178.
118. Madronich S. The atmosphere and UV-B radiation at ground level. In: Young AR,

Bjorn LO, Moan J, et al, eds. *Environmental UV Photobiology*. New York, Plenum Press, 1993, pp 1-39.
119. Feister U, Grewe R. Spectral albedo measurements in the UV and visible region over different types of surfaces. *Photochem Photobiol* 1995; 62:736-744.
120. Hoover HL. Solar ultraviolet irradiation of human cornea, lens, and retina: equations of ocular irradiation. *Applied Optics* 1986; 25: 359-367.
121. Sliney DH. Physical factors in cataractogensis: ambient ultraviolet radiation and temperature. *Invest Ophthalmol Vis Sci* 1986; 27:781-790.
122. Sliney DH. Ocular injury due to light toxicity. *Int Ophthalmol Clin* 1988; 28:246-250.
123. Sliney DH. Epidemiological studies of sunlight and cataract: the critical factor of ultraviolet exposure geometry. *Ophthalmic Epidemiol* 1994; 1:107-119.
124. Sliney DH. UV radiation ocular dosimetry. *Doc Ophthalmol* 1995; 88:243-254.
125. Winn B, Whitaker D, Elliott DB, et al. Factors affecting light-adapted pupil size in normal human subjects. *Invest Ophthalmol Vis Sci* 1994; 35:1132-1137.
126. Weale RA. Sunglasses: an ocular hazard? *Br J Ophthalmol* 1986; 70:769-771.
127. Hoover HL. Sunglasses, pupil dilation, and solar ultraviolet irradiation of the human lens and retina. *Applied Optics* 1987; 26:689-695.
128. Pitts D. Sunlight as an ultraviolet source. *Optom Vis Sci* 1990; 67:401-406.
129. Stolarski R, Bojkov R, Bishop L, et al. Measured trends in stratospheric ozone. *Science* 1992; 256:342-349.
130. Madronich S. The radiation equation. *Nature* 1995; 377:682-683.
131. Lubin D, Jensen EH. Effects of clouds and stratospheric ozone depletion on ultraviolet radiation trends. *Nature* 1995; 377:710-713.
132. Zigman S. Photobiology of the lens. In Maisel H, ed: *The Ocular Lens: Structure, Function, and Pathology* . New York, Marcel Dekker Inc, 1985, pp 301-347.
133. Urbach F. Potential effects of altered solar ultraviolet radiation on human skin cancer. *Photochem Photobiol* 1989; 50:507-513.
134. Moan J, Dahlback A. The relationship between skin cancers, solar radiation, and ozone depletion. *Br J Cancer* 1992; 65:916-921.
135. Smith RC, Prezeliu BB, Baker KS, et al. Ozone depletion: ultraviolet radiation, and phytoplankton biology in Antarctic waters. *Science* 1992; 255:952-958.
136. Schein OD, Vicencio C, Munoz B, et al. Ocular and dermatologic health effects of ultraviolet radiation exposure from the ozone hole in southern Chile. *Am J Public Health* 1995; 85:546-550.
137. Soret JL. Sur la transparence des milieux de l'oeil pour les rayons ultra-violets. *Comptes Rendus Hebdomadaires des Séances de 1 Académie des Sciences* 1879; 88:1012-1015.
138. Martin EK. The effects of ultraviolet rays upon the eye. *Proc Roy Soc London* [Biol] 1912; 85:319-330.
139. Burge WE. The mode of action of ultraviolet radiation in injuring living cells with special reference to those constituting the eye. *Am J Physiol* 1915; 39:335-344.
140. Duke-Elder WS. The pathological action of light upon the eye. *Lancet* 1926; 1:1137-1141.
141. Duke-Elder WS, Duke-Elder PM. A histological study on the action of short-waved light upon the eye, with a note on "inclusion bodies." *Br J Ophthlamol* 1929; 13:1-37.
142. Bachem A. Ophthalmic ultraviolet action spectra. *Am J Ophthalmol* 1956; 41:969-975.
143. Boettner EA, Wolter JR. Transmission of the ocular media. *Invest Ophthalmol* 1962, 1:776-783.
144. Ambach W, Blumthaler M, Schöpt T, et al. Spectral transmission of the optical media of the human eye with respect to keratitis and cataract formation. *Doc Ophthalmol* 1994; 88:165-173.
145. Keates RH, Genstler DE, Tarabichi S. Ultraviolet light transmission of the lens capsule. *Ophthalmic Surg* 1982; 13:374-376.

146. Murata Y. Light absorption characteristics of the lens capsule. *Ophthalmic Res* 1987; 19:107-112.
147. Said FS, Weale RA. The variation with age of the spectral transmissivity of the living human crystalline lens. *Gerontologica* 1959; 3:213-231.
148. Weale RA. Senescent vision: is it all the fault of the lens? *Eye* 1987; 1:217-221.
149. Weale RA. Age and the transmittance of the human crystalline lens. *J Physiol* 1988; 395:577-587.
150. Weale RA. The lenticular nucleus, light and the retina. *Exp Eye Res* 1991; 53:213-218.
151. Marshall J, Beaconsfield M, Rothery S. The anatomy and development of the human lens and zonules. *Trans Ophthalmol Soc UK* 1982; 102:423-440.
152. Rafferty NS. Lens morphology. In: Maisel H, ed. *The OcularLens: Structure, Function and Pathology*. New York, Marcel Dekker Inc, 1985, pp 1-60.
153. Kleiman NJ, Worgul BV. Lens. *Duane's Foundations of Clinical Ophthalmology*. Philadelphia, JB Lippincott, 1994, pp 1-39.
154. Duke-Elder WS. *Text-Book of Ophthalmology. Vol I: The Development, Form, and Function of the Visual Apparatus*. St Louis, CV Mosby, 1946.
155. Smith P. On the growth of the crystalline lens. *Trans Ophthal Soc UK* 1883; 3:79-99.
156. Smith P. On the size of the cornea in relation to age, sex, refraction, and primary glaucoma. *Trans Ophthalmol Soc UK* 1891; 10:68-78.
157. Tscherning MH. *Optique Physiologique*. Paris, Carré et Naud, 1898.
158. Fuchs E; Duane A, trans. *Text-Book of Ophthalmology*. Third Edition. Philadelphia, JB Lippincott, 1908.
159. Salzmann M; Brown EV, trans. *The Anatomy and Histology of the Human Eyeball in the Normal State: Its Development and Senescence*. Chicago, University of Chicago Press, 1912.
160. Spalteholtz W. *Hand-Atlas of Human Anatomy. Vol III. Viscera, Brain, Nerves, Sense-Organs*. 5th ed in English. Philadelphia, JB Lippincott, 1925.
161. Huggert A. The thickness of the cortex of the crystalline lens in different ages. *Acta Ophthalmol* 1946; 24:43-62.
162. Weekers R, Delmarcelle Y, Luyckx-Bacus J, et al. Morphological changes of the lens with age and cataract. *The Human Lens in Relation to Cataract*. New York, Elsevier (Excerpta Medica), 1973, pp 25-43. Ciba Foundation Symposium 19.
163. Delmarcelle Y, Collignon J, Luyckx J, Weekers R. Étude biométrique du globe oculaire dans le glaucome á angle fermé. *Bull Soc Fr Ophthalmol* 1971; 84:449-457.
164. Hoffer KJ. Axial dimensions of the human cataractous lens. *Arch Ophthalmol* 1993; 111:914-918.
165. Straatsma BR, Lightfoot DO, Barke RM, et al. Lens capsule and epithelium in age-related cataract. *Am J Ophthalmol* 1991; 112:283-296.
166. Stafford JR, Rosen TS, Merriam JC. Prenatal cocaine exposure and the development of the human eye. *Ophthalmol* 1994; 101:301-308.
167. Isenberg SJ, Neumann D, Cheong PW, et al: Growth of the internal and external eye in term and preterm infants. *Ophthalmol* 1995; 102:827-830.
168. Sasaki K, Hiiragi M, Sakamoto Y. Changes of crystalline lens transparency with age in healthy individuals. *Lens Research* 1986; 3:239-251.
169. Patel S, Marshall J, Fitzke FW III. Refractive index of the human corneal epithelium and stroma. *J Refrac Surg* 1995; 11:100-105.
170. Hemenger RP, Garner LF, Ooi CS. Change with age of the refractive index gradient of the human ocular lens. *Invest Ophthalmol Vis Sci* 1995; 36:703-707.
171. Lotmar W. Theoretical model with aspherics. *J Opt Soc Am* 1971; 6:1522-1529.
172. Zissis GJ, Larocca AJ. Optical radiators and sources. In: Driscoll WG, Vaughan W, eds. *Handbook of Optics*. New York, McGraw-Hill, 1978, pp 1-83.
173. Bird RE, Hulstrom RL, Kliman AW, et al. Solar spectral measurements in the terres-

trial environment. *Appl Optics* 1982; 21:1430-1436.
174. Merriam GR Jr. A clinical study of radiation cataracts. *Trans Am Ophthalmol Soc* 1956; 54:611-653.
175. Campbell CJ, Koester CJ, Rittler MC, et al. *Physiological Optics*. New York, Harper & Row, 1974, pp 100-104.
176. Morys M,Berger D. The accurate measurement of biologically effective ultraviolet radiation. (Presented at the International Symposium on High Latitude Optics, July 1993, Tromso, Norway.) Philadephia, Solar Light Co, 1994.
177. Narayanan P, Merriam JC, Vazquez ME, et al. Experimental model of light focusing of the peripheral cornea. *Invest Ophthalmol Vis Sci* 1996; 37:37-41.
178. Young AR, Bjorn LO, Moan J, et al, eds. *Environmental UV Photobiology*. New York, Plenum Press, 1993.
179. Lerman S. Ocular phototoxicity. *N Engl J Med* 1988; 319:1475-1478.
180. Söderberg PG. Acute cataract in the rat after exposure to radiation in the 300 nm wavelength region. *Acta Ophthalmol* 1988; 66:141-152.
181. Söderberg PG. Experimental cataract induced by ultraviolet radiation. *Acta Ophthalmol Suppl* 1990; 196:1-75.
182. Zigman S. Ocular light damage. *Photochem Photobiol* 1993; 57:1060-1068.
183. Eaton JW. UV-mediated cataractogensis: a radical perspective. *Doc Ophthalmol* 1995; 88:233-242.
184. Hightower KR. A review of the evidence that ultraviolet radiation is a risk factor in cataractogenesis. *Doc Ophthalmol* 1995; 88:205-220.
185. Vrensen GF: UV-B and early cortical and nuclear changes in the human lens. *Doc Ophthalmol* 1995; 88:255-261.
186. Sutherland JC, Griffin KP. Absorption spectrum of DNA for wavelengths greater than 300 nm. *Radiat Res* 1981; 86:399-409.
187. Andley UP, Lewis RM, Reddan JR, et al. Action spectrum for cytotoxicity in the UV-A and UV-B wavelength region in cultured lens epithelial cells. *Invest Ophthalmol Vis Sci* 1994; 35:367-373.
188. Coohill TP, Jacobson ED. Action spectra in mammalian cells exposed to ultraviolet radiation. *Photochem Photobiol* 1981; 33:941-945.
189. Jones CA, Huberman E, Cunningham ML, et al. Mutagenesis and cytotoxicity in human epithelial cells by far and near ultraviolet radiations: action spectra. *Radiat Res* 1987; 110:244-254.
190. Jose JG, Yielding KL. "Unscheduled" DNA synthesis in lens epithelium following ultraviolet irradiation. *Exp Eye Res* 1977; 24:113-119.
191. Morison WL, Parrish JA, McAuliffe DJ, et al. Sensitivity of mononuclear cells to UV radiation: effect on subsequent stimulation with phytohemagglutinin. *Photochem Photobiol* 1980; 32:99-101.
192. Peak MR, Peak JG. Single-strand breaks induced in *Bacillus subtilis* DNA by ultraviolet light: action spectrum and properties. *Photochem Photobiol* 1982; 35:675-680.
193. Grabner G, Brenner W. Unscheduled DNA repair in human lens epithelium following "in vivo" and "in vitro" ultraviolet irradiation. *Ophthalmic Res* 1982; 14:160-166.
194. Söderberg PG, Philipson BT, Lindström B. Unscheduled DNA synthesis in lens epithelium after in vivo exposure to UV radiation in the 300 nm wavelength region. *Acta Ophthalmol* 1986; 64:162-168.
195. Andley UP, Walsh A, Kochevar IE, et al. Effect of ultraviolet-B radiation on protein synthesis in cultured lens epithelial cells. *Curr Eye Res* 1990; 9:1099-1106.
196. Kleiman NJ, Wang R-R, Spector A. Ultraviolet light induced DNA damage and repair in bovine lens epithelial cells. *Curr Eye Res* 1990, 9:1185-1193.
197. Sidjamin D, Zigman S, Reddan J. DNA damage and repair in rabbit lens epithelial cells following UV-A radiation. *Curr Eye Res* 1993; 12:773-781.

198. von Sallmann L. The lens epithelium in the pathogenesis of cataract. *Am J Ophthalmol* 1957; 44:159-170.
199. Zigman S, Groff J, Yulo T, et al. The response of mouse ocular tissue to continuous near-UV light exposure. *Invest Ophthalmol* 1975; 14:710-713.
200. Zigman S, Paxhia T, McDaniel T, et al. Effect of chronic near-ultraviolet radiation on the grey squirrel lens in vivo. *Invest Ophthalmol Vis Sci* 1991; 32:1723-1732.
201. Hightower KR. The role of the lens epithelium in development of UV cataract. *Curr Eye Res* 1995; 14:71-78.
202. Leip O, Breipohe W, Wegener A, et al. Distribution pattern of viable mitochondria in bovine lens epithelial cells. *Dev Ophthalmol* 1994; 26:90-96.
203. Hightower KR, McCready JP, Borchman D. Membrane damage in UV-irradiated lenses. *Photochem Photobiol* 1994; 59:485-490.
204. Shoji Y. Sur la cysteine du cristallin et ses rapports avec les rayons ultra-violets. *Arch Ophtalmol* 1931; 48:28-33.
205. Clark JH. The effect of ultraviolet radiation on lens protein in the presence of salts and the relation of radiation to industrial and senile cataract. *Am J Physiol* 1935; 113:538-547.
206. East EJ, Chang RC, Yu N-T. Raman spectroscopic measurement of total sulfhydryl in intact lens as affected by aging and ultraviolet irradiation. *Biol Chem* 1978; 253:1436-1441.
207. Kuck JF. Effect of long-wave ultraviolet light on the lens. IV. Leucine metabolism in normal human lenses in vitro. *Ophthalmic Res* 1983; 15:216-219.
208. Iwata MA, Iwata S. Effects of UV-cutting filters on aggregation of lens protein. *Jpn J Ophthalmol* 1985; 29:460-467.
209. Yu N-T, Bando M, Kuck JF. Localization of UV-induced changes in mouse lens. *Exp Eye Res* 1990; 50:327-329.
210. Thomas DM, Papadopoulou O, Mahendroo PP, et al. Phosphorus-31 NMR study of the effects of UV on squirrel lenses. *Exp Eye Res* 1993; 57:59-65.
211. Zigman S, Griess G, Yulo T, et al. Ocular protein alteration by near UV light. *Exp Eye Res* 1973; 15:255-264.
212. Tung WA, Chylack LT, Andley UP. Lens hexokinase deactivation by near-uv irradiation. *Curr Eye Res* 1988; 7:257-263.
213. Torriglia A, Zigman S. The effect of near-UV light on Na-K-ATPase of the rat lens. *Curr Eye Res* 1988; 7:539-548.
214. Hightower KR, McCready J. Mechanisms involved in cataract development following near-ultraviolet radiation of cultured lenses. *Curr Eye Res* 1992; 11:679- 689.
215. Dovrat A, Weinreb O. Recovery of lens optics and epithelial enzymes after ultraviolet-A radiation. *Invest Ophthalmol Vis Sci* 1995; 36:2417-2424.
216. Li D-Y, Borkmann RF. Photodamage to calf lenses in vitro by excimer laser radiation at 308, 337 and 350 nm. *Invest Ophthalmol Vis Sci* 1990; 31:2180-2184.
217. Stuart DD, Sivak JG, Cullen AP, et al. UV-B radiation and the optical properties of cultured bovine lenses. *Curr Eye Res* 1991; 10:177-184.
218. Hightower KR, McCready J. Physiological effects of UV-B irradiation on cultured rabbit lens. *Invest Ophthalmol Vis Sci* 1992; 33:1783-1787.
219. Stuart DD, Cullen AP, Sivak JG, et al. Optical effects of UV-A and UV-B radiation on the cultured bovine lens. *Curr Eye Res* 1994; 13:371-376.
220. Dillon J. The photophysics and photobiology of the eye. *J Photochem Photobiol* 1991; 10:23-40.
221. Dillon J. UV-B as a pro-aging and pro-cataract factor. *Doc Ophthalmol* 1995; 88:339-344.
222. Cooper GF, Robson JG. The yellow colour of the lens of man and other primates. *J Physiol* 1969; 203:411-417.

223. Zigman S, Shultz J, Yulo T. Possible roles of near UV light in the cataractous process. *Exp Eye Res* 1973; 15:201-208.
224. Borkman RF, Lerman S. Evidence for a free radical mechanism in aging and uv-irradiated ocular lenses. *Exp Eye Res* 1977; 25: 303-309.
225. Borkman RF. Cataracts and photochemical damage. *Human Cataract Formation.* London, Pitman, 1984, pp 88-109. Ciba Foundation Symposium 106.
226. Eaton JW. UV-mediated cataractogenesis: a radical perspective. *Doc Ophthalmol* 1995; 88:233-242.
227. Gillardon F, Zimmermann M, Uhlmann E. Expression of c-Fos and c-Jun in cornea, lens, and retina after ultraviolet irradiation of the rat eye and effects of topical antisense oligodeoxynucleotides. *Br J Ophthalmol* 1995; 79:277-281.
228. Li W-C, Kuszak JR, Dunn K, et al. Lens epithelial cell apoptosis appears to be a common cellular basis for non-congenital cataract development in humans and animals. *J Cell Biol* 1995; 130:169-181.
229. Kuszak JR, Sivak JG, Weerheim JA. Lens optical quality is a direct function of lens sutural architecture. *Invest Ophthalmol Vis Sci* 1991; 32:2119-2129.
230. Brown NP, Harris ML, Shun-shin GA, et al. Is cortical spoke cataract due to lens fibre breaks? The relationship between fibre folds, fibre breaks, water clefts and spoke cataract. *Eye* 1993; 7:672-679
231. Hess C. Versuche über die Einwirkung ultravioletten Lichtes auf die Linse. *Arch Augenheilkd* 1907; 35:185-196.
232. MacKeen D, Fine S, Fine BS. Production of cataracts in rabbits with the ultraviolet laser. *Ophthalmic Res* 1973; 5:317-324.
233. Zigman S, Yulo T, Schultz J. Cataract induction in mice exposed to near UV light. *Ophthalmic Res* 1974; 6:259-270.
234. Zigman S, Vaughan T. Near-ultraviolet light effect on the lenses and retinas of mice. *Invest Ophthalmol* 1974; 13:462-465.
235. Ebbers RW. Ocular effects of a 325 nm ultraviolet laser. *Am J Optom Physiol Optic* 1975; 52:216-223.
236. Zuchlich JA, Connolly JS. Ocular damage induced by near-ultraviolet laser radiation. *Invest Ophthalmol* 1976; 15:760-764.
237. Cullen AP, Monteith-McMaster CA. Damage to the rainbow trout (*Oncorhyncus mykiss*) lens following an acute dose of UVB. *Curr Eye Res* 1993; 12:97-106.
238. Pitts DG, Cullen AP, Hacker PD. Ocular effects of ultraviolet radiation from 295 to 365 nm. *Invest Ophthalmol Vis Sci* 1977; 16:932-939.
239. Jose JG, Pitts, DG. Wavelength dependency of cataracts in albino mice following chronic exposure. *Exp Eye Res* 1985; 41:545-563.
240. Jose JG. Posterior cataract induction by UV-B radiation in albino mice. *Exp Eye Res* 1986; 42:11 -20.
241. Zigman S, Paxhia T, Waldron W. Effects of near-UV radiation on the protein of the grey squirrel lens. *Curr Eye Res* 1988; 7:531-537.
242. Hightower KR, McCready J. Comparative effect of UV-A and UV-B on cultured rabbit lens. *Photochem Photobiol* 1993; 58:827-30.
243. Wegener AR. In vivo studies on the effect of UV-radiation on the eye lens in animals. *Doc Ophthalmol* 1995; 88:221-232.
244. Fisher RF. Elastic constants of the human lens capsule. *J Physiol* 1969; 201:1-19.
245. Fisher RF. The significance of the shape of the lens and capsular energy changes in accommodation. *J Physiol* 1969; 201: 21-47.
246. Fisher RF. Senile cataract: a comparative study between lens fibre stress and cuneiform opacity formation. *Trans Ophthal Soc UK* 1970; 90:93-109.
247. Fisher RF. The structure and function of basement membrane (lens capsule) in relation to diabetes and cataract. *Trans Ophthalmol Soc UK* 1985; 104:755-759.

248. Fisher RF. The influence of age on some ocular basement membranes. *Eye* 1987; 1:184-189.
249. Minassian DC, Mehra V, Verrey J-D. Dehydrational crises: a major risk factor in blinding cataract. *Br J Ophthalmol* 1989; 73:100-105.
250. Van Heyningen R, Harding JJ. A case-control study of cataract in Oxfordshire: some risk factors. *Br J Ophthalmol* 1988; 72:804-808.
251. Harding JJ, Harding RS, Egerton M. Risk factors for cataract in Oxfordshire: diabetes, peripheral neuropathy, myopia, glaucoma and diarrhoea. *Acta Ophthalmol* 1989; 67:510-517.
252. Harding J. The untenability of the sunlight hypothesis of cataractogenesis. *Doc Ophthalmol* 1995; 88:345-349.
253. Leyton GB. Effects of slow starvation. *Lancet* 1946; 2:73-79.
254. Report of the Ninth Meeting of the WHO Programme Advisory Group on the Prevention of Blindness, March 5-8, 1991. Geneva, Switzerland, World Health Organization, 1991, publication 91.22.
255. Wong L, Ho SC, Coggon D, et al. Sunlight exposure, antioxidant status, and cataract in Hong Kong fishermen. *J Epidemiol Comm Health* 1993; 47:46-49.
256. Darrell RW, Bachrach CA. Pterygium among veterans. *Arch Ophthalmol* 1963; 70:158-169.
257. Chylack LT. Mechanisms of senile cataract formation. *Ophthalmol* 1984; 91:596-602.
258. Kahn HA, Leibowitz HM, Granley JP, et al. The Framingham Eye Study. II. Association of ophthalmic pathology with single variables previously measured in the Framingham Heart Study. *Am J Epidemiol* 1977; 106:33-41.
259. Clayton RM, Cuthbert J, Duffy J, et al. Some risk factors associated with cataract in SE Scotland: a pilot study. *Trans Ophthalmol Soc UK* 1982; 102:331-336.
260. Leske MC, Chylack LT, Wu S-Y, et al. The lens opacities case-control study: risk factors for cataract. *Arch Ophthalmol* 1991; 109:244-251.
261. Leske MC, Wu S-Y, Hyman L, et al. Biochemical factors in the lens opacities case-control study. *Arch Ophthalmol* 1995; 113:1113-1119.
262. Mares-Perlman JA, Brady WE, Klein BE, et al. Serum carotenoids and tocopherols and severity of nuclear and cortical opacitites. *Invest Ophthalmol Vis Sci* 1995; 36:276-288.
263. Christen WG, Manson JE, Seddon JM, et al. A prospective study of cigarette smoking and risk of cataract in men. *J Am Med Assoc* 1992; 268:989-993.
264. Hankinson SE, Willett WC, Colditz GA, et al. A prospective study of cigarette smoking and risk of cataract surgery in women. *J Am Med Assoc* 1992, 268:994-998.
265. Klein BE, Klein R, Jensen SC, et al. Hypertension and lens opacities from the Beaver Dam Eye Study. *Am J Ophthalmol* 1995; 119:640-646.
266. Glynn RJ, Christen WG, Manson JE, et al. Body mass index: an independent predictor of cataract. *Arch Ophthalmol* 1995; 113:1131-1137.
267. Schoenfeld ER, Leske MC, Wu S-Y. Recent epidemiologic studies on nutrition and cataract in India, Italy, and the United States. *J Am Coll Nutrition* 1993; 12:521-526.
268. Heiba IM, Elston RC, Klein BE, Klein R. Evidence for a major gene for cortical cataract. *Invest Ophthalmol Vis Sci* 1995; 36:227-235.
269. Hyman L. Epidemiology of eye disease in the elderly. *Eye* 1987; 1:330-341.
270. Report of the Tenth Meeting of the WHO Programme Advisory Group on the Prevention of Blindness, Geneva, March 2-5, 1993. Geneva, Switzerland, World Health Organization, 1993, publication 93.30.
271. Said M-E, Goldstein H, Korra A, et al. Prevalence and causes of blindness in urban and rural areas of Egypt. *Public Health Rep* 1970; 85:587-599.
272. Tabbara KF, Ross-Degnan D. Blindness in Saudi Arabia. *JAMA* 1986; 255:3378-3384.
273. Minassian DC, Mehra V. 3.8 million blinded by cataract each year: projections from the first epidemiological study of incidence of cataract blindness in India. *Br J Ophthalmol*

1990; 74:341-343.
274. Report of the Lens and Cataract Panel. *Vision Research: A National Plan 1994-1998.* Washington, DC: US Dept of Health and Human Services; 1993:155-197; Public Health Service publication NIH 93-3186.
275. Häkkinen L. Vision of the elderly and its use in the social environment. *Scand J Soc Med* 1984; 35:1-60.
276. Rouhiainen H, Terasvirta M. Kuopio eye survey (KEYS). *Acta Ophthalmol* 1990; 68:554-558.
277. Hirvelä H, Luukinen H, Laatikainen L. Prevalence and risk factors of lens opacities in the elderly in Finland. *Ophthalmol* 1995; 102:108-117.
278. Gibson JM, Rosenthal AR, Lavery J. A study of the prevalence of eye disease in the elderly in an English community. *Trans Ophthalmol Soc UK* 1985; 104:196-203.
279. Leske MC, Sperduto RD. The epidemiology of senile cataracts: a review. *Am J Epidemiol* 1983; 118:152-165.
280. Kupfer C. The conquest of cataract: a global challenge. *Trans Ophthalmol Soc UK* 1984; 104:1-10.
281. Mann I. *Culture, Race, Climate and Eye Disease: An Introduction to the Study of Geographical Ophthalmology.* Springfield, Ill, Charles C Thomas, 1966.
282. Dawson CR, Schwab IR. Epidemiology of cataract: a major cause of preventable blindness. *Bull WHO* 1981; 59:493-501.
283. Goldstein H. The reported demography and causes of blindness throughout the world. *Adv Ophthalmol* 1980; 40:1-99.
284. Rosenthal FS, Safran M, Taylor HR. The ocular dose of ultraviolet radiation from sunlight exposure. *Photochem Photobiol* 1985; 42:163-171.
285. Rosenthal FS, Bakalian AE, Taylor HR. The effect of prescription eyewear on ocular exposure to ultraviolet radiation. *Am J Public Health* 1986; 76:1216-1220.
286. Duncan DD, Schneider W, West KJ, et al. The development of personal dosimeters for use in the visible and ultraviolet wavelength regions. *Photochem Photobiol* 1995; 62:94-100.